2022

Microvascular Consequences of Engineered Nanomaterial Inhalation Exposure and Subsequent Reproductive Outcomes

Krista Lee Garner
kg0048@mix.wvu.edu

MICROVASCULAR CONSEQUENCES OF ENGINEERED NANOMATERIAL INHALATION EXPOSURE AND SUBSEQUENT REPRODUCTIVE OUTCOMES

KRISTA LEE GARNER

Dissertation submitted to the

School of Medicine at West Virginia University

In partial fulfillment of the requirements for the degree of

Doctor of Philosophy

In

Cellular and Integrative Physiology

Stanley Hileman, Ph.D., Chair

Timothy Nurkiewicz, Ph.D., Mentor

Salik Hussain, Ph.D.

Eric Kelley, Ph.D.

Robert Dailey, Ph.D.

Daniel Conklin, Ph.D., External Examiner

Department of Physiology and Pharmacology

Morgantown, West Virginia

2022

Keywords: Microcirculation, Toxicology, Nano-Titanium Dioxide, Angiotensin II, Gestation

Abstract

Microvascular Consequences of Toxicant Inhalation Exposure and Subsequent Reproductive Outcomes

Krista L. Garner

Nano-titanium dioxide (nano-TiO_2) is a commonly utilized engineered nanomaterial found ubiquitously in consumer products. While benefits of ENM utilization in are undeniable, nanoparticle inhalation has been linked to cardiovascular consequences and altered microvascular responses. Given these outcomes, it is important to explore vulnerable timepoints, such as gestation, as robust vascular adaptations are essential for maternofetal health.

The first aim of this dissertation was to assess myogenic responsiveness following maternal nano-TiO_2 inhalation. Fetal aortic responses were evaluated on gestational day (GD) 20 to assess how exposure may impact the F1 generation. Myogenic responsiveness within the uterine radial arteries were unaffected. Endothelium-dependent relaxation was found to be reduced within the fetal aortas of the exposure group.

The second aim was to evaluate the window of gestation that is most susceptible to maternal exposure. Exposure groups were divided into early (EE), mid (ME) and late (LE) and uterine radial artery responses were assessed on GD 20. The EE group showed increased sensitivity to Ang II and exhibited decreased protein level of angiotensin II type 2 receptor. EE resulted in reduced pup mass and placental efficiency, suggesting Ang II vasoconstriction may play a role in poor perfusion, resulting in reduced pup size.

The third aim was to further evaluate the susceptible time-point of gestational exposure by assessing placental physiology. Placental hemodynamics were not influenced by exposure, nor were Ang II receptor protein level, suggesting that the reduced pup mass within the EE group may be dependent upon uterine vascular function and not placental hemodynamics.

Acknowledgements

Over my 5-year journey at WVU, I have met many incredible people that have no doubt contributed to who I am today as a scientist. The individuals in this section have aided me in my journey as a graduate student and I am entirely thankful for their support, of which without none of this would have been possible.

My first thanks must go to my mentor, Dr. Timothy Nurkiewicz, who has encouraged me throughout my journey as a graduate student. Thank you for always showing me support and instilling me with an interest in cardiovascular toxicology—and yes, I will always remember Claude Bernard. I must also personally thank my committee chair, Dr. Stan Hileman, who was always available to listen and offer advice. In addition, I want to thank all of my committee members, including Dr. Eric Kelley, Dr. Salik Hussain, and Dr. Robert Dailey, whose valuable guidance gave me the tools to successfully complete my dissertation.

I would also like to thank all Nurkiewicz lab members, past and present, who have trained me in techniques, that without I would not have been able to accomplish my Ph.D. I will miss our enlightening and often hilarious conversations during tissue harvest days. The faculty, staff and graduate students within the physiology and pharmacology department also deserve acknowledgement for their collaborative spirit and sense of community present within our department.

A special thanks must go out to the friends I have gained here at WVU, who have made some of the most trying moments bearable and have been a source of laughter in my life. Emily Burrage, I do not know what I would have done without you and our trips to Los. Thank you for offering welcomed distractions, but also keeping me on track. Julie Griffith,

thank you for being such a wonderful and caring lab mate. I will always think of your hilariously sassy quotes. Last, but not least, Dr. Lizzie Bowdridge—Two words: De nada. I am so thankful to have not only found a friend in you, but also a mentor. You are a true inspiration (and I am sure Wes would agree) and have made a profound impact on me as a scientist and as a friend.

I would like to thank my friends and family back home who have consistently offered support and comfort during this experience. Phone calls to them never went unanswered and for that I am truly grateful. A special thanks goes to the wonderful children in my life, Harper, Greer and Wyatt, who made visits back home full of joy and laughter.

I would also like to thank my late father, James Garner, who I miss dearly. He always believed in me and pushed me to be the best. During my most challenging moments, I have often heard his words “they can kill you, but they can’t eat you.” While I always got the gist of the saying, I never fully understood this quote until recently looking up the last portion of it: “…because you’re too tough!”. It has always given me strength to step out of my comfort zone, which is no doubt necessary when pursuing a Ph.D.

Finally, I want to say thank you to my caring partner, Anthony, who has stood by me throughout my Ph.D., and has offered immense support. Thank you for your encouragement, comfort and unconditional love.

Table of Contents

Glossary of Abbreviations

˚C	Degrees Celsius
µg	Micrograms
µl	Microliters
µm	Micrometers
3D	Three dimensional
ABS	Acrylonitrile butadiene styrene
ACE	Angiotensin converting enzyme
ACE2	Angiotensin converting enzyme 2
ACh	Acetylcholine
ADH	Anti-diuretic hormone
ADMA	Asymmetric dimethylarginine
Ang-1	Angiopoietin-1
Ang-2	Angiopoietin-2
Ang I	Angiotensin I
Ang II	Angiotensin II
ANOVA	Analysis of variance
APS	Aerodynamic particle sizer

AT_1-AA	AT_1 autoantibodies
AT_1R	Angiotensin type 1 receptor
AT_2R	Angiotensin type 2 receptor
AuNPs	Gold nanoparticles
B_2	Bradykinin
B_2R	Bradykinin receptor
BPA	Bisphenol A
BPM	Beats per minute
C	Mass concentration
Ca^{2+}- free PSS	Calcium-free physiological salt solution
$CaCl_2$	Calcium chloride
CeO_2	Cerium dioxide
CMD	Count median diameter
CNTs	Carbon nanotubes
COX	Cyclooxygenase
CYP17	Cytochrome p450c17
D	Lung deposition
DAG	Diacylglycerol

Dcon	Control diameter
DES	Diethylstilbestrol
DHEA	Dehydroepiandrosterone
Di	Internal diameter
Dm	Maximal diameter
DMT	Danish MyoTechnologies
DOHaD	Developmental origins of health and disease
Dss	Steady state diameter
E_2	Estradiol
E_3	Estriol
EDTA	Ethylenediaminetetraacetic acid
EE	Early exposed
ELPI	Electrical low-pressure impactor
ENM	Engineered nanomaterials
eNOS	endothelial nitric oxide synthase
ET-1	Endothelin-1
F	Deposition fraction
FMPS	Fast mobility particle sizer

GD	Gestational day
GLUT-1	Glucose transport protein
H&E	Hematoxylin and eosin
HEPA	High-efficiency particulate air
HPAG	High-pressure acoustical generator
IARC	International Agency for Research on Cancer
ICAM-1	Intercellular adhesion molecule 1
ID	Internal diameter
IFN- ɣ	Interferon gamma
IL-1β	Interleukin-1β
IL-6	Interleukin-6
IP3	Inositol triphosphate
IUGR	Intrauterine growth restriction
K+PSS	High-potassium physiological salt solution
KCl	Potassium chloride
kDa	Kilodalton
KH_2PO_4	Potassium phosphate
Kiss	Kisspeptin

LE	Late exposed
LPS	Lipopolysaccharide
M	Molar
m^3	Meters cubed
MAP	Mean arterial pressure
MAPK	Mitogen-activated protein kinase
MasR	Mas receptor
ME	Mid exposed
mg	Milligrams
MgO	Magnesium oxide
$MgSO_4$	Magnesium sulfate
MI	Myocardial infarction
MKP-1	Mitogen-activated protein kinase phosphatase
MLCK	Myosin light chain kinase
MLCP	Myosin light chain phosphatase
mM	Millimolar
mm Hg	Millimeters of mercury
MMAD	Mass median aerodynamic diameter

MOUDI	Micro-orifice uniform deposit impactor
mV	Millivolts
MWCNTs	Multi-walled carbon nanotubes
N	Animal number
n	Vessel number
N/m	Newtons per meter
NaCl	Sodium chloride
NaH_2PO_4	Sodium phosphate
$NaHCO_3$	Sodium bicarbonate
Nano-TiO_2	Titanium dioxide nanoparticles
NE	Norepinephrine
NF-kB	Nuclear factor kappa B
$NiCl_2$	Nickel chloride
NIOSH	National Institute for Occupational Safety and Health
nM	Nanomolar
nm	Nanometer
NO	Nitric oxide
NOS	Nitric oxide synthase

OSHA	Occupational Safety and Health Administration
O_3	Ozone
OD	Outer diameter
PAI-1	Plasminogen activator inhibitor-1
PBS	Phosphate buffered saline
P4	Progesterone
PE	Phenylephrine
PEG	Polyethylene glycol
PGI_2	Prostacyclin
PI3K	Phosphatidylinositol 3-kinase
PKC	Protein kinase C
PLC	Phospholipase C
PSS	Physiological salt solution
RAS	Renin-angiotensin system
RAAS	Renin-angiotensin-aldosterone system
ROS	Reactive oxygen species
QDs	Quantum dots
SD	Standard deviation

SE	Standard error
SEM	Scanning electron microscopy
sFLT-1	Soluble fms-like tyrosine receptor-1
SMPS	Scanning-mobility particle size
SNAP	S-Nitroso-N-acetyl-DL-penicillamine
SOD	Superoxide dismutase
SWCNTs	Single-walled carbon nanotubes
T	Exposure duration
TNF-α	Tumor necrosis factor alpha
uNK	Uterine natural killer cells
V	Minute ventilation
VCAM-1	Vascular cell adhesion protein 1
VEGF	Vascular endothelial growth factor
VOCs	Volatile organic compounds
WLR	Wall-to-lumen ratio
WT	Wall thickness
ZnO	Zinc oxide

List of Figures

Chapter 1:

Chapter 2:

List of Tables

Chapter 2

Chapter 3

Chapter 5

I. Literature Review

Engineered nanomaterials (ENM) have no doubt advanced society through their impact on human health. Due to their unique physicochemical properties, ENM are found ubiquitously in day-to-day life as they are used to improve material robustness, enable more efficient drug delivery, and provide antimicrobial properties [1]. While ENM have improved many aspects of human life, it is important to consider that exposure to these advanced materials may have untoward consequences. Due to their impressive chemical and physical properties, exposure through routes such as inhalation may lead to negative downstream health outcomes not originally intended. In 1993 a link between air pollution inhalation and mortality, especially due to cardiovascular events, was first reported [2]. Since then, our lab and others have explored such consequences and have linked nanoparticle inhalation exposure to negative cardiovascular events such as acute hypertension [3, 4] and arrhythmia [4]. Further, microvascular dysfunction has been observed following ENM inhalation exposure within various vascular beds [5, 6], including the uterine microcirculation during gestation as well as umbilical vasculature [7-10]. Due to these findings, it is crucial to explore potential negative outcomes from inhalation exposure during pregnancy, in which unmatched microvascular growth and cardiovascular adaptation take place. Unique adaptions to pregnancy can be clearly witnessed when examining maternal uterine microvascular growth and placental development during gestation [11]. If perturbations were to occur during these sensitive windows of development, adverse consequences to the mother as well as the fetus may occur, leading to gestational complications and poor health outcomes.

While many adaptations to pregnancy occur, components of the renin-angiotensin-aldosterone system (RAAS) are crucial during gestation for increasing blood volume to support the fetus as well as vascular growth and have been shown to be altered following inhalation exposure to ENM such as nano-titanium dioxide (nano-TiO_2) [9]. Given the important roles of RAAS throughout gestation, as well as its implications for preeclampsia [12], it is important to determine how exposure during key periods of pregnancy may affect microvascular responses within the maternal uterus as well as the placenta. Additionally, it is important to pinpoint when during gestation exposure causes the most detrimental impacts, as gestational ENM exposure in an occupational setting is likely to occur in early and mid-gestation.

A. ENM Utilization and Advanced Materials

A.1. ENM Properties. Engineered nanomaterials (ENM) are anthropogenic particles that are ≤ 100 nm in size in at least one dimension. ENM can be used to produce advanced materials that are utilized for biomedical applications, nanomedicine [1], and every day-use consumer products [13]. These advanced materials are the result of nanotechnology innovations that are improving the medical field and consumer products. ENM have special properties that allow for these innovational uses, such as their size and size distribution, shape and morphology, charge, high surface area-mass ratio, and chemical composition. However, these properties may also increase the potential toxicity of these materials. The risk of ENM exposure also increases when considering the lifecycle of these advanced materials. Not only is there exposure risk during production and use of these products, but also during their destruction and recycling. ENM exposure has been linked to cardiovascular morbidity and mortality, and this may be due to mechanisms such

as endothelial dysfunction, thrombosis, and systemic inflammation [14, 15]. To better understand these negative consequences associated with advanced materials, it is important to understand their properties that contribute to their possible toxicities and the applications through which humans are exposed.

A.1.1. Carbonaceous Nanoparticles

Carbonaceous nanoparticles are utilized in a diverse set of applications due to their exceptional structural characteristics. Carbon nanomaterials exist in a wide variety of allotropic forms and are utilized due to their high tensile strength [16]. Due to this, they are found in a multitude of consumer products as discussed below. Additionally, they are utilized in medical applications due their electrical conductivity and are used for biomedical imaging [17]. There are a multitude of structural forms of carbon-based nanoparticles, but here, the two most commonly utilized examples are discussed.

A.1.1.1. Graphene

Graphene consists of a two-dimensional sheet of carbon atoms. These particles have physiochemical properties that allow for applications where high surface area, electrical conductivity, and lightweight, but strong mechanical strength are advantageous. Due to the light weight and exceptional strength of graphene it has been incorporated into sports equipment and aerospace parts. Additionally, graphene and graphene composites have been utilized for several other applications such as energy battery storage [18, 19] and filtration since they possess a capacity for absorbing organic contaminants. Graphene layers have been utilized in carbon air filters for the removal of volatile organic compounds [20] as well as absorption of pesticides [21]. These applications reflect the versatility of

these nanomaterials and how consumer markets can beneficially harness their physical and chemical properties.

A.1.1.2. Carbon Nanotubes

Carbon nanotubes (CNTs) can be formed into either single walled carbon nanotubes (SWCNTs) or multi-walled carbon nanotubes (MWCNTs) and are utilized in a wide variety of materials and applications. There are several properties that can be altered in CNTs that can change their physicochemical capabilities, such as aspect ratio and length, which have also been shown to correlate with toxicity [22]. CNTs are utilized to enhance textiles, such as their incorporation into cotton fabrics, which are inherently water absorbent and flammable. After doing so, these CNT encased cotton fibers become increasingly water resistant, UV resistant, flame retardant and mechanically stronger. This hybrid material improves the resiliency of the cotton threads and allows for the possibility of cotton to meet military specifications [23]. SWCNTs have also found a use in biological imaging. In 2004 it was shown that SWCNT's intrinsic near-infrared fluorescence can be utilized to monitor macrophage-like cells after phagocytosis of the particles [24]. Near-infrared florescence allows for higher resolution and greater penetration depth for imaging [25]. MWNTs can be found in a variety of composite materials. The inherent strength of the structure increases the load bearing ability of resins mixed with CNTs and polymers. Additionally, when mixed in paints CNTs can aid in anticorrosion coatings as well as reduce biofouling [26]. Thus, due to the intrinsic properties of these ENM, the addition of CNTs to various products can significantly enhance and improve their functionality.

A.1.2. Organic Nanoparticles

Organic nanoparticles are another subsection of nanoparticles that can be utilized due to their unique properties. These particles of are particular interest within the material sciences as they are fashioned after organic molecules and are found to have increased biocompatibility. In addition to having high biocompatibility, they are of particular interest in the biomedical field due to their low cost of production and low cytotoxicity [27]. Two of the more highly utilized organic nanoparticles are discussed below.

A.1.2.1. Liposomes

Liposomes are formed from water insoluble polar lipids with a polar head and nonpolar tail. They can be created from cholesterol or other natural phospholipids that form a bilayer vesicle with an outer hydrophobic region of nonpolar tails and a hydrophilic region within the center of the vesicle [28]. These artificial vesicles are ideal for drug delivery due to their small size and duel hydrophobic and hydrophilic nature. As they are composed of basic components of the cell wall, liposomes are biocompatible, allowing them to easily be transferred within the body to the desired target through the addition of site-specific modifications [29]. Additionally, they protect drugs from potential immunological break down, leading to enhancement of the therapeutic agents and increasing drug half-life. Currently, several liposomal drugs are on the market. One such drug is Doxil®, a chemotherapy drug that when given as a free drug bolus to cancer patients showed high cytotoxicity and a resultant cardiomyopathy. Doxil® is cell-cycle specific and works by inducing cell cycle arrest via increased Fas expression. This leads to enhanced caspase activation resulting in intracellular apoptotic signaling [30]. By liposomally encapsulating the drug, not only was toxicity reduced, but half-life and drug retention improved. This was due to a reduction of liposome detection by the immune

system, allowing for the drug to get closer to the tumor and exhibit cytotoxicity most specifically to tumor cells [31].

A.1.2.2. Polymers

Polymer nanospheres or nanocapsules, similar to liposomes, can be used to carry biologically active molecules such as drugs and fluorescent or nucleic material. Polymer nanoparticles can either be naturally produced and extracted or be synthetic polymers, depending on the desired function. For drug delivery, natural polymers such as polyethylene glycol (PEG) may be derived and added to drugs for delivery. PEGylation is a process that has been used to improve immune responses to these nanoparticles. Not only does PEG have relatively low toxicity [32], it exhibits reduced phagocytosis from macrophages [33]. These organic nanomaterials can be utilized to overcome immunological destruction and active drug toxicity, thereby improving pharmacological outcomes.

A.1.3. Inorganic Nanoparticles

Inorganic nanoparticles are biocompatible components utilized for several medical applications, including the conjugation of ligands, imaging techniques for various diagnoses, improving antioxidant activity, and enhancing drug delivery [17]. These nanomaterials can also be incorporated into consumer products due to their unique photocatalytic and antibacterial properties. For example, metal oxides and silver nanoparticles can be added to fabrics to kill bacteria, reduce odors within clothing and increase durability [34]. Given the versatility of these ENM, it is not surprising that

nanoparticle technology use in these particular consumer markets has grown exponentially.

A.1.3.1. Quantum Dots

Quantum dots (QDs) are zero dimensional crystalline inorganic solids that exhibit a range in size of just a few nanometers and act as semiconductors due to their high surface-to-volume ratio. QDs are used for photonics and photoluminescent dyes [35] and can be highly useful in imaging and diagnostic applications within the medical field as they allow for brighter imaging as well as decreased degradation of signal, resulting in a higher resolution. Fluorescent QDs have been utilized to visualize capillaries within live murine brains, demonstrating an application for in vivo angiography [36]. QDs can even be utilized to track metastatic cancer cells using antibodies. In a 2004 study, researchers were able to track tumor cells labeled with quantum dots following injection into mice, allowing them to assess the extravasation of cells throughout the body [37]. Development of these and future uses for QDs will undoubtedly improve applications for assessing and treating human health issues.

A.1.3.2. Metallic Nanoparticles

Examples of metal nanoparticles include gold, silver and iron oxide. Gold nanoparticles (AuNPs) have been utilized in diagnostic imagining techniques due to their biocompatibility and nontoxic properties as well as for their negative charge which can be useful for creation of gold nanoconjugates [38]. The size of nanomaterials has been shown to impact the rate at which they are absorbed into the body as well as the biodistribution of particles. Nanoparticles have the ability to transport through cell barriers,

leading to translocation of particles into the blood stream and into target tissues. Additionally, the size and composition of the particles can contribute to their persistence within the body, as size can influence uptake by macrophages. Opsonization, the tagging of foreign material to be eliminated via phagocytes, and which can occur through blood protein corona formation once the particles have entered the blood stream, has been shown to be reduced for particles less than 100 nm compared to larger particles greater than 100 nm [33]. Consistent with that thought, AuNPs were shown to have a size dependent rate of macrophage uptake when cultured with J774A.1 murine macrophages. AuNPs of 90 nm in size were shown to be more readily taken up by these cells compared to the smaller 15 nm particles [39]. If macrophages are unable to recognize the particles as foreign, then presence of the foreign material will persist in the body for a longer period of time.

A.1.3.3. Metal Oxides

Metal oxide nanoparticles have antioxidant and catalytic properties making them well suited for diverse biomedical applications. Cerium dioxide (CeO_2) has been shown to have anti-inflammatory properties and significant redox capabilities. This is primarily due to a lattice structure that allows oxygen mobility and numerous active spots within the structure for redox reactions and scavenging [40]. The antibacterial capabilities of metal oxides such as magnesium oxide (MgO) nanoparticles have also been explored. For example, dental restorative cement enhanced with MgO nanoparticles shows resistance to *streptococcus mutans* and *streptococcus sobrinus* when mixed with commonly utilized glass ionomer cement [41]. Other metal oxides such as zinc oxide (ZnO) have been explored for drug delivery and anticancer drugs. ZnO nanoparticles were shown to cause

histone modification in bladder cancer cells, resulting in reduced cancer cell proliferation and migration via an epigenetic mechanism [42]. These inorganic nanoparticles have become a valuable material within the health care and consumer industries due to their intrinsic properties and versatility.

A.2. Nano-Titanium Dioxide. The primary nanomaterial of focus in this dissertation is nano-TiO_2. TiO_2 has a white pigment with a high refractive index and is used in many paints, inks, cosmetics and even toothpastes. Nano-TiO_2 is found in many cosmetics and sunscreens due to its ability to protect against UV radiation through light scattering and absorption, resulting in decreased risk for skin cancer [43]. Additionally, nano-TiO_2 has been utilized for its photocatalytic and antibacterial properties. The catalytic properties of these nanomaterials allow them to be used in water treatment [44] as well as to be embedded into textiles for self-cleaning capabilities [45]. Nano-TiO_2 has also been utilized in many medical implant devices, including those used in hip and knee replacements [46]. Given its versatility and stability, it is of no surprise that humans are at an increased risk of coming into contact with these nanoparticles and while the benefits of these materials are apparent, little is known about the potentially harmful consequences of exposure. Currently, titanium dioxide is classified as a group 2B carcinogen by the International Agency for Research on Cancer (IARC), identifying the compound as a possible carcinogen to humans [47]. Given this, it is of particular importance to examine the consequences of exposure.

A.3. Lifecycle of advanced materials. Advanced materials incorporate nanoparticles to improve specific features of a product. With the increase in use of these products comes the increased probability of human contact and the potential to experience adverse

reactions. The simplified lifecycle of ENM has four steps to consider when assessing exposure and contact: the collection/processing of the raw materials, the manufacturing of the advanced material, the use of the advanced material, and the destruction, recycling or disposal of the advanced material/ENM [48]. At each step, differing exposure levels and routes of exposure need to be taken into consideration when assessing risk.

Occupational exposures are of great concern during the first two steps of the advanced material lifecycle, including the creation of ENM and the manufacturing of the advanced material. The research in this dissertation focuses on these steps of the advanced material timeline. Routes of exposure to personnel include inhalation, dermal, and inadvertent ingestion due to surface transfer, airborne particles and lung clearance [49]. Inhalation remains the primary route of ENM exposure [50]. Given the size and aerodynamic properties of nanoparticles, inhalational exposure in particular is of great concern, as particle within the nano size range have the ability to deposit within the entire respiratory tract as well have a higher deposition fraction within the terminal alveoli compared to fine particulate matter [51]. This allows particles to embed deep within the lung where gas exchange occurs.

Concerns over consumer exposure should also be taken into consideration with the finished product. This is of particular concern when products are being used for drug delivery, biological imaging, or medical implants—as exposure to the body is due to direct injection, ingestion, topical application, or inhalation. Accidental exposure may also take place with products such as surface coatings, plastics or textiles impregnated with these nanomaterials and should also be considered when assessing risk.

Finally, given the potential biopersistence of these particles, the inevitable breakdown of the product should be of concern to consumers, as well as to the occupational workers who may destroy/recycle these products. When considering the impact that these advanced materials and ENM have as a whole it becomes apparent that there may not only be beneficial outcomes, but also the potential for unintended harmful side effects as toxicity is determined by exposure and dose of the toxin. With increased exposure comes the distinct possibility of an increase in toxicologic effects that need to be explored, especially as the field of nanotechnology continues to evolve and diversify.

B. Pregnancy and Toxicology

B.1. Critical development during pregnancy in humans and rats. Pregnancy in humans is divided into trimesters, which represent distinct time-periods of anatomical change and fetal development. In humans, gestation lasts 10 months, encompassing the time from conception and implantation to parturition. In rats, gestation only lasts 21-23 days [52], but the similarities to humans during fetal and placental development make rats a useful model for assessing toxicant exposure. When assessing consequences of exposure during distinct periods of development, rat gestation can be broken into early, mid and late time points of pregnancy, akin to human trimesters and representing embryonic growth, fetal development and fetal growth, respectively [53]. The information from this section is graphically displayed within Fig. 1.

B.1.1. First Trimester

The first trimester in humans lasts from 0 to 13 weeks. During this time a myriad of critical developments take place. By day 5 post-fertilization blastocyst formation has occurred

followed by implantation within the endometrium on gestational day (GD) 7. The yolk sac undergoes its formation from GD 7 through GD 16 [54] and helps to support embryogenesis before placental development. The primary yolk sac forms prior to blastocyst implantation and then is replaced by the secondary yolk sac. The secondary yolk sac is the first site of hematopoiesis and blood island formation [55]. Additionally, the yolk sac supplies nutrients and supports gas exchange to the embryo through maternal gland secretions until the formation of the placenta [56], which begins to develop around week 4. The embryo is supported by the yolk sac until the end of the first trimester, after which it disappears and the definitive placenta is fully formed [57]. Additionally, maternal spiral artery remodeling occurs within the uterus during the first 22 weeks of pregnancy. The uterine tissue prepares for trophoblast invasion with the formation of the decidua and initiation of spiral artery remodeling by uterine natural killer cells (uNK). uNK aid in spiral artery remodeling through the secretion of angiogenic factors such as interferon gamma (IFN-ɣ), vascular endothelial growth factor (VEGF), angiopoietin (ang)-1 and ang-2 [58]. By week 8 extravillous trophoblast cells begin to invade into the spiral arteries causing vascular enlargement [59] as well as endothelial cell loss and fibrinoid necrosis, which decreases vasoconstrictor responses as well as decreases basal vascular resistance [60, 61]. Collectively, this permits for an increase in blood flow to the developing placenta and fetus. By about week 8 the embryo is considered a fetus, with major organ systems now formed, but still immature. In rats, implantation occurs on GD 5 and, similarly to humans, the formation of the visceral yolk sac allows for hematopoiesis. Blood islands, structures around the embryo that eventually form the circulatory system, begin to form and give rise to angioblasts, with vasculogenesis beginning by GD 10 [62, 63]. The visceral yolk

sac continues to grow and provides metabolic, endocrine and hematopoietic functions to the placenta proper until just prior to parturition [64]. Uterine spiral artery remodeling begins for rats on GD 6.5-9.5, and is similarly driven by the action of natural killer cells and followed by endovascular invasive trophoblast cells, causing alterations within the spiral arteries at GD 11.5 that persists into late pregnancy [65].

B.1.2. Second Trimester

The second trimester in humans occurs between weeks 14-26 of gestation. As mentioned above, all the organ systems are present, but are immature or not currently depended upon. By week 20-24 the ability to secrete surfactant is gained, allowing for inflation of the lungs [66]. Hippocampal formation also begins early in the second trimester and is essential for memory and cognition [67]. By weeks 18-20 the placenta is fully formed but continues to grow during gestation. The human placenta is discoid in shape and classified as chorioallantoic. This placenta is formed from the trophectoderm of the embryo, which differentiate into trophoblast giant cells and spongiotrophoblasts. This placenta is additionally classified as hemochorial, where the maternal blood is in direct contract with the fetal chorionic villi [68]. The human and rodent placenta are very similar in their classification. Rat placenta is completely developed by GD 11.5 [69] and is also discoid and hemochorial.

The structure of human and rat placentas are somewhat different, but generally analogous with one another. The first layer of the placenta is the decidua, which is considered to be the maternal compartment. This membrane is important as a nutrient source (glycogen and lipid storage) as well as the production of prolactin and prostaglandins [70] and insulin-like growth factor protein in humans [71]. The decidua is

also critical for protection against heavy metal toxicity and oxidative stress as it has metallothioneins which are present beginning at GD 9 in rodents [57, 72]. Metallothioneins can bind heavy metals intracellularly as well as harmful oxidant radicals through their cysteine residues [73]. The subsequent layer is the basal plate in humans and the junctional zone (or basal zone) in rats. This zone is comprised of trophoblast giant cells, glycogen cells (for glycogen storage, which begin to appear around GD 12 in rodents) and spongiotrophoblast cells. This section of the placenta plays a critical role in the production and secretion of steroid hormones such as progesterone (P4) and testosterone. Spongiotrophoblast cells are also believed to secrete hormones important for placental development and maintenance, such as insulin-like growth factor [74]. The third layer of the placenta is the fetal-placental interface. In humans, this is called the placental villi and in rats, the labyrinth zone. This is the section of the placenta that is directly attached to the umbilical cord, contains fetal capillaries, and is the location where materno-fetal nutrient and waste exchange occurs. In rats, the labyrinth zone reaches peak proliferation by GD 13 and slowly decreases in cellular proliferation towards the end of pregnancy [57].

A key difference between the human and rat placenta is the steroid hormone biosynthetic capabilities of these organs. Human placentas contain P450scc and 3β-HSD and can synthesize P4 and pregnenolone from cholesterol. However, they lack cytochrome p450c17 (CYP17) and, as a result, are unable to synthesize dehydroepiandrosterone (DHEA). The fetal adrenal gland contains CYP17, so this tissue can synthesize DHEA, which is subsequently converted by the placenta to estriol (E_3). During human gestation, the placenta is the primary source of E_3 production. In contrast, CYP17 is present within

the rat placenta, allowing for the direct production of androgen by the placenta. However, it lacks the aromatase enzyme [75] and, thus, estradiol (E_2) is not produced from the rat placenta. Instead, the main source of E_2 during gestation in the rat is the ovaries [76].

B.1.3. Third Trimester

The third trimester in humans occurs between gestational weeks 27-40 and is when the most rapid fetal growth occurs. All of the foundational systems and organs have been developed and are now increasing in size. The placenta will continue to grow until parturition in humans and in rats. The junctional zone reaches full maturity within rat placentas at GD 15, and then begins to decrease in size [57], which correlates with decreased levels of P4 towards the end of pregnancy. Alternatively, the labyrinth zone continues to grow and becomes the largest component of the fetal placenta [57].

B.2. Toxicant exposure during pregnancy. Given the variety and number of crucial events that must take place within each trimester of pregnancy, it is not surprising that toxicant exposure during specific key windows of gestation may result in varied fetal outcomes. Depending on the toxicant, toxicant dose, and exposure route, maternal and fetal consequences may arise from exposure during specific critical windows of development. The first trimester encompasses embryonic development while the second and third trimester contains fetal development and growth. Development encompasses a process in which cellular organisms become more complex and organs become functional whereas growth means size and mass will increase overtime [77]. Determination of such critical windows for various toxicants is of utmost importance for risk assessments in regard to pregnant women and their offspring.

B.2.1. Early Stage

The first trimester in humans can be the most crucial for fetal survival and health, as this is when 80% of miscarriages occur [78]. This is an important time period as the fetus begins to develop organs and lays the foundation for systems critical for survival. Maternal toxicant exposure within early gestation has been shown to cause detrimental effects to placental function, fetal health and even motor and cognition of offspring, as detailed in the following paragraphs.

Implantation, an initial and crucial step for embryonic survival, has been shown to be affected by early gestational exposure to toxicants [79-81]. Arecoline alkaloid, an addictive substance found in areca nuts and utilized in Eastern countries, was shown to alter reproductive outcomes in mice following ingestion over 3 days starting day 4.5 post-coitus. Blastocysts were collected on post-coitus day 4.5 and were cultured to assess growth with various doses of arecoline at 24, 48 and 72 hours after culture. The authors reported significant decreases in blastocyst size and trophoblast outgrowth at all time-points [79]. Additionally, pregnant mice in that study were fed arecoline and embryo attachment was assessed at 7.5 days post-coitus. The number of implanted embryos was significantly decreased in the highest dose group (2.40 ± 5.37 embryos) compared to controls (11.25 ± 0.96 embryos) [79]. The mechanism of action is undetermined at this time, but is believed to be related to inducing the phosphorylation of ATM kinase, thereby leading to p53 phosphorylation and cell cycle arrest [82]. Another example of how toxicants can negatively impact implantation and uterine receptivity are endocrine disruptors (ED) [80]. Bisphenol A (BPA), an industrial chemical used to manufacture plastics since the 1950's, is one such ED that has received extensive study. In one such

study, pregnancy mice were injected subcutaneously once per day with BPA from GD 0.5 to 3.5 and blastocyst implantation was assessed on GD 5.5. The authors reported that exposure resulted in significantly reduced implantation site growth and size [81].

Exposure to heavy metals, such as nickel, during early gestation has also been shown to negatively impact reproduction. Nickel is an industrial pollutant that has been shown to cause embryotoxicity. In a study from 1981, female mice were injected with a single intraperitoneal injection of $NiCl_2$ at GD 1, 2, 3, 4, 5 or 6 and were euthanized at GD 19 for assessment. The number of implantation sites were significantly lower in the GD 1 group with 10.8 ± 0.51 pups per litter compared to 12.0 ± 0.42 in the controls [83]. While litter size was only minimally reduced, the GD 1 group showed the largest number of abnormal fetuses with conditions such as hematomas, exencephaly, anemic phenotype and hypodevelopment, suggesting that GD 1 exposure is a sensitive period for nickel exposure [83]. $NiCl_2$ has been shown to have accumulate in embryos during early gestational exposure, suggesting a direct effect of the heavy metal on the embryos themselves [84].

Zinc oxide nanoparticles (ZnO NPs) are an example of a commonly utilized advanced material for which humans are at an increased risk of exposure. In a study from 2021, mice were administered various doses of ZnO NPs by oral gavage from GD 3.5 to 9.5 and were euthanized for assessment of reproductive endpoints on GD 10.5 [85]. The nanoparticles translocated to the uterus and uterine atrophy was noted during histopathological examination. The authors suggest that translocation of these nanoparticles resulted in increased reactive oxygen species (ROS) production, leading to oxidative stress and induction of apoptosis. Additionally, an increased abortion rate

(66.67%) was reported as well as decreased fetal weight within the highest dose group (0.039 ± 0.002 g/pup) compared to the control fetuses (0.051 ± 0.004 g/pup) [85]. AuNPs also caused similar results in pregnant mice injected for 3 days during early pregnancy (starting at embryonic day 5.5) compared to late pregnancy exposure (starting at embryonic day 11.5). Early exposure groups showed a 53.5% abortion rate with evidence of AuNPs reaching the fetal tissues, raising the possibility of a direct effect. The authors reported that these nanoparticles tend to form aggregates and due to the fewer number of cells present within the embryo during early gestation compared to late gestation, the nanoparticle aggregates may have a more serious impact on the earlier embryo than what would be seen in more mature fetuses [86]. Nano-TiO_2 has also been shown to alter fetal umbilical vascular responses, even with only a single day exposure on GD 4 in rats. Umbilical veins were shown to have a reduced response to endothelium-dependent and independent vasodilation at GD 20 [10]. Inhalation exposure to nano-TiO_2 has been shown to cause immunological responses arising from the lungs that may contribute to this dysfunction [6], but there may also be direct effects, as nano-TiO_2 is capable of translocating to the placenta [87]. This reflects how a toxicological insult in early pregnancy could translate to lasting consequences throughout gestation.

One toxicant shown to have effects post-partum following early gestational exposure is phthalate. Phthalate is an unstable plasticizing agent which can easily transfer to food and has been used as an additive in advanced materials [88, 89]. Phthalates are known to be linked to endocrine disruption and neurodevelopmental disorders, but not until 2020 were the in-utero effects of exposure occurring specifically during early gestation assessed. The authors examined neurodevelopmental function in children at 4 years of

age following gestational exposure and found that motor and cognition scores were significantly decreased in offspring exposed to phthalates early in pregnancy compared to the control group. One potential mechanism of action is believed to be neuronal degeneration due to hypoactivity of sodium/potassium-ATPase, which has been shown to effect structures such as the hippocampus. This is due to the region's rapid changes in structure and plasticity during development [90]. Additionally, males were more adversely affected than females, underscoring the sex-dependent effects of some toxicants following exposure [91].

B.2.2. Mid Stage

Exposures during mid gestation also yield reproductive consequences as maternal vascular and placental dysfunction have been reported after exposure during this period. In 2021 it was demonstrated that pregnant rats inhaling ozone (O_3) on GD 10 showed increased uterine artery resistance as assessed by echocardiographic measurements [92]. Normally, resistance within the uterine artery decreases from GD 8 to GD 20, and this is reflected in their data. This decrease though is significantly ameliorated with exposure on GD 10, as indicated by the reduced decrease in the uterine artery resistance index, which could lead to decreased blood flow to the fetus [92]. Additionally, expression of several placental mRNA were altered in a manner similar to that seen in preeclamptic patients. MMP10 was significantly decreased while Cd36 and Fzd1 were increased, suggesting not only negative impact on uterine vasculature, but potentially the placenta as well [92]. The alterations seen in this study show how exposure may lead to issues like preeclampsia, which have a genesis earlier in pregnancy, but do not become pronounced until late pregnancy.

Effects on placental development and function are also important to consider following exposure due to its critical role in pregnancy. The labyrinth zone is a major part of mid gestational function and an often examined toxicological target site [57]. Diethylstilbestrol (DES) is a synthetic estrogen that was once prescribed to aid in preventing miscarriages. Kagawa et al. examined how pregnant mice orally exposed to DES from early- to mid-gestation (GD 4-8) exhibited altered placentogenesis and fetal survival [93]. Exposure resulted in a 70.8% mortality rate compared to 1.9% in the control group and DES significantly decreased embryo size as well. Additionally, the placenta showed a significantly thinner labyrinth zone and therefore a decrease in glucose transport protein-1 (GLUT-1), expression of which is typically highly upregulated during early pregnancy. Not surprisingly then, further evidence suggested that this affected glucose transport, as fetal blood glucose levels were significantly decreased [93]. The authors suggested that exposure during mid-gestation may alter placental anatomy and thereby physiology, resulting in poor nutrient delivery and lower fetal survival.

Exposure during mid-gestation also results in detrimental effects on offspring postnatally, such as in their neuronal development. Wang et al. investigated how sevoflurane, a commonly used maternal anesthetic during the second trimester, may affect postnatal cognitive function and critical fetal hippocampal development during this gestational window. At GD 14, pregnant rats were placed under a low or high level of sevoflurane anesthesia for 2 hours. At post-natal day 28, behavioral analyses were conducted using the Morris Water Maze, a navigation test and a spatial navigation test. The high dose group showed an increase in path length and escape latency time during the navigation test as well as a decrease in spatial exploration [94]. The high level of anesthesia led to

offspring with significant learning and memory impairments following only a single exposure within the second trimester. Alterations in rat behavior and cognition due to nano-TiO_2 inhalation has also been reported for male offspring of mid- to late-gestationally exposed dams. Male offspring were subjected to behavioral tests once adulthood was reached (20 ± 1 weeks) and displayed impairment of short-term memory compared to the control group. Latency time to finding a visible platform was also increased through the first three trials, but not the fourth trial, which indicated that locomotor or visual differences were not present, but instead that motivation differences between groups were the more likely explanation [95]. Nano-TiO_2 gestational exposure has been shown to result in cerebral cortex damage within offspring [96], which could be due to the ability for these particles to translocate to the fetal brain [87]. These studies reflect how exposure during mid-gestation can lead to altered behavioral outcomes in adulthood, highlighting the importance of mid-gestational development as a critical period in which toxicant exposure can have negative health outcomes.

B.2.3. Late Stage

Late gestational toxicant exposure can also lead to detrimental fetal and reproductive effects. The ED, cadmium, is a bio persistent environmental pollutant that has been shown to disrupt endocrine steroidogenesis. In a study from 2020 pregnant mice were exposed to cadmium containing drinking water at either early (GD 0-6), mid (GD 7-12) or late gestation (GD 13-17). Fetal mass, length, and % rate of fetal growth restriction was significantly affected within the late exposure group, leading to smaller pups and an increased rate of fetal growth restriction. Liver, lung, and brain development were also shown to only be impaired, when assessed relative to body weight, within the late

exposure group. The low passage of cadmium (<0.1%) from maternal circulation to the fetus suggest that growth restriction cannot be fully related to direct effects on the fetus [97]. Placental structure and P4 synthesis were also assessed and placentas exposed in late gestation showed a decrease in blood sinusoid and blood vessel area within the labyrinth zone as well as a decrease in placental P4 and proteins/enzymes involved in the P4 biosynthetic pathway [98]. This highlights the possibility that exposure, even within the final stages of pregnancy, can cause reproductive effects such altered placental biosynthesis of P4, which is critical for placental development and fetal survival. This may then lead to poor placental vascularization, and therefore fetal growth restriction.

Another ED previously discussed, BPA, was examined during early (GD 5.5-12.5) and late (GD 11.5-18.5) gestation in mice [99]. Mice were exposed daily through oral gavage and then anxiety-like behavior was assessed in the offspring through an elevated plus maze test on postnatal week 10. Female offspring from the late-exposed BPA group, but not the early-exposed group, showed a decrease in total distance moved, time spent in open arms of the maze, and number of entries made into open arms of the maze, reflecting heighted anxiogenic behavior [99]. These data reflect how late gestational exposure during a critical window of development may influence progeny behavior into adulthood.

C. The Virgin and Pregnant Microcirculation

C.1. The importance of the microcirculation. The microcirculation is composed of a network of microvessels that allows for the delivery of nutrients and waste exchange at target tissues, controls blood flow within the circulation and plays an important role in the immune response. The microvascular network begins with arterioles that branch from

resistance arteries within the vascular bed. Arterioles are small reactive vessels that respond to metabolic demands of the terminal tissue and hemodynamic influences of the cardiovascular system. The arterioles then lead into the capillary bed where the nutrient and oxygen exchange occur. Lymphatics, which originate at the capillary level, are also part of the microcirculation wherein extravascular fluid is carried to the venous system. Finally, after the capillaries, venules lead to larger veins carrying deoxygenated blood back to the heart. Additionally, venules play an important role in host responses [100]. The cardiovascular system is entirely lined with endothelial cells, which come into direct contact with blood. The arterioles also contain a layer of smooth muscle cells, which allow for resistance control and optimized nutrient/waste exchange.

The microcirculation is also crucial for an immune response. Post capillary venules are the site at which leukocyte rolling takes place, as the endothelial cells within this portion of the microcirculation have a higher expression of adhesion molecules, and there is slow fluid velocity and increased permeability. Endothelial cells will upregulate adhesion proteins to allow for leukocyte attachments at sites of inflammation [100]. Before leukocyte attachment, endothelial cells must become activated. Cytokines indicating inflammation or damage (TNF-α, lL-1β), ROS or LPS are some examples of signals that will result in endothelial activation and the presentation of adhesion molecules. Chemokines within the circulation can cause endothelial cell contraction, resulting in increased vascular permeability. With inflammatory stimulation the endothelial cells will begin to express adhesion molecules such as P-selectin and E-selectin, resulting in leukocyte capture and rolling along the endothelial surface. ICAM-1 and VCAM-1 allow for further slow rolling and arrest followed by firm adhesion of the leukocytes [100, 101].

The process then leads to transendothelial migration into the tissue [101]. This ability of the endothelial cells to cause leukocyte adhesion allows for transmigration of the leukocytes into the tissue at the sight of damage.

Microvascular endothelial cells respond to mediators of arteriolar tone by responding to shear stress within the microcirculation. Shear stress is the force exerted on blood vessel walls due to the flow of blood, which can be estimated using Poiseulle's law, where increased blood viscosity and flow rate can cause an increase in shear stress [102]. An increase in radius of the blood vessel, on the other hand, will cause a decrease in shear stress. Therefore, through mechanotransduction, an increase in shear stress stimulates the endothelial cells to respond by opening non-specific cation channels, resulting in increasing intracellular calcium, leading to production of nitric oxide (NO) and prostacyclin (PGI_2) that will cause smooth muscle vasodilation and increase the radius of the arterioles [103]. Additionally, the arterioles may respond to increased pressure within the vessel. The arterioles are the site whereby the body controls vascular peripheral resistance. Once the blood enters the arterioles, blood pressure drops, thus protecting downstream terminal tissues and allowing for proper nutrient exchange to occur in the capillaries. One example of autoregulation within the arterioles to respond to their environment is called the myogenic response. Transmural pressure within the blood vessels is the differences between intra- and extraluminal pressure. When there is an increase in transluminal pressure, vessel wall tension will increase and vascular smooth muscle cells will experience stretch. This mechanical stimulation will lead to depolarization of the smooth muscle cells and activate voltage gated calcium channels, initiating vasoconstriction [104]. As another level of control, the microcirculation also responds to metabolic

demands (oxygen and pH) as well as circulatory factors (ACh, bradykinin, norepinephrine, etc.). These circulating factors have the ability to compete with the autoregulatory tone that resides within the arterioles [105]. In doing so, and through autoregulation via myogenic responses and shear stress, the vessel will become smaller and will decrease downstream blood pressure, regulating blood flow to downstream organs.

C.2. The Uterine Microcirculation. Pregnancy is a period of time in which cardiovascular alterations, specifically microvascular growth and adaption, are unmatched. Over a time period of 9 months in humans, or 21 days in rats, incredible developments and adjustments must take place to allow for both maternal and fetal survival. If the microcirculation is unable to adjust if dysfunction occurs, then the results could lead to health complications or even death. The primary site of microvascular adaptation occurs within the uterine circulation to allow for proper delivery of nutrients to the placenta and growing fetus. To understand the alterations during pregnancy within this vascular bed, we must first consider the virgin uterine microcirculation.

C.2.1. Virgin Uterus

The rat reproductive system consists of two ovaries and two uterine horns that receive blood flow from the branching of the left and right internal iliac arteries into the respective uterine arteries. Additionally, blood flow also is received from the ovarian arteries that branch from the abdominal aorta; this results in bidirectional blood flow through the uterine arteries [106, 107]. Branching from the uterine arteries is a network of arteries and arterioles that decrease in size and arcuate arteries that form an arcading network within the myometrium. These further branch into radial arteries and then basal and spiral arterioles that infiltrate deep into the endometrium. Here, the capillaries exchange

nutrients and waste within the uterus and blood is carried into venules and veins that match flow with the arterial network. The uterine and ovarian veins then carry deoxygenated blood to the inferior vena cava and back to the heart [106]. This vascular network supports the virgin uterus, but once conception occurs, there are many adaptations that must occur to ensure optimal maternal and fetal health.

C.2.2. Pregnant Uterus

During pregnancy, blood volume increases by approximately 45% with cardiac output and heart rate increasing throughout pregnancy [108]. Given this, one may expect blood pressure to increase. While this does occur in pathological conditions, such as preeclampsia or gestational hypertension, that is not the case in a healthy pregnancy. During normal gestation, blood pressure in the first and second trimester are lower than nonpregnant blood pressure measurements and will then increase to nonpregnant levels during the final trimester [108]. This is due to a decrease in systemic vascular resistance, including the microcirculation, as well as physiological remodeling within the maternal circulation. While arteriolar tone decreases during pregnancy, venous tone via sympathetic outflow will increase, resulting in distribution of blood within the systemic circuit and into the placenta [109]. These adaptations are essential to allow for increased blood volume and blood flow to the uterus, placenta, and fetus.

Pressor responsiveness in pregnant rats was shown to be markedly decreased to angiotensin II (Ang II), norepinephrine (NE) and vasopressin compared to nonpregnant rats [110]. If the sensitivity to the Ang II pressor response is not reduced during pregnancy, gestational hypertension may occur [111]. This highlights the importance of a decrease in sensitivity to Ang II during pregnancy. Through this decrease in pressor

response the body is able to adequately handle the increased blood volume and cardiac output, which is essential for proper perfusion of the uterus.

In addition to the changes described above, anatomical adaptations such as angiogenesis, the growth of existing vessels, and neovascularization (the growth of new vessels), take place to achieve decreased uterine vascular resistance. Passive diameter of blood vessels within the uterine circulation approximately doubles in size during pregnancy in both humans and rats and experiences outward hypertrophic growth, with little wall growth into the lumen [107]. Both arteries and veins experience this outward growth, and this change seems to initiate in smaller vessels before expanding to the uterine artery and vein. Elongation of the blood vessels is also reported with arcuate arteries in rats increasing in length by approximately 20% [112]. Spiral arterioles within the uterus will also begin to widen in diameter and lose contractile functionality as endovascular trophoblasts invade the vessels and destroy vascular smooth muscle [61, 113]. Along with elongation and outward hypertrophic growth, branching and neovascularization can also occur. By increasing the branching complexity of the vascular bed, peripheral resistance decreases, thereby increasing blood flow and perfusion of the uterus, placenta and fetus.

There are several factors that encourage the growth and adaptation of the vascular network including hormones, NO, shear stress, vascular mediators, and the renin-angiotensin-aldosterone system (RAAS), which will be covered in detail in the following section. Studies have shown that E_2 can enhance the vascular endothelial growth factor (VEGF) vasodilatory response and secretion of NO [114]. VEGF is a major angiogenic factor responsible for endothelial proliferation and vasodilation that is directly stimulated

by E_2 [115]. E_2 has also been implicated in the process of endovascular trophoblast invasion [116]. Shear stress is another plausible mechanism for inducing alterations in the vasculature. Placentation and spiral artery widening should cause a decrease in downstream resistance, causing an increase in shear stress and flow velocity in upstream vessels [117]. The subsequent outward growth of these upstream vessels would then result in normalization of the shear stress. Through a multitude of mediators, vascular growth and adaptation occur to support the increased blood volume and increased blood flow necessary for fetal survival and maternal health.

D. The Renin-Angiotensin-Aldosterone System

D.1. Overview. The renin-angiotensin-aldosterone system (RAAS) is a multi-organ signaling cascade mainly known for its important role in renal regulation of blood pressure and electrolyte/fluid balance. The first enzyme released in the cascade is renin from the kidney. This is released from the juxtaglomerular cells when the macula densa within the kidney sense a decrease in flow rate or a decrease in sodium chloride (NaCl), which may be due to a drop in blood pressure and/or loss of blood volume. Renin then cleaves the peptide angiotensinogen, which is released from the liver, into angiotensin I (Ang I). Ang I can then be converted by angiotensin converting enzyme (ACE) into angiotensin II (Ang II) [118]. ACE is canonically found within the lungs and renal endothelium [119], but is also found locally in blood vessel endothelium [120] as well as within placental tissue [121]. Ang II is the main bioactive peptide hormone and is known to have many roles in the regulation of blood pressure and blood flow. Ang II causes an increase in peripheral resistance through arteriolar vasoconstriction, stimulates an increase in sodium and water retention in the kidneys, as well as promotes sympathetic outflow, all of which result in

increased blood volume, resistance and blood pressure. Furthermore, Ang II stimulates the release of aldosterone from the adrenal gland, further causing sodium and water reabsorption and potassium excretion through the insertion of additional sodium-potassium ATPase exchangers and sodium channels in the kidneys [118] . Ang II also causes the release of anti-diuretic hormone (ADH) from the posterior pituitary gland. This hormone stimulates water reabsorption within the kidneys via upregulating aquaporin channels within the collecting duct as well as increasing thirst. Once water and electrolyte retention effectively increase, causing an increase in circulating blood volume, then juxtaglomerular apparatus perfusion in the kidney will increase, and renin release from the kidneys will decrease.

D.2. Angiotensin receptors and function. Ang II mainly exerts its vasoconstrictive effects through angiotensin type I receptor (AT_1R). Within vascular smooth muscle, Ang II binds to AT_1R and intracellular signaling is linked to both G protein-dependent and -independent pathways. Activation of AT_1R coupled to Gαq results in phospholipase C (PLC) activation leading to inositol triphosphate (IP3) and diacylglycerol (DAG) formation. IP3 can then bind to its receptor on the sarcoplasmic reticulum and induce intracellular calcium release that then activates myosin light chain kinase (MLCK), resulting in smooth muscle contraction. DAG can lead to the activation of protein kinase C (PKC), producing a substrate that can directly inhibit myosin light chain phosphatase (MLCP). Similarly, the RhoA/Rho-kinase pathway is also stimulated through the activation of AT_1R leading to inhibition of MLCP activity. AT1R activation may also lead to transactivation of EGF receptors via release of soluble EGF by matrix metalloproteinases induced through PLC activation. This indirectly activates the mitogen-activated protein kinase (MAPK) pathway,

resulting in proliferation and hypertrophy of vascular smooth muscle cells [122]. AT_1R is also present on endothelial cells as well as vascular smooth muscle. AT_1R has been shown to reduce NO activity through an increase in ROS production and asymmetric dimethylarginine (ADMA) generation, which leads to eNOS inactivation. AT_1R has also been linked to endothelin-1 (ET-1) production, resulting in vasoconstriction and ACE activation as well as increased production of cyclooxygenase (COX) products such as thromboxane [123]. Therefore, stimulation of AT_1R-induced signaling results in a vasoconstrictive and proinflammatory phenotype mediated by actions within both endothelial cells and vascular smooth muscle.

Vascular dysfunction, fibrosis, and hypertension can also be exaggerated when Ang II activates NADPH oxidases via the AT_1R receptor, causing an increase in ROS production which can lead to an increase in oxidative stress and inflammatory mediators [124]. This pathway may also play a role in atherogenesis as it induces aortic smooth muscle cell migration and IL-6 release that leads to MMP-9 promotion, as ROS production via Ang II was shown to activate NF-kB [125]. Enhancement of superoxide production and other ROS production through this pathway can also lead to apoptosis by decreasing antioxidants as well as by upregulating LOX-1, which can cause a decrease in expression of anti-apoptotic proteins such as bcl-2 and NOS [126, 127]. Further, they have been shown to play a role in leukocyte capture and rolling [128]. Additionally, eNOS can be bound and inactivated within endothelial cells by endothelin-1 ET_B receptor or AT_1R, thereby decreasing NO levels. Interestingly, AT_1R has been linked to both apoptotic and antiapoptotic effects, which may be related to the state of cellular growth or vascular bed phenotype. Through activating the PI3K/AKT pathway, survivin protein and mRNA

expression was increased, resulting in antiapoptotic effects in retinal vascular endothelial cells [129]. Due to the physiological importance of the AT_1R receptor and diversity of Ang II activity, it has become a useful and highly marketed drug target.

Ang II may also act through the angiotensin type II receptor (AT_2R). AT_2R is a G protein-coupled receptor that is Gαi/Gαs. Actions through Gαi protein will result in mitogen-activated protein kinase phosphatase 1 (MKP-1) activation leading to bcl-2 inhibition inducing apoptosis [130]. Activation through the Gαs protein causes an increase in SHP-1. SHP-1 can act by inhibiting the ERK1/2 pathway, resulting in reduction of proliferation and migration [130]. While AT_1R is found extensively through the adult body, AT_2R is transiently upregulated within fetal tissue and then reduced to lower levels than AT_1R in adults [131]. Although found at lower levels in adult tissue, it does have an important role in opposing AT_1R effects and is upregulated following cardiovascular or neurological injuries, such as during myocardial infarction (MI) [132] or brain ischemia [133]. The importance of this is highlighted by the effects of AT_2R expression on infarct size and progression. AT_2R knockout mice recovering from an MI had a significantly reduced survival rate as well as greater left ventricle dilation, which may lead to congestive heart failure [134]. Additionally, AT_2R stimulation has neuroprotective effects and improves motor function following stroke induction in rats [135]. These protective effects are related to increased perfusion within blood vessels in the area of the infarct following injury.

Vasodilation following AT_2R activation is due to an increase in Na-H ion exchanger expression, resulting in an acidic intracellular environment that triggers kininogenase activity, resulting in bradykinin production [127]. Bradykinin can then bind to bradykinin B_2 receptors (B_2R) on endothelial cells, resulting in eNOS induction and increased NO

release [127]. Additionally, bradykinin can affect both the endothelial and vascular smooth muscle cells by inducing extracellular or intracellular superoxide dismutase (SOD), resulting in a reduction in superoxide and therefore increasing bioavailability of NO [127].

While Ang II is the main bioactive peptide hormone within this system, it is important to discuss the breakdown of Ang II into other functional peptides. Ang II may be cleaved by angiotensin converting enzyme 2 (ACE2) to form angiotensin (1-7) or from converting angiotensin I to angiotensin (1-9) by ACE2 and then to angiotensin (1-7) by ACE. Angiotensin (1-7) is an agonist for the Mas receptor (MasR) which opposes the canonical pathway of Ang II and AT_1R, as does the activation of AT_2R. This arm of the RAAS axis is believed to be protective, offering vasodilatory, antifibrotic and antihypertensive effects [136, 137]. MasR is a G protein-coupled receptor that acts through the phosphatidylinositol 3-kinase (PI3K)/Akt pathway to activate eNOS release of NO. MasR activation can also suppress Ang II-induced production of aldosterone by inhibiting the phosphorylation of JAK/STAT proteins within adrenal cells [138]. MasR activation via administration of recombinant hACE2 inhibits the activation of NADPH oxidase induced by Ang II, reducing super oxide production [139]. Due to these combined effects, it has been investigated as a potential therapeutic pathway to attenuate hypertension.

Finally, Ang II can be converted into angiotensin III (2-8) via aminopeptidase A and subsequently angiotensin IV (3-8) via aminopeptidase N. Angiotensin IV can bind to angiotensin receptor type IV (AT_4R), also known as insulin-regulated membrane aminopeptidase (IRAP). These receptors are found in a wide variety of tissues, including the brain, lung, heart, kidney, adrenal glands, and vasculature. Work examining AT_4R binding has focused on the role of the receptor in memory retention and improved learning

[140]. For example, angiotensin IV is a potential target for treating Alzheimer's disease. It has been implicated in mediating cognition, memory and the anti-inflammatory effects of Losartan, a commonly administered AT_1R antagonist for hypertension treatment that has shown promise for delaying Alzheimer's disease progression [141]. Given that IRAP is an enzyme known to break down peptide hormones such as vasopressin, oxytocin and somatostatin, a potential role of Angiotensin IV may be to bind to and inhibit IRAP and allow for increased half-life of these peptides within the circulation [142]. Vasopressin, oxytocin and somatostatin have all been implicated in improving cognition, and thus may represent the mechanism by which Angiotensin IV has its effects [143]. When it comes to roles of Angiotensin IV in the microcirculation, AT_4R activation has been linked to an increase in intracellular calcium release and increased eNOS activity in endothelial cells [144], but has also been shown to be a weak AT_1R agonist, resulting in vasoconstriction in some vascular beds [145].

D.3. Angiotensin II and Pregnancy

As mentioned above, blood volume must increase during pregnancy to support the increased need for nutrient and oxygen in the uterus and placenta, which would mean a requisite induction of RAAS. Simultaneously though, peripheral resistance must decrease to allow for proper perfusion of the placenta. As Ang II is a robust vasoconstrictor, this would seemingly contradict the imposition of reduced peripheral resistance, but during a healthy pregnancy, adaptations take place to alter sensitivity to Ang II. In a normotensive pregnancy, almost all components of RAAS are increased to support an increase in blood volume, with the exception of ACE expression. Additionally, Ang II activity and AT_1R sensitivity is decreased and ACE2 activity and Angiotensin (1-7) circulating levels are

increased [146, 147]. Sensitivity of AT_1R is thought to be decreased in part due to inactivation by ROS, which would be increased in normal or pathological pregnancy. Abdalla et. al demonstrated that during a normal pregnancy AT_1R tends to exist in monomeric states and hydrogen peroxide tends to cause an aggregation of these receptors that leads to deactivation [148]. Additionally, the Angiotensin (1-7) component is thought to further counterbalance Ang II through its antiangiogenic, antimitotic and vasodilatory properties. The importance of RAAS is underscored by the fact that local components of this system are found within the uterus as well as the placenta.

Along with the direct contributions of angiotensin (1-7) to decrease peripheral resistance, it has also been shown to increase vasodilation by inducing prostacyclin release through the COX pathway present within the endothelium [149]. In the endothelium, arachidonic acid is converted to prostaglandin H2 via COX-1 and then to prostacyclin via prostacyclin synthase. Prostacyclin will then increase cAMP via adenylate cyclase, which inhibits myosin light chain kinase within smooth muscle, resulting in vasodilation [150]. Additionally, increased P4 levels, which occur throughout pregnancy, have been shown to inhibit adrenergic agonist-induced vasoconstriction [146, 151]. While not directly affecting RAAS, this would reduce overall maternal peripheral resistance. Additionally, estradiol, which also increases during pregnancy, has been shown to contribute to increased expression of AT_2R. Mishra et. al demonstrated that estradiol affects protein levels of AT_2R, but not AT_1R, which results in decreased vasoconstriction within the uterine arteries of pregnant rats [152]. This demonstrates that hormones such as P4 and estradiol may significantly influence RAAS and maternal hemodynamics as a whole. RAAS is a complicated and intricate system that must be altered appropriately during

pregnancy. If these adaptations do not occur, then this may lead to a gestational complications and even maternal and fetal morbidity or mortality.

D.4. Angiotensin II and Preeclampsia

Preeclampsia affects 4.6% pregnancies per year and is a major cause of maternal and fetal morbidity and mortality [153]. While the exact mechanism underlying preeclampsia remains poorly understood, the diagnosis is determined by the presence of hypertension and proteinuria after 20 weeks of pregnancy. In a preeclamptic pregnancy, many components of the RAAS system are improperly altered. Angiotensinogen and renin activity is decreased, meaning blood volume levels will be decreased compared to a healthy pregnancy. Furthermore, while circulating levels of Ang II are decreased, the sensitivity of the AT_1R is actually increased [146]. To further support vasoconstriction, ACE2 activity is decreased, therefore reducing circulating Angiotensin (1-7) [146], which normally would promote vasodilation. These changes thereby result in an even greater reduction in blood flow, which contributes to a hostile gestational environment.

One mechanism that contributes to increased sensitivity to AT_1R-mediated vasoconstriction may be influenced by receptor dimerization. As mentioned earlier, in a healthy pregnancy monomeric AT_1R are inactivated via ROS, but during preeclampsia there is an increase in AT_1R forming heterodimers with B_2R. Abdalla et. al demonstrated that these heterodimers not only show resistance to hydrogen peroxide deactivation, but exhibit enhanced Ang II-mediated signaling, which could contribute to the heightened AT_1R sensitivity seen in preeclamptic patients [148]. Placental chorionic villi from pathological pregnancies show an increase in Ang II/AT_1R expression, but a decrease in the angiotensin (1-7)/MasR arm of the RAAS system, which may further contribute to the

pathology of preeclampsia [154]. Additionally, decreased circulating levels of estradiol have been reported in preeclamptic pregnancies [155]. If estradiol affects AT_2R density, this may lead to a decrease in vasodilatory Ang II receptors within the uterine circulation. Furthermore, estradiol was shown to have a direct effect on VEGF gene transcription within the endometrium [156]. Given the decrease in circulating levels of estradiol that occur during preeclampsia, the resultant decrease in circulating VEGF would be expected to impair angiogenesis and result in decreased perfusion.

Another mechanism that is believed to play a role in the pathology of preeclampsia is reduced trophoblast invasion and spiral artery remodeling. For example, the presence of active AT_1R has been shown to play a key role in regulating genes essential for a healthy pregnancy. Placental trophoblast cells express an abundance of AT_1R that have been linked to regulation of genes responsible for angiogenesis and invasion including soluble fms-like tyrosine receptor-1 (sFLT-1) and plasminogen activator inhibitor-1 (PAI-1) [157]. PAI-1 is an inhibitor of plasminogen activator that is mainly responsible for the suppression of the fibrinolytic system during pregnancy. PAI-1 has a direct effect on endovascular trophoblast cells by limiting trophoblast invasion and decreasing extracellular matrix degradation [158]. sFLT-1 is a circulating antagonist to VEGF and placental growth factor, which reduces angiogenesis. Zhou et. al demonstrated that sFLT-1 levels increase in a dose dependent manner to Ang II within trophoblast cells *in vitro*. This resulted in poor cell migration and tube formation, suggesting that AT_1R activation influences angiogenesis in preeclampsia [159]. Inhibiting angiogenesis, remodeling and trophoblast invasion leads to poor placental perfusion, which further contributes to hypertension and poor maternal and fetal health outcomes.

A role for AT_1R autoantibodies (AT_1-AA) has also been suggested in preeclampsia. These autoantibodies circulate at higher levels in preeclamptic pregnancies and activate AT_1R [160]. Furthermore, hypoxic conditions, such as that seen in preeclampsia, will stimulate the secretion of AT_1-AA [161] and AT_1-AA can subsequently increase oxidative stress by binding to trophoblast cells and activating NADPH-oxidase [162]. Furthermore, AT_1R activation will cause an increase in sFLT-1 and PAI-1, as described above. While the underlying mechanism(s) that cause preeclampsia has/have not been fully elucidated, it is clear that RAAS, and specifically Ang II and its receptors, play a large role in its pathology. Further exploration of their roles clearly needs to be undertaken.

E. Microvascular Dysfunction Associated with Nano-TiO_2 Exposure

Nano-TiO_2 inhalation exposure has been linked to microvascular dysfunction [5, 6, 8]. Pregnancy is a vulnerable period in which vascular adaptation and growth is paramount to maternal and fetal survival. Additionally, given that women may be unaware they are pregnant at the beginning of gestation and given that they remain in the work force usually until their third trimester, exposure during the manufacturing of products that use nano-TiO_2 is of great concern. Currently, the literature focusing on the consequences of maternal exposure to these nanoparticles is limited. The evaluation of the outcomes on maternal, fetal and multi-generational health needs to be fully explored to fully understand the potential impact of these exposures.

E.1.Maternal microvascular dysfunction.

Microvascular dysfunction following maternal inhalation exposure to nano-TiO_2 has been reported within the uterine circulation [8, 10, 163]. This is of great importance as uterine

adaptation to pregnancy is critical to support increased blood flow to, and decreased resistance within, the placentofetal unit [152]. Bowdridge et. al and Fournier et al. demonstrated how inhalation exposure affects uterine artery responses to vasoactive agonists [8, 10]. A single inhalation exposure to nano-TiO_2 during GD 4 or GD 12 resulted in decreased uterine artery relaxation to an endothelium-dependent vasodilatory agent ACh, as well as reduced adrenergic α_1 tension generation with exposure on GD 4, 12 or 17 [10]. Bowdridge et. al also demonstrated that the uterine artery exhibited increased sensitivity to kisspeptin, resulting in increased vasoconstriction following maternal exposure for 6 days starting mid-gestation [8]. It was also found that repeated maternal inhalation exposure to nano-TiO_2 from mid to late gestation resulted in anatomical alterations to the uterine artery with a significant decrease in internal vessel diameter [8]. Given how outward hypertrophic growth is critical to support increased blood flow to the uterus [11], this is of great concern. Taken together, these data supports the finding that inhalation exposure to nano-TiO_2 during pregnancy may alter vasoactive adaptations and blood flow during pregnancy and consequently lead to aberrant uterine hemodynamics.

A mechanism by which these alterations occur could be via the reduced circulating levels of estradiol that are observed following maternal inhalation exposure [8]. Estradiol has been shown to alter leukocyte trafficking following nano-TiO_2 inhalation exposure. Leukocyte trafficking was shown to decrease during proestrus in rats but was significantly increased following inhalation exposure to nano-TiO_2 [163]. Proestrus represents a preparatory stage of reproduction. If inflammatory responses are induced during this time period, then the uterine environment may not be receptive for implantation following ovulation. Further, plasma estradiol levels on GD 20 were shown to be significantly

decreased following a 6 day mid- to late-gestation nano-TiO_2 inhalation exposure [8]. As estradiol has been shown to be important for vascular growth and vasodilation [114, 115] as well as for RAAS adaptation during pregnancy [152], estradiol disruption can have devastating consequences for health outcomes during pregnancy, such as the development of preeclampsia.

E.2. Placental dysfunction following maternal exposure.

The placenta is an important organ during pregnancy that must be functional for proper growth and survival of the fetus. Maternal exposure of mice to nano-TiO_2 during the first 13 days of gestation decreased the area of labyrinth zones, that are critical for nutrient and waste exchange, reduced vascularization, and decreased uNK cells that are critical for placentation and vascular remodeling [164]. Placental mRNA expression for genes required for labyrinth development and trophoblast differentiation were significantly reduced and proteins associated with apoptosis significantly increased within placental tissue following exposure [164]. If placental growth and attachment is impaired, then hemodynamics will be altered resulting in poor perfusion.

Vascular function of the umbilical artery and vein have also been examined following inhalation exposure to nano-TiO_2. The fetal perfusion of the placenta allows the delivery of waste and the return of nutrients from the placenta, contrary to maternal perfusion. Umbilical veins examined on GD 20 following a single maternal exposure on GD 4 showed an increased response to endothelium-dependent and -independent relaxation [10], suggesting altered vascular tone following exposure. Alternatively, maternal inhalation exposure for 6 days from mid- to late-gestation decreased the vasodilatory response in uterine veins to acetylcholine (ACh) and increased passive inner diameter

[9]. The umbilical artery was also shown to have decreased responsiveness to endothelium-dependent and -independent vasodilation as well as an increased sensitivity to adrenergic vasoconstriction [9]. These alterations could increase tension within the umbilical vessels resulting in increased vascular resistance and poor fetal perfusion.

Placental efficiency is defined as the mass of the pup divided by the mass of the placenta, where a larger pup supported by a smaller placenta would represent high placental efficiency [165]. A decrease in placental efficiency has been reported following maternal inhalation exposure to nano-TiO_2, as smaller pup sizes have been associated with larger placentas [8]. This may be related to altered placental hemodynamics that occur after maternal inhalation exposure. An increase in placental vascular resistance was observed following *ex-vivo* incubation in normal superfusates as well as calcium-free perfusion solution [9]. Additionally, outflow pressure was significantly decreased compared to controls during treatment with endothelium-dependent vasodilation agents and Ang II treatment, suggesting increased vasoconstriction within the placental microvascular networks [9]. Increased placental resistance will lead to decreased blood flow, resulting in poor nutrient and waste exchange and subsequently negative fetal health consequences.

E.3. Fetal Consequences and developmental origins of health and disease (DOHaD). While maternal consequences from direct exposure can occur, fetal consequences have also been reported. Fetal mass has been shown to be significantly decreased following maternal toxicant inhalation exposure [8], which may be ascribed to poor perfusion during gestation. Not only was maternal and placental vascular dysfunction reported following exposure, but fetal vascular responses were also altered. On GD 20 fetal aortic isometric

tension generation was tested via wire myography and showed increased contraction to adrenergic stimulation [10], which could alter fetal hemodynamics within the fetus and may have lasting effects following birth.

Changes in gene expression or epigenetic modification may also play a role in laying the foundation for future disease within the offspring of maternal exposure. Originally coined by epidemiologist David Barker, the Barker hypothesis, which is now referred to the developmental origins of health and disease (DOHaD), states that a hostile gestational environment may lead to poor adult health outcomes later in life, such as increased susceptibility to disease [166-168]. This connection between the gestational environment and alterations of the fetal transcriptome have been shown in past studies. Stapleton et al. exposed pregnant dams to nano-TiO_2 aerosols and collected fetal hearts at the end of gestation on GD 20 [169]. RNA sequencing and transcriptomic analysis was performed to assess which pathways were altered by nano-TiO_2 exposure. With the results showing most of the effects residing within the kidney and liver. This included pathways involved in renal necrosis, liver hyperplasia/hyperproliferation, renal damage and autophagy. Additionally, the authors reported an increased propensity for infection due to alterations in pathways involving infectious disease [169]. This study demonstrated how fetal transcriptomes can be altered by maternal inhalation exposure to ENM and how this may predispose offspring to future disease. Further research has shown not only epigenetic remodeling following maternal exposure, but also cardiac dysfunction in young adult offspring [170, 171]. Nano-TiO_2 inhalation exposure during gestation also resulted in adult offspring with modified cognition. Engler-Chiurazzi et. al found that male adult offspring presented with significant working memory impairments compared to control offspring, as

well as decreases in motivation, suggesting behavioral alterations [95]. These results suggest that exposure in utero may lead to psychological deficits that manifest or persist into adulthood. With physiological and behavioral alterations apparent in offspring from maternally exposed dams, it is of great importance to tease out potential mechanisms and to further identify the dangers of these exposures. Furthermore, it is crucial to examine when during gestation exposure results in the most devastation to maternal and fetal health. Slight differences resulting within early gestation due to exposure may lay the foundation for devastating consequences later in life.

F. Conclusion

The benefits of diverse ENM applications and advanced materials in human endeavors are undeniable and, with the growth of this technology, the exposure potential to these products continues to rise. The importance of investigating the effects of maternal inhalation exposure to such toxicants is two-fold: 1) Women are exposed to ENM in industrial settings well into their third trimester. This is of great importance as different time-points of exposure may result in various degrees or types of reproductive impacts and fetal consequences. Determining what gestational windows are susceptible to these insults is crucial to better understand the real-world ramifications of exposures, 2) ENM exposure has been linked to cardiovascular consequences and microvascular dysfunction. Given how paramount microvascular adaptation and growth is to pregnancy, this would likely be a very vulnerable time period for ENM exposure and could have devastating effects to fetal and maternal health. We must be able to identify what adverse health outcomes are related to exposure and when the greatest detriment occurs to be

able to protect future generations as well as to better treat these consequences in the future.

Furthermore, investigation into consequences for offspring is of importance. ENM exposure has been linked to cardiac and behavioral deficits and evidence exists to show that the impact of exposures can persist well into adulthood. Future research into maternal, fetal and offspring consequences are necessary to comprehensively understand the effect of ENM inhalation exposure during gestation.

Purpose of Dissertation

Given the increased utilization of ENM containing products and advanced materials, it is of importance to fully identify the microvascular and reproductive consequences associated with exposure. To do so, the following studies were designed to assess how exposure can affect microvascular function as well as how that dysfunction may play a role in resultant reproductive consequences. Therefore, the central hypothesis of my dissertation was that maternal inhalation exposure to nano-TiO_2 will result in maternal microvascular dysfunction and fetal vascular consequences. Additionally, I believed that the gestational period in which exposure occurs will result in differing maternal and placental microvascular consequences contributing to poor fetal outcomes. Given that early gestation lays the foundation for fetal development, I believed that this time period would be the post sensitive to maternal inhalation exposure to nano-TiO_2. The specific aims of the studies are listed below.

Study 1:

This study aimed to assess how maternal inhalation exposure may affect autoregulation within the uterine microcirculation and fetal vascular function. To do so, pregnant dams were exposed to nano-TiO_2 aerosols and myogenic responsiveness was assessed via pressure myography. Fetal aortic tension was also assessed to investigate fetal vascular alterations following gestational exposure.

Study 2:

The aim of this study was to determine the critical time-point of gestational exposure most harmful to uterine microvascular function and fetal outcomes. Pregnant dams were exposed to nano-TiO_2 aerosols either during early, mid or late gestation. Placental efficiency was calculated and uterine radial artery response to endothelium-dependent and -independent agents as well as to the adrenergic response and angiotensin II vasoconstriction were assessed. The role that Ang II may play was also explored by assessing receptor protein levels within the uterine artery.

Study 3:

The aim of this study was to develop a novel technique to assess placental hemodynamics. As such, this study is a technical report that provides users with the means to assess pressure and flow within placental units. This allows researchers an improved approach for assessing placental microvascular function and resistance following toxicant exposure.

Study 4:

The aim of this study was to determine which critical window of gestational exposure most affects placental function. Pregnant dams were exposed to nano-TiO_2 aerosols either

during early, mid or late gestation and placental hemodynamics were assessed with and without the presences of dilatory and constrictive agonists, including Ang II. Further, Ang II receptor protein levels were assessed within the placenta and placental zones were measured to determine if anatomical changes were apparent following exposure. This studied aimed to identify anatomical and physiological consequences to the placenta during distinct windows of exposure.

Study 5:

The aim of this study was to investigate the consequences of mixed exposures to 3D printer emissions, which contain both particulate matter and gas. This aim was developed to explore ENM exposure during the “use” period of acrylonitrile butadiene styrene (ABS) filaments. This study was performed in tandem with another study to assess microvascular dysfunction within the mesenteric circulation following inhalation exposure.

References

1. Albalawi, F., et al., *Engineered Nanomaterials: The Challenges and Opportunities for Nanomedicines.* Int J Nanomedicine, 2021. **16**: p. 161-184.
2. Dockery, D.W., et al., *An association between air pollution and mortality in six U.S. cities.* N Engl J Med, 1993. **329**(24): p. 1753-9.
3. Stefaniak, A.B., et al., *Inhalation exposure to three-dimensional printer emissions stimulates acute hypertension and microvascular dysfunction.* Toxicol Appl Pharmacol, 2017. **335**: p. 1-5.
4. Guo, N.L., et al., *Pilot deep RNA sequencing of worker blood samples from Singapore printing industry for occupational risk assessment.* NanoImpact, 2020. **19**.
5. Abukabda, A.B., et al., *Heterogeneous Vascular Bed Responses to Pulmonary Titanium Dioxide Nanoparticle Exposure.* Front Cardiovasc Med, 2017. **4**: p. 33.
6. Abukabda, A.B., et al., *Group II innate lymphoid cells and microvascular dysfunction from pulmonary titanium dioxide nanoparticle exposure.* Part Fibre Toxicol, 2018. **15**(1): p. 43.
7. Stapleton, P.A., et al., *Microvascular and mitochondrial dysfunction in the female F1 generation after gestational TiO2 nanoparticle exposure.* Nanotoxicology, 2015. **9**(8): p. 941-51.
8. Bowdridge, E.C., et al., *Maternal Engineered Nanomaterial Inhalation During Gestation Disrupts Vascular Kisspeptin Reactivity.* Toxicol Sci, 2019. **169**(2): p. 524-533.
9. Abukabda, A.B., et al., *Maternal titanium dioxide nanomaterial inhalation exposure compromises placental hemodynamics.* Toxicology and Applied Pharmacology, 2019. **367**: p. 51-61.
10. Fournier, S.B., et al., *Effect of Gestational Age on Maternofetal Vascular Function Following Single Maternal Engineered Nanoparticle Exposure.* Cardiovasc Toxicol, 2019. **19**(4): p. 321-333.
11. Osol, G. and M. Mandala, *Maternal uterine vascular remodeling during pregnancy.* Physiology (Bethesda, Md.), 2009. **24**: p. 58-71.

12. Levine, R.J., et al., *Circulating Angiogenic Factors and the Risk of Preeclampsia.* New England Journal of Medicine, 2004. **350**(7): p. 672-683.

13. Kessler, R., *Engineered nanoparticles in consumer products: understanding a new ingredient.* Environ Health Perspect, 2011. **119**(3): p. a120-5.

14. Mann, E.E., et al., *Changes in cardiopulmonary function induced by nanoparticles.* Wiley Interdiscip Rev Nanomed Nanobiotechnol, 2012. **4**(6): p. 691-702.

15. Mostovenko, E., et al., *Indirect mediators of systemic health outcomes following nanoparticle inhalation exposure.* Pharmacol Ther, 2022: p. 108120.

16. Kashani, H., et al., *Extraordinary tensile strength and ductility of scalable nanoporous graphene.* Sci Adv, 2019. **5**(2): p. eaat6951.

17. Mauricio, M.D., et al., *Nanoparticles in Medicine: A Focus on Vascular Oxidative Stress.* Oxid Med Cell Longev, 2018. **2018**: p. 6231482.

18. Wang, H.e.a., *Advanced asymmetrical supercapacitors based on graphene hybrid materials.* Nano Research, 2011. **4**: p. 729-736.

19. Ou, L., et al., *Toxicity of graphene-family nanoparticles: a general review of the origins and mechanisms.* Part Fibre Toxicol, 2016. **13**(1): p. 57.

20. Nwali, C.J., *Volatile Organic Compounds Removal by Adsorption on Activated Carbon Filters.* International Journal of Advanced Research in Chemical Science, 2014. **1**(3): p. 38-43.

21. Maliyekkal, S.M., et al., *Graphene: a reusable substrate for unprecedented adsorption of pesticides.* Small, 2013. **9**(2): p. 273-83.

22. Fraser, K., et al., *Physicochemical characterization and genotoxicity of the broad class of carbon nanotubes and nanofibers used or produced in U.S. facilities.* Part Fibre Toxicol, 2020. **17**(1): p. 62.

23. Liu, Y.Y.e.a., *Functionalization of cotton with carbon nanotubes.* Journal of Materials Chemistry, 2008. **18**: p. 3454-3460.

24. Cherukuri, P., et al., *Near-infrared fluorescence microscopy of single-walled carbon nanotubes in phagocytic cells.* J Am Chem Soc, 2004. **126**(48): p. 15638-9.

25. Harrison, B.S. and A. Atala, *Carbon nanotube applications for tissue engineering.* Biomaterials, 2007. **28**(2): p. 344-53.

26. De Volder, M.F., et al., *Carbon nanotubes: present and future commercial applications.* Science, 2013. **339**(6119): p. 535-9.

27. Virlan, M.J., et al., *Organic Nanomaterials and Their Applications in the Treatment of Oral Diseases.* Molecules, 2016. **21**(2).

28. Nakhaei, P., et al., *Liposomes: Structure, Biomedical Applications, and Stability Parameters With Emphasis on Cholesterol.* Front Bioeng Biotechnol, 2021. **9**: p. 705886.

29. Fernandez-Fernandez, A., R. Manchanda, and A.J. McGoron, *Theranostic applications of nanomaterials in cancer: drug delivery, image-guided therapy, and multifunctional platforms.* Appl Biochem Biotechnol, 2011. **165**(7-8): p. 1628-51.

30. Kim, H.S., Y.S. Lee, and D.K. Kim, *Doxorubicin exerts cytotoxic effects through cell cycle arrest and Fas-mediated cell death.* Pharmacology, 2009. **84**(5): p. 300-9.

31. Lasic, D.D., *Doxorubicin in sterically stabilized liposomes.* Nature, 1996. **380**(6574): p. 561-2.

32. Webster, R., et. al, *PEG and PEG conjugates toxicity: towards an understanding of the toxicity of PEG and its relevance to PEGlyated biologicals*, in *Pegylated Protein Drugs: Basic Science and Clinical Applications. Milestones in Drug Therapy*. 2009, Birkhauser Basel. p. 127-146.

33. Palombo, M., et al., *Pharmaceutical and toxicological properties of engineered nanomaterials for drug delivery.* Annu Rev Pharmacol Toxicol, 2014. **54**: p. 581-98.

34. Yetisen, A.K., et al., *Nanotechnology in Textiles.* ACS Nano, 2016. **10**(3): p. 3042-68.

35. Murphy, C.J., *Optical sensing with quantum dots.* Anal Chem, 2002. **74**(19): p. 520A-526A.

36. Levene, M.J., et al., *In vivo multiphoton microscopy of deep brain tissue.* J Neurophysiol, 2004. **91**(4): p. 1908-12.

37. Voura, E.B., et al., *Tracking metastatic tumor cell extravasation with quantum dot nanocrystals and fluorescence emission-scanning microscopy.* Nat Med, 2004. **10**(9): p. 993-8.

38. El-Sayed, I.H., X. Huang, and M.A. El-Sayed, *Surface plasmon resonance scattering and absorption of anti-EGFR antibody conjugated gold nanoparticles in cancer diagnostics: applications in oral cancer.* Nano Lett, 2005. **5**(5): p. 829-34.

39. Walkey, C.D., et al., *Nanoparticle size and surface chemistry determine serum protein adsorption and macrophage uptake.* J Am Chem Soc, 2012. **134**(4): p. 2139-47.

40. Chen, B.H. and B. Stephen Inbaraj, *Various physicochemical and surface properties controlling the bioactivity of cerium oxide nanoparticles.* Crit Rev Biotechnol, 2018. **38**(7): p. 1003-1024.

41. Noori, A.J. and F.A. Kareem, *The effect of magnesium oxide nanoparticles on the antibacterial and antibiofilm properties of glass-ionomer cement.* Heliyon, 2019. **5**(10): p. e02568.

42. Zhang, T., et al., *Anticancer Effects of Zinc Oxide Nanoparticles Through Altering the Methylation Status of Histone on Bladder Cancer Cells.* Int J Nanomedicine, 2020. **15**: p. 1457-1468.

43. McSweeney, P.C., *The safety of nanoparticles in sunscreens: An update for general practice.* Aust Fam Physician, 2016. **45**(6): p. 397-9.

44. Chong, M.N., et al., *Recent developments in photocatalytic water treatment technology: a review.* Water Res, 2010. **44**(10): p. 2997-3027.

45. Meilert, K.T., et. al, *Photocatalytic self-cleaning of modified cotton textiles by TiO2 clusters attached by chemical spacers.* Journal of Molecular Catalysis A: Chemical, 2005. **237**(1-2): p. 101-108.

46. Sul, Y.T., *Electrochemical growth behavior, surface properties, and enhanced in vivo bone response of TiO2 nanotubes on microstructured surfaces of blasted, screw-shaped titanium implants.* Int J Nanomedicine, 2010. **5**: p. 87-100.

47. IARC, *IARC Monographs on the Evaluation of Carcinogenic Risk to Humans: Carbon Black, Titanium Dioxide, and Talc*. Vol. 93. 2010.

48. Dhingra, R., et. al, *Sustainable Nanotechnology: Through Green Methods and Life-Cycle Thinking.* Sustainability, 2010. **2**: p. 3323-3338.

49. Basinas, I., et al., *A Systematic Review of the Routes and Forms of Exposure to Engineered Nanomaterials.* Ann Work Expo Health, 2018. **62**(6): p. 639-662.

50. 2009-116, N.P.N., *Current Intelligence Bulletin 60: Interim Guidance for Medical Screening and Hazard Surveillance for Workers Potentially Exposed to Engineered Nanoparticles*. 2009.

51. Stapleton, P.A., et al., *Xenobiotic particle exposure and microvascular endpoints: a call to arms.* Microcirculation, 2012. **19**(2): p. 126-42.

52. *Sprague Dawley Rat: Preferred for Safety and Efficacy, Surgical Modification and Reproductive Studies*, I. Taconic Biosciences, Editor. p. 7-8.

53. Garner, K.L., Bowdridge, E. C., Griffith, J. A., DeVallance, E., Seman, M. G., Engels, K. J., Groth, C. P., Goldsmith, W. T., Wix, K., Batchelor, T. P., & Nurkiewicz, T. R., *Maternal Nanomaterial Inhalation Exposure: Critical Gestational Period in the Uterine Microcirculation is Angiotensin II Dependent.* Cardiovascular Toxicology, 2022.

54. Cross, J.C., Rossant, J., *Development of the Embryo*, in *Fetal Growth and Development*, R.H.a.A.D. Bocking, Editor. 2001, Cambrige University Press: Cambridge, United Kingdom. p. 1-4.

55. Takashina, T., *Haemopoiesis in the human yolk sac.* J Anat, 1987. **151**: p. 125-35.

56. Ross, C. and T.E. Boroviak, *Origin and function of the yolk sac in primate embryogenesis.* Nat Commun, 2020. **11**(1): p. 3760.

57. Furukawa, S., N. Tsuji, and A. Sugiyama, *Morphology and physiology of rat placenta for toxicological evaluation.* J Toxicol Pathol, 2019. **32**(1): p. 1-17.

58. Robson, A., et al., *Uterine natural killer cells initiate spiral artery remodeling in human pregnancy.* FASEB J, 2012. **26**(12): p. 4876-85.

59. Pijnenborg, R., et al., *Trophoblastic invasion of human decidua from 8 to 18 weeks of pregnancy.* Placenta, 1980. **1**(1): p. 3-19.

60. Brosens, I., W.B. Robertson, and H.G. Dixon, *The physiological response of the vessels of the placental bed to normal pregnancy.* J Pathol Bacteriol, 1967. **93**(2): p. 569-79.

61. Kam, E.P., et al., *The role of trophoblast in the physiological change in decidual spiral arteries.* Hum Reprod, 1999. **14**(8): p. 2131-8.

62. Risau, W. and I. Flamme, *Vasculogenesis.* Annu Rev Cell Dev Biol, 1995. **11**: p. 73-91.

63. Garcia, M.D. and I.V. Larina, *Vascular development and hemodynamic force in the mouse yolk sac.* Front Physiol, 2014. **5**: p. 308.

64. Beckman, D.A., et al., *Experimental manipulation of the rodent visceral yolk sac.* Teratology, 1990. **41**(4): p. 395-404.

65. Soares, M.J., et al., *Rat placentation: an experimental model for investigating the hemochorial maternal-fetal interface.* Placenta, 2012. **33**(4): p. 233-43.

66. Nunn, J.F., *Respiration in Neonates and Children*, in *Applied Respiratory Physiology*. 1987. p. 342-349.

67. Ge, X., et al., *Development of the human fetal hippocampal formation during early second trimester.* Neuroimage, 2015. **119**: p. 33-43.

68. Rai, A. and J.C. Cross, *Development of the hemochorial maternal vascular spaces in the placenta through endothelial and vasculogenic mimicry.* Dev Biol, 2014. **387**(2): p. 131-41.

69. Jollie, W.P., *Development, morphology, and function of the yolk-sac placenta of laboratory rodents.* Teratology, 1990. **41**(4): p. 361-81.

70. Wooding, P., Burton, G., *Comparative Placentation*. 2008: Springer.

71. Bell, S.C., et al., *Major secretory protein of human decidualized endometrium in pregnancy is an insulin-like growth factor-binding protein.* J Endocrinol, 1988. **118**(2): p. 317-28.

72. Xu, Y., R. Xiao, and Y. Li, *Effect of ethanol on the development of visceral yolk sac.* Hum Reprod, 2005. **20**(9): p. 2509-16.

73. Kumari, M.V., M. Hiramatsu, and M. Ebadi, *Free radical scavenging actions of metallothionein isoforms I and II.* Free Radic Res, 1998. **29**(2): p. 93-101.

74. Han, V.K. and A.M. Carter, *Spatial and temporal patterns of expression of messenger RNA for insulin-like growth factors and their binding proteins in the placenta of man and laboratory animals.* Placenta, 2000. **21**(4): p. 289-305.

75. Stocco, C., *Tissue physiology and pathology of aromatase.* Steroids, 2012. **77**(1-2): p. 27-35.

76. Itoh, K., et al., *Placental steroidogenesis in rats is independent of signaling pathways induced by retinoic acids.* Gen Comp Endocrinol, 2009. **163**(3): p. 285-91.

77. *Franscisco, . (2017, October 3). Differences Between Growth and Development in Biology. Difference Between Similar Terms and Objects. http://www.differencebetween.net/science/biology-science/differences-between-growth-and-development-in-biology/.*

78. Dugas, C. and V.H. Slane, *Miscarriage*, in *StatPearls*. 2022: Treasure Island (FL).

79. Liu, S.T., et al., *A preliminary report on the toxicity of arecoline on early pregnancy in mice.* Food Chem Toxicol, 2011. **49**(1): p. 144-8.

80. Varayoud, J., et al., *Long-lasting effects of neonatal bisphenol A exposure on the implantation process.* Vitam Horm, 2014. **94**: p. 253-75.

81. Tran, D.N., et al., *Effects of Bisphenol A and 4-tert-Octylphenol on Embryo Implantation Failure in Mouse.* Int J Environ Res Public Health, 2018. **15**(8).

82. Tsai, Y.S., et al., *Arecoline, a major alkaloid of areca nut, inhibits p53, represses DNA repair, and triggers DNA damage response in human epithelial cells.* Toxicology, 2008. **249**(2-3): p. 230-7.

83. Storeng, R. and J. Jonsen, *Nickel toxicity in early embryogenesis in mice.* Toxicology, 1981. **20**(1): p. 45-51.

84. Olsen, I. and J. Jonsen, *Whole-body autoradiography of 63Ni in mice throughout gestation.* Toxicology, 1979. **12**(2): p. 165-72.

85. Chen, L., et al., *The effect of reproductive toxicity induced by ZnO NPs in mice during early pregnancy through mitochondrial apoptotic pathway.* Environ Toxicol, 2021. **36**(6): p. 1143-1151.

86. Yang, H., et al., *Murine exposure to gold nanoparticles during early pregnancy promotes abortion by inhibiting ectodermal differentiation.* Mol Med, 2018. **24**(1): p. 62.

87. Yamashita, K., et al., *Silica and titanium dioxide nanoparticles cause pregnancy complications in mice.* Nat Nanotechnol, 2011. **6**(5): p. 321-8.

88. Kim, I.H., et al., *Swelling and drug release behavior of tablets coated with aqueous hydroxypropyl methylcellulose phthalate (HPMCP) nanoparticles.* J Control Release, 2003. **89**(2): p. 225-33.

89. Mukherjee, R. and S. De, *Adsorptive removal of phenolic compounds using cellulose acetate phthalate-alumina nanoparticle mixed matrix membrane.* J Hazard Mater, 2014. **265**: p. 8-19.

90. Holahan, M.R. and C.A. Smith, *Phthalates and neurotoxic effects on hippocampal network plasticity.* Neurotoxicology, 2015. **48**: p. 21-34.

91. Torres-Olascoaga, L.A., et al., *Early Gestational Exposure to High-Molecular-Weight Phthalates and Its Association with 48-Month-Old Children's Motor and Cognitive Scores.* Int J Environ Res Public Health, 2020. **17**(21).

92. Garcia, M., et al., *Early Gestational Exposure to Inhaled Ozone Impairs Maternal Uterine Artery and Cardiac Function.* Toxicol Sci, 2021. **179**(1): p. 121-134.

93. Kagawa, N., Y. Saito, and T. Nagao, *Early to middle gestational exposure to diethylstilbestrol impairs the development of labyrinth zone in mouse placenta.* Congenit Anom (Kyoto), 2014. **54**(2): p. 116-9.

94. Wang, Y., et al., *Mid-gestational sevoflurane exposure inhibits fetal neural stem cell proliferation and impairs postnatal learning and memory function in a dose-dependent manner.* Dev Biol, 2018. **435**(2): p. 185-197.

95. Engler-Chiurazzi, E.B., et al., *Impacts of prenatal nanomaterial exposure on male adult Sprague-Dawley rat behavior and cognition.* J Toxicol Environ Health A, 2016. **79**(11): p. 447-52.

96. Su, J., et al., *Pregnancy exposure of titanium dioxide nanoparticles causes intestinal dysbiosis and neurobehavioral impairments that are not significant postnatally but emerge in adulthood of offspring.* J Nanobiotechnology, 2021. **19**(1): p. 234.

97. Whelton, B.D., J.M. Toomey, and M.H. Bhattacharyya, *Cadmium-109 metabolism in mice. IV. Diet versus maternal stores as a source of cadmium transfer to mouse fetuses and pups during gestation and lactation.* J Toxicol Environ Health, 1993. **40**(4): p. 531-46.

98. Xiong, Y.W., et al., *Maternal cadmium exposure during late pregnancy causes fetal growth restriction via inhibiting placental progesterone synthesis.* Ecotoxicol Environ Saf, 2020. **187**: p. 109879.

99. Ohtani, N., et al., *Late pregnancy is vulnerable period for exposure to BPA.* J Vet Med Sci, 2018. **80**(3): p. 536-543.

100. Ley, K., *The Microcirculation in inflammation*, in *Handbook of Physiology: Microcirculation*, R.F. Tuma, et. al, Editor. 2008.

101. Patten, D.A. and S. Shetty, *More Than Just a Removal Service: Scavenger Receptors in Leukocyte Trafficking.* Front Immunol, 2018. **9**: p. 2904.

102. Rodriguez, I. and M. Gonzalez, *Physiological mechanisms of vascular response induced by shear stress and effect of exercise in systemic and placental circulation.* Front Pharmacol, 2014. **5**: p. 209.

103. Ngai, C.Y., Yao, X., *Vascular Responses to Shear Stress: The Involvement of Mechanosensors in Endothelial Cells.* The Open Circulation and Vascular Journal, 2010. **3**: p. 85-94.

104. Schubert, R. and M.J. Mulvany, *The myogenic response: established facts and attractive hypotheses.* Clin Sci (Lond), 1999. **96**(4): p. 313-26.

105. Davis, M.J.e.a., *Local Regulation of Microvascular Perfusion*, in *Handbook of Physiology: Microcirculation*, R.F. Tuma, et. al, Editor. 2008.

106. Burbank, F., *Hemodynamic Changes in the Uterus and its Blood Vessels in Pregnancy*, in *Textbook of Postpartum Hemorrhage; An Essential Clinical Reference for Effective Managment*. 2012, Sapiens.

107. Mandala, M. and G. Osol, *Physiological Remodelling of the Maternal Uterine Circulation during Pregnancy.* Basic & Clinical Pharmacology & Toxicology, 2012. **110**(1): p. 12-18.

108. Sanghavi, M. and J.D. Rutherford, *Cardiovascular physiology of pregnancy.* Circulation, 2014. **130**(12): p. 1003-8.

109. Edouard, D.A., et al., *Venous and arterial behavior during normal pregnancy.* Am J Physiol, 1998. **274**(5): p. H1605-12.

110. Paller, M.S., *Mechanism of decreased pressor responsiveness to ANG II, NE, and vasopressin in pregnant rats.* Am J Physiol, 1984. **247**(1 Pt 2): p. H100-8.

111. Gant, N.F., et al., *A study of angiotensin II pressor response throughout primigravid pregnancy.* J Clin Invest, 1973. **52**(11): p. 2682-9.

112. Cipolla, M. and G. Osol, *Hypertrophic and hyperplastic effects of pregnancy on the rat uterine arterial wall.* American Journal of Obstetrics & Gynecology, 1994. **171**(3): p. 805-811.

113. Gokina, N.I., M. Mandala, and G. Osol, *Induction of localized differences in rat uterine radial artery behavior and structure during gestation.* Am J Obstet Gynecol, 2003. **189**(5): p. 1489-93.

114. Storment, J.M., M. Meyer, and G. Osol, *Estrogen augments the vasodilatory effects of vascular endothelial growth factor in the uterine circulation of the rat.* Am J Obstet Gynecol, 2000. **183**(2): p. 449-53.

115. Ni, Y., et al., *Pregnancy augments uteroplacental vascular endothelial growth factor gene expression and vasodilator effects.* Am J Physiol, 1997. **273**(2 Pt 2): p. H938-44.

116. Mandala, M., *Influence of Estrogens on Uterine Vascular Adaptation in Normal and Preeclamptic Pregnancies.* Int J Mol Sci, 2020. **21**(7).

117. Ben Driss, A., et al., *Arterial expansive remodeling induced by high flow rates.* Am J Physiol, 1997. **272**(2 Pt 2): p. H851-8.

118. Fountain, J.H. and S.L. Lappin, *Physiology, Renin Angiotensin System*, in *StatPearls*. 2022: Treasure Island (FL).

119. Bernstein, K.E., et al., *Renal angiotensin-converting enzyme and blood pressure control.* Curr Opin Nephrol Hypertens, 2014. **23**(2): p. 106-12.

120. Rogerson, F.M., et al., *Presence of angiotensin converting enzyme in the adventitia of large blood vessels.* J Hypertens, 1992. **10**(7): p. 615-20.

121. Yart, L., et al., *Role of the Uteroplacental Renin-Angiotensin System in Placental Development and Function, and Its Implication in the Preeclampsia Pathogenesis.* Biomedicines, 2021. **9**(10).

122. Kanaide, H., et al., *Cellular mechanism of vasoconstriction induced by angiotensin II: it remains to be determined.* Circ Res, 2003. **93**(11): p. 1015-7.

123. MacKenzie, A., *Endothelium-derived vasoactive agents, AT1 receptors and inflammation.* Pharmacol Ther, 2011. **131**(2): p. 187-203.

124. Touyz, R.M., et al., *Oxidative Stress: A Unifying Paradigm in Hypertension.* Can J Cardiol, 2020. **36**(5): p. 659-670.

125. Tsai, M.H., et al., *CO-releasing molecules CORM2 attenuates angiotensin II-induced human aortic smooth muscle cell migration through inhibition of ROS/IL-6 generation and matrix metalloproteinases-9 expression.* Redox Biol, 2017. **12**: p. 377-388.

126. Li, D.Y., et al., *Upregulation of endothelial receptor for oxidized low-density lipoprotein (LOX-1) in cultured human coronary artery endothelial cells by angiotensin II type 1 receptor activation.* Circ Res, 1999. **84**(9): p. 1043-9.

127. Watanabe, T., T.A. Barker, and B.C. Berk, *Angiotensin II and the endothelium: diverse signals and effects.* Hypertension, 2005. **45**(2): p. 163-9.

128. Honjo, M., et al., *Lectin-like oxidized LDL receptor-1 is a cell-adhesion molecule involved in endotoxin-induced inflammation.* Proc Natl Acad Sci U S A, 2003. **100**(3): p. 1274-9.

129. Ohashi, H., et al., *Phosphatidylinositol 3-kinase/Akt regulates angiotensin II-induced inhibition of apoptosis in microvascular endothelial cells by governing survivin expression and suppression of caspase-3 activity.* Circ Res, 2004. **94**(6): p. 785-93.

130. Porrello, E.R., L.M. Delbridge, and W.G. Thomas, *The angiotensin II type 2 (AT2) receptor: an enigmatic seven transmembrane receptor.* Front Biosci (Landmark Ed), 2009. **14**(3): p. 958-72.

131. Aguilera, G., et al., *Developmental changes in angiotensin II receptor subtypes and AT1 receptor mRNA in rat kidney.* Kidney Int, 1994. **46**(4): p. 973-9.

132. Busche, S., et al., *Expression of angiotensin AT(1) and AT(2) receptors in adult rat cardiomyocytes after myocardial infarction. A single-cell reverse transcriptase-polymerase chain reaction study.* Am J Pathol, 2000. **157**(2): p. 605-11.

133. Li, J., et al., *Angiotensin AT2 receptor protects against cerebral ischemia-induced neuronal injury.* FASEB J, 2005. **19**(6): p. 617-9.

134. Oishi, Y., et al., *Cardioprotective role of AT2 receptor in postinfarction left ventricular remodeling.* Hypertension, 2003. **41**(3 Pt 2): p. 814-8.

135. McCarthy, C.A., et al., *Angiotensin AT2 receptor stimulation causes neuroprotection in a conscious rat model of stroke.* Stroke, 2009. **40**(4): p. 1482-9.

136. Touyz, R.M. and A.C. Montezano, *Angiotensin-(1-7) and Vascular Function: The Clinical Context.* Hypertension, 2018. **71**(1): p. 68-69.

137. Rentzsch, B., et al., *Transgenic angiotensin-converting enzyme 2 overexpression in vessels of SHRSP rats reduces blood pressure and improves endothelial function.* Hypertension, 2008. **52**(5): p. 967-73.

138. Itcho, K., et al., *Angiotensin 1-7 suppresses angiotensin II mediated aldosterone production via JAK/STAT signaling inhibition.* J Steroid Biochem Mol Biol, 2019. **185**: p. 137-141.

139. Lo, J., et al., *Angiotensin-converting enzyme 2 antagonizes angiotensin II-induced pressor response and NADPH oxidase activation in Wistar-Kyoto rats and spontaneously hypertensive rats.* Exp Physiol, 2013. **98**(1): p. 109-22.

140. Chai, S.Y., et al., *The angiotensin IV/AT4 receptor.* Cell Mol Life Sci, 2004. **61**(21): p. 2728-37.

141. Royea, J., et al., *Angiotensin IV Receptors Mediate the Cognitive and Cerebrovascular Benefits of Losartan in a Mouse Model of Alzheimer's Disease.* J Neurosci, 2017. **37**(22): p. 5562-5573.

142. Lew, R.A., et al., *Angiotensin AT4 ligands are potent, competitive inhibitors of insulin regulated aminopeptidase (IRAP).* J Neurochem, 2003. **86**(2): p. 344-50.

143. Kovacs, G.L. and D. De Wied, *Peptidergic modulation of learning and memory processes.* Pharmacol Rev, 1994. **46**(3): p. 269-91.

144. Chen, S., J.M. Patel, and E.R. Block, *Angiotensin IV-mediated pulmonary artery vasorelaxation is due to endothelial intracellular calcium release.* Am J Physiol Lung Cell Mol Physiol, 2000. **279**(5): p. L849-56.

145. Gardiner, S.M., et al., *Regional haemodynamic effects of angiotensin II (3-8) in conscious rats.* Br J Pharmacol, 1993. **110**(1): p. 159-62.

146. Yang, J., et al., *The role of the renin-angiotensin-aldosterone system in preeclampsia: genetic polymorphisms and microRNA.* J Mol Endocrinol, 2013. **50**(2): p. R53-66.

147. Neves, L.A., et al., *Pregnancy enhances the angiotensin (Ang)-(1-7) vasodilator response in mesenteric arteries and increases the renal concentration and urinary excretion of Ang-(1-7).* Endocrinology, 2003. **144**(8): p. 3338-43.

148. AbdAlla, S., et al., *Increased AT(1) receptor heterodimers in preeclampsia mediate enhanced angiotensin II responsiveness.* Nat Med, 2001. **7**(9): p. 1003-9.

149. Muthalif, M.M., et al., *Signal transduction mechanisms involved in angiotensin-(1-7)-stimulated arachidonic acid release and prostanoid synthesis in rabbit aortic smooth muscle cells.* J Pharmacol Exp Ther, 1998. **284**(1): p. 388-98.

150. Steinhorn, R.H., *Nitric oxide and beyond: new insights and therapies for pulmonary hypertension.* J Perinatol, 2008. **28 Suppl 3**: p. S67-71.

151. Barbagallo, M., et al., *Vascular Effects of Progesterone : Role of Cellular Calcium Regulation.* Hypertension, 2001. **37**(1): p. 142-147.

152. Mishra, J.S., K. Gopalakrishnan, and S. Kumar, *Pregnancy upregulates angiotensin type 2 receptor expression and increases blood flow in uterine arteries of rats.* Biol Reprod, 2018. **99**(5): p. 1091-1099.

153. Abalos, E., et al., *Global and regional estimates of preeclampsia and eclampsia: a systematic review.* Eur J Obstet Gynecol Reprod Biol, 2013. **170**(1): p. 1-7.

154. Anton, L., et al., *Activation of local chorionic villi angiotensin II levels but not angiotensin (1-7) in preeclampsia.* Hypertension, 2008. **51**(4): p. 1066-72.

155. Salas, S.P., et al., *Time course of maternal plasma volume and hormonal changes in women with preeclampsia or fetal growth restriction.* Hypertension, 2006. **47**(2): p. 203-8.

156. Mueller, M.D., et al., *Regulation of vascular endothelial growth factor (VEGF) gene transcription by estrogen receptors alpha and beta.* Proc Natl Acad Sci U S A, 2000. **97**(20): p. 10972-7.

157. Vaughan, D.E., S.A. Lazos, and K. Tong, *Angiotensin II regulates the expression of plasminogen activator inhibitor-1 in cultured endothelial cells. A potential link between the renin-angiotensin system and thrombosis.* J Clin Invest, 1995. **95**(3): p. 995-1001.

158. Ye, Y., et al., *Role of Plasminogen Activator Inhibitor Type 1 in Pathologies of Female Reproductive Diseases.* Int J Mol Sci, 2017. **18**(8).

159. Zhou, C.C., et al., *Angiotensin II induces soluble fms-Like tyrosine kinase-1 release via calcineurin signaling pathway in pregnancy.* Circ Res, 2007. **100**(1): p. 88-95.

160. Wallukat, G., et al., *Patients with preeclampsia develop agonistic autoantibodies against the angiotensin AT1 receptor.* J Clin Invest, 1999. **103**(7): p. 945-52.

161. LaMarca, B., et al., *Autoantibodies to the angiotensin type I receptor in response to placental ischemia and tumor necrosis factor alpha in pregnant rats.* Hypertension, 2008. **52**(6): p. 1168-72.

162. Dechend, R., et al., *AT1 receptor agonistic antibodies from preeclamptic patients stimulate NADPH oxidase.* Circulation, 2003. **107**(12): p. 1632-9.

163. Stapleton, P.A., et al., *Estrous cycle-dependent modulation of in vivo microvascular dysfunction after nanomaterial inhalation.* Reprod Toxicol, 2018. **78**: p. 20-28.

164. Zhang, L., et al., *Gestational exposure to titanium dioxide nanoparticles impairs the placentation through dysregulation of vascularization, proliferation and apoptosis in mice.* Int J Nanomedicine, 2018. **13**: p. 777-789.

165. Wilson, M.E. and S.P. Ford, *Comparative aspects of placental efficiency.* Reprod Suppl, 2001. **58**: p. 223-32.

166. Barker, D.J., *The fetal and infant origins of adult disease.* Bmj, 1990. **301**(6761): p. 1111.

167. Barker, D.J. and C.N. Martyn, *The maternal and fetal origins of cardiovascular disease.* J Epidemiol Community Health, 1992. **46**(1): p. 8-11.

168. Arima, Y. and H. Fukuoka, *Developmental origins of health and disease theory in cardiology.* J Cardiol, 2020. **76**(1): p. 14-17.

169. Stapleton, P.A., et al., *Maternal engineered nanomaterial inhalation during gestation alters the fetal transcriptome.* Part Fibre Toxicol, 2018. **15**(1): p. 3.

170. Kunovac, A., et al., *ROS promote epigenetic remodeling and cardiac dysfunction in offspring following maternal engineered nanomaterial (ENM) exposure.* Part Fibre Toxicol, 2019. **16**(1): p. 24.

171. Kunovac, A., et al., *Enhanced antioxidant capacity prevents epitranscriptomic and cardiac alterations in adult offspring gestationally-exposed to ENM.* Nanotoxicology, 2021. **15**(6): p. 812-831.

Figure Legends

Fig. 1 Critical gestational timepoints in human and rat pregnancies. The first, second and third trimesters are graphically represented within human pregnancy as well as a similarly segmented within the rat pregnancy timeline. GD = gestational day

Fig. 1

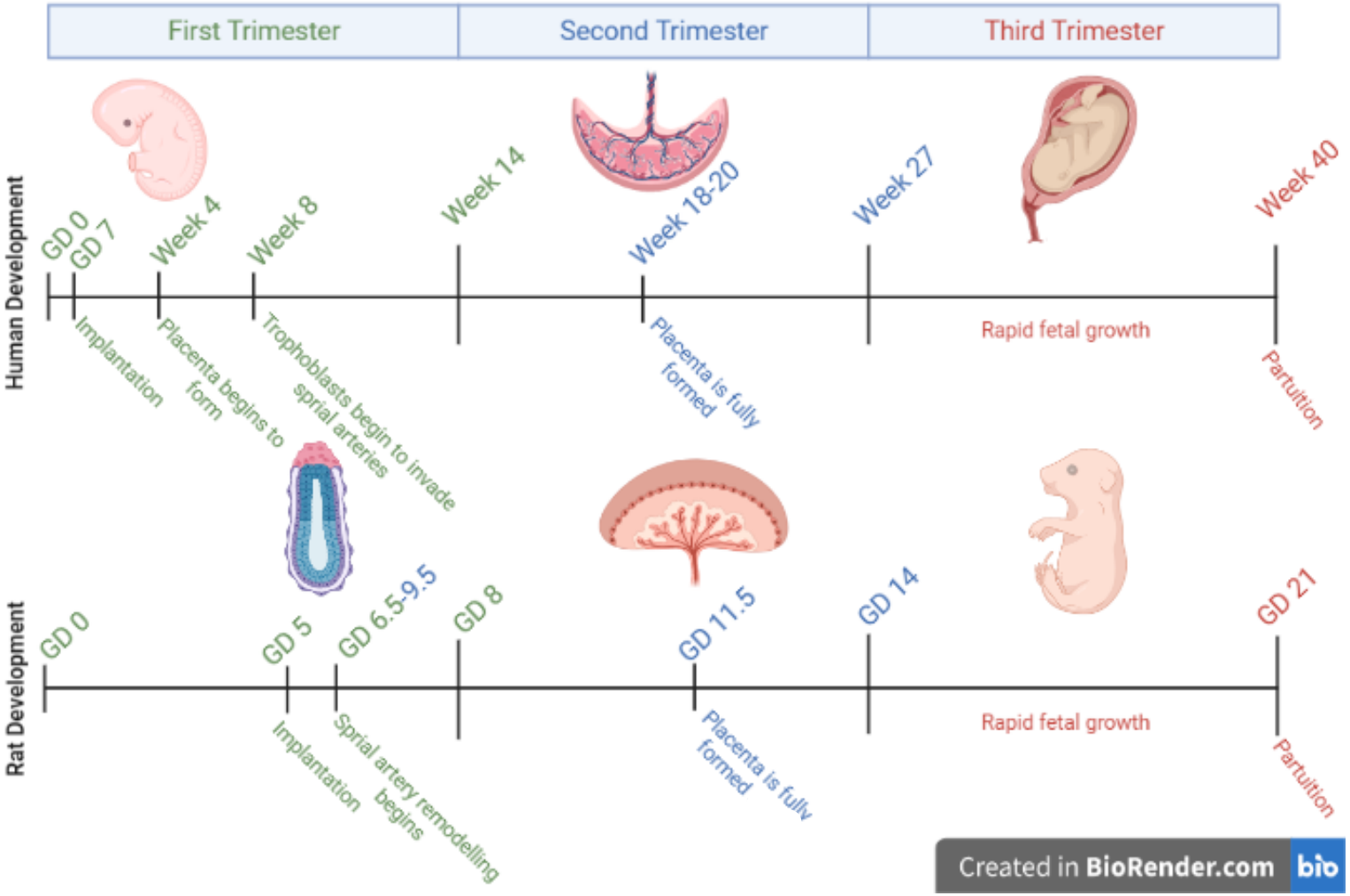
First Trimester
Second Trimester
Third Trimester
Human Development
GD 0
GD 7
Week 4
Week 8
Week 14
Week 18-20
Week 27
Week 40
Implantation
Placenta begins to form
Trophoblasts begin to invade sprial arteries
Placenta is fully formed
Rapid fetal growth
Partuition
Rat Development
GD 0
GD 5
GD 6.5-9.5
GD 8
GD 11.5
GD 14
GD 21
Implantation
Sprial artery remodelling begins
Placenta is fully formed
Rapid fetal growth
Partuition
Created in BioRender.com
bio

II. Chapter 2

Maternal Engineered Nanomaterial Inhalation Exposure does not Compromise Maternal Myogenic Response but Alters Fetal Vascular Reactivity

Authors:

Garner, K.L.

Abukabda, A.B.

Bowdridge, E.C.

McBride, C.R.

Goldsmith, W.T.

Batchelor, T.P.

Nurkiewicz, T.R.

Affiliations:

Department of Physiology and Pharmacology, West Virginia University School of Medicine, Morgantown, WV

Center for Inhalation Toxicology (iTOX), West Virginia University School of Medicine, Morgantown, WV

Abstract

Maternal inhalation exposure to nano-titanium dioxide (nano-TiO_2), ubiquitously used in a variety of advanced materials, has been linked to microvascular dysfunction within the maternal circulation and poor reproductive outcomes. While studies are beginning to examine these consequences more research is required to fully understand the extent of this exposure. This study evaluated maternal myogenic response and fetal aortic responses following maternal inhalation exposure. Pregnant dams were exposed to nano-TiO_2 aerosols for 6 days at a concentration of 11.7± 1.0 mg/m^3. On GD 20, blood pressure measurements were taken and uterine radial arteries were excised from the dams for myogenic responsiveness evaluations via pressure myography. Additionally, fetal aortas were dissected and tension generation was assessed via wire myography. Maternal blood pressure and heart rate was not altered, nor was the uterine radial artery myogenic response with or without adrenergic stimulation. Fetal aortic relaxation to endothelium dependent stimulation was significantly reduced in the exposure group compared to the control, suggesting maternal exposure can lead to vascular dysfunction within the fetal circulation. Surprisingly, fetal dry mass was significantly increased in the exposure group (0.62 ± 0.02 g) compared to the control (0.55 ± 0.01 g). Additionally, litter size between the exposure group (13 ± 1) and control group (10 ± 1) was significantly different. While these results were surprising, it is concerning that fetal circulation was altered following maternal exposure, suggesting that gestational exposure can have further effects on fetal health. These consequences may persist into adulthood and could predispose future generations to adverse cardiovascular events.

Introduction

Nano-titanium dioxide (nano-TiO2) is a prominent engineered nanomaterial (ENM) used in a wide variety of applications. These advanced materials, while beneficial in many applications such as nanomedicine and water treatment [1, 2], need to be fully examined to completely grasp the toxicological effects of exposure. Due to the prominence of these materials, the chances of exposure are incredibly high and therefore the risks associated with exposure are of the utmost importance. Inhalation exposure to these nanomaterials have been linked to cardiovascular consequences [3, 4] and poor reproductive outcomes in a maternal model of exposure [5-8]. Given that gestation is a time period of rapid cardiovascular adaptations that are imperative to maternofetal health, a gestational model of inhalation exposure is critical to evaluate nano-TiO_2 consequences.

Arterioles within the microcirculation are responsible for vascular resistance and controlling blood flow into downstream organs. Without the proper responsiveness within these networks, the appropriate blood flow may not be delivered accordingly. Local mechanisms responsible for these responses include metabolic factors such as oxygen/pH, adenosine, osmolarity and reactive oxygen species (ROS) as well as direct adjustments due to sheer stress and pressure [9]. Myogenic response is the response of vascular smooth muscle to contract when there is an increase in transmural pressure or dilate when there is a decrease in transmural pressure within the circulation [9]. By doing so, the arterioles can keep blood flow consistent and protect downstream tissues. Myogenic responsiveness alters wall tension to regulate flow and is an important protective mechanism within the microcirculation. Myogenic tone has been shown to decrease in late pregnant mouse mesenteric arterioles and within the uterine artery

compared to nonpregnant responses [10] which is critical to allow for increased blood flow without increasing blood pressure during pregnancy. Myogenic tone is a resting level of contractility. This allows the vessel to respond to transmural pressure via constriction or dilation. The first experiments within this study assessed if myogenic response within the uterine microcirculation was altered following maternal inhalation exposure to nano-TiO_2. We hypothesized that since poor fetal outcomes had been observed in past gestational studies in rats [7] as well as reduced response to sheer stress [11], that myogenic response would be increased in the exposure group, resulting in inability to maintain blood flow consistently to the uterus and essentially the fetoplacental unit.

Further, we wanted to assess how fetal vascular responsiveness on gestational day (GD) 20 would be affected following maternal exposure. To do so, aortic response to vasoagonists were examined via wire myography. Given the microvascular dysfunction reported within the maternal circulation, our hypothesis was that these effects would also be found within the fetal circulation and that aortic dysfunction would be present within the exposed group pups. This examination is critical to assess how maternal inhalation exposure to these abundantly found ENM may result in maternal and fetal consequences, allowing for a more in-depth toxicological assessment.

Materials and Methods

Animal Characteristics

Female Sprague-Dawley rats were purchased from Hilltop Laboratories (Scottdale, PA) and housed in an AAALAC approved facility at West Virginia University (WVU). Rats were housed under a regulated temperature of 20-26 ˚C, relative humidity of 30-70% and 12:12 h light-dark cycle. Rats were assigned randomly to control or exposure groups. Rats had

ad libitum access to food and water and were acclimated for 48-72 h prior to mating. Gestational day (GD) 0 was identified by the presence of sperm following vaginal swab. Dams were euthanized on GD 20. All procedures were approved by the WVU Institutional Animal Care and Use Committee.

Engineered Nanomaterial

Nano-TiO_2 was purchased from Evonik (Aeroxide P25, Parsippany, New Jersey). Powder is composed of anatase (80%) and rutile (20%) TiO_2 and has been shown to have a primary particle size of 21 nm, a surface area of 48.08 m^2/g [12], and a Zeta potential of -56.6 mV [13].

Aerosol Generation

A high-pressure acoustical generator (HPAG, IEStechno, Morgantown, West Virginia) was utilized for nano-TiO_2 aerosol generation. The output of the generator was fed into a Venturi pump (JS-60M, Vaccon, Medway, Massachusetts), further deagglomeration of the particles. The nano-TiO_2 aerosol/air mix then entered the whole-body exposure chamber. A personal DataRAM (pDR-1500; Thermo Environmental Instruments Inc., Franklin, Massachusetts) was utilized for sampling the exposure chamber air to determine the real-time aerosol mass concentration. The software utilized feed-back loops to automatically adjust the acoustic energy to maintain the targeted, stable mass concentration during the exposure. Gravimetric measurements were conducted on Teflon filters simultaneously with the DataRAM measurements to obtain a calibration factor. The gravimetric measurements were conducted during each exposure to assess mass concentration measurements reported in this study. Water saturated bedding material

was used in the exposure chamber to maintain comfortable humidity (30%-70%). Control animal chambers were held at similar temperature and humidity conditions but were exposed to HEPA-filtered air only.

Aerosol Characterization

Size distribution and mass concentration assessment of the exposure paradigm occurred through various measurements during the exposure runs. Measurements of the Aerosol size distributions within the exposure chamber were obtained while maintaining a mass concentration of 12 mg/m^3 with: a high-resolution electrical low-pressure impactor (ELPI+, Dekati, Tampere, Finland), a scanning mobility particle sizer (SMPS 3938, TSI Inc., St. Paul, Minnesota), and an aerodynamic particle sizer (APS 3321, TSI Inc., St. Paul, Minnesota).

Exposure Paradigm

Exposure group was exposed to nano-TiO_2 aerosols in a whole-body chamber at a concentration of 12 mg/m^3 for 6 days, 6 h/day. All control groups were exposed to filtered air at 25 ml/min for 5-7 days, 6 h/day. Exposures began after GD 7. Estimation of lung deposition (D) with nano-TiO_2 [14] was determined using the equation: D=F●V●C●T, in which F is the deposition fraction (10%), V is the minute ventilation (208.3 cc), C is the mass concentration (mg/m^3), and T is the exposure duration (minutes) [15]. This exposure paradigm produced an estimated cumulative lung deposition of 539 ± 10 µg. These calculations represent cumulative lung deposition and do not account for clearance (MPPD Software v 2.11, Arlington, Virginia).

Euthanasia and Tissue Harvest

On GD 20, dams were anesthetized with 5% isoflurane and maintained during surgery under 2.5% isoflurane. Dams were placed on a heating pad to maintain a 37 ˚C body temperature. The trachea was intubated to ensure a patent airway and the right carotid artery was cannulated for blood collection. Mean arterial pressure (MAP) was acquired through PowerLab830 (AD Instruments).

Both uterine horns were surgically excised, and 1-3 pups were removed and placed in physiological salt solution (PSS, in mmol/L: 119 nM NaCl, 4.7 mM KCl, 1.18 mM KH_2PO_4, 1.17 mM $MgSO_4$, 2.5 mM $CaCl_2$, 25 mM $NaHCO_3$, 0.027 mM EDTA, 5.5 mM glucose) and the remaining pups and placenta were removed and weighed. The aortas were dissected from the pups and tension generation was assessed as detailed in the Wire Myography section. The uterus was placed in a dissection dish containing 4 ˚C PSS (in mmol/L: 129.8 NaCl, 5.4 KCl, 0.5 NaH_2PO_4, 0.83 $MgSO_4$, 19.0 $NaHCO_3$, 1.8 $CaCl_2$, 5.5 glucose) and was utilized for vascular assessments as detailed in the Pressure Myography section.

Fetal Aorta Tension Assessment: Wire Myography

Wire myography was utilized to assess tension generation within fetal aortas. 2-3 mm segments were cut and placed in a wire myography chamber (AD Instruments, DMT 620M) with 5 mL PSS and bubbled with 95% O_2 / 5% CO_2 at 37 ˚C. Vessels were incubated for 30 minutes and then max contractile response was determined by utilizing high-potassium PSS (K+PSS, in mmol/L: 123.7 nM KCl, 1.18 mM KH_2PO_4, 1.17 mM $MgSO_4$, 2.5 mM $CaCl_2$, 25 mM $NaHCO_3$, 0.027 mM EDTA, 5.5 mM glucose. Vessels were then relaxed by washing out K+PSS with PSS washes until baseline tension was reached. Contractile response was assessed via cumulative doses of U46619 (10^{-14} - 10^{-7} M).

Relaxation responses were assessed via cumulative doses of endothelium-dependent vasodilator acetylcholine (ACh, 10^{-9} - 10^{-4} M) and endothelium-independent vasodilator S-nitroso-N-acetyl-DL-penicillamine (SNAP, 10^{-10} - 10^{-3} M).

Wire Myography Calculations

Tension developed by the vessels with K+PSS is the maximum tension. Tension generated from treatment with agonists (PE, ACh, or SNAP) was recorded and the percentage of maximum tension generation was calculated using the following formula:

$$\boldsymbol{Percent\ Maximum\ Tension}\ (\%) = \left(\frac{\boldsymbol{Tension\ with\ Agonists\ in\ mN}}{\boldsymbol{Maximum\ Tension\ in\ mN}}\right) \times \mathbf{100}\%$$

Pressure Myography

Uterine vascular myogenic responses were assessed to elucidate alterations in reactivity following inhalation exposure. Radial arteries were dissected and transferred to an isolated vessel chamber (Living Systems Instrumentation, Burlington, Vermont) containing PSS. The arteries were cannulated on glass pipette tips (Living Systems Instrumentation, Burlington, Vermont), secured with 6-0 silk suture (AD Surgical, Sunnyvale, California), pressurized to 60 mm Hg, and superfused (rate of 10 ml/min) with PSS warmed to 37 ˚C and oxygenated (21% O_2/5% CO_2). Inner and outer vessel diameter was measured with video calipers (Colorado Video, Boulder, Colorado). The vessels were allowed to develop spontaneous tone before vascular reactivity was assessed. The degree of constriction by a blood vessel relative to its maximally dilated states is spontaneous tone. Vascular tone ranges from 0% (complete relaxation, maximum dilation) to 100% (complete lumen closure, maximum constriction).

Radial arteries were measured with increasing pressure from 0-120 mm Hg in 15 mm Hg increments. The steady state diameter was recorded following the increase of pressure. Vessels were then incubated with propranolol (3 x 10^{-6} M) for 10 minutes to block β adrenergic receptors and were then treated with norepinephrine (NE, 1 x $10^{-8\ -\ -5}$ M). Adrenergic influence on the myogenic response was assessed by measuring vessel diameter from 0-120 mm Hg in 15 mm Hg increments. Following the final curve, the vessel was carefully washed with fresh, warmed, and oxygenated PSS until the agonist was removed. The PSS was removed and replaced with Ca^{2+} -free PSS for 30 minutes to allow maximum passive diameter to be determined.

Pressure Myography Calculations

Spontaneous tone was calculated through the following equation:

$$\boldsymbol{Spontaneous\ Tone}\ (\%) = \left[\frac{(\boldsymbol{Dm} - \boldsymbol{Di})}{(\boldsymbol{Di})}\right] \times \mathbf{100}\%$$

Dm is the maximal diameter and Di is the initial steady-state diameter prior to the experimental treatments. The vasoactive responses were normalized to the maximal diameter using the equation: normalized diameter= Dss/Dm. Dss is steady state diameter at each pressure change. The vasoactive response to NE were calculated using the following equation:

$$\boldsymbol{Diameter}\ (\%\ \boldsymbol{Constriction}) = -\left[\frac{(\boldsymbol{Dcon} - \boldsymbol{Dss})}{(\boldsymbol{Dcon})}\right] \times \mathbf{100}\%$$

Dcon is the diameter prior to starting the treatment and Dss is the steady-state diameter following the addition of each treatment dose.

WT is the wall thickness of the vessel. This is calculated by measuring both the inner (ID) and outer (OD) passive diameters at the end of the Ca^{2+} free wash using the following equation:

$$\boldsymbol{WT = \frac{(OD - ID)}{2}}$$

Wall-to-lumen ratio (WLR) was calculated using the following equation:

$$\boldsymbol{WLR = \frac{WT}{ID}}$$

Statistics

Animal and vessel characteristics were assessed via unpaired student t test. Two-way repeated measures analysis of variance (ANOVA) was utilized to evaluate point-by-point differences in dose response curves for ACh, SNAP and myogenic response data. Šídák's post hoc analysis was performed when significance was found. When equal variance was not met, the Greenhouse-Geiger correction was utilized. U46619 dose response was evaluated using a mixed-effects model utilizing the Greenhouse-Geiger correction. Šídák's post hoc analysis was performed when significance was found. Statistical analyses were calculated via GraphPad Prism 9 (San Diego, California). N represents the number of animals whereas n represents vessel number. That data in this study is reported as the mean ± standard error (SE). Significance was set at $p \leq 0.05$.

Results

Nano-TiO_2 Aerosol Characterization

The average real-time aerosol mass concentration during exposures had a target of 12 mg/m^3 (Fig. 1a). Mass concentration was 11.7± 1.0 mg/m^3. The aerosol aerodynamic

diameter (assessed via the ELPI) had a count median diameter (CMD) of 167 nm with a standard deviation of 1.92 (Fig. 1b). Aerosol diameter was also assessed via the SMPS and APS and had a combined CMD of 118 nm with a standard deviation of 2.09 (Fig. 1c). We have extensively characterized morphology of the agglomerates via electron microscopy [6, 7].

Animal Characteristics

Exposed and control dams were similar in age, weight, heart rate and mean arterial pressure (Table 1). Litter size was different between the groups with exposed dams having larger litters (13±1) compared to the control (10±1) (Table 2). Wet pup mass and wet placental mass were not different, but dried pup mass was significantly increased in the exposed group (0.62±0.02) compared to the control (0.55±0.01) (Table 2).

Uterine Radial Artery Characteristics

Isolated uterine radial arteries had similar inner diameter, passive inner diameter, and passive outer diameter (Table 3). Wall thickness, wall to lumen ratio (WLR) and wall tension were not different between the groups (Table 3).

Uterine Radial Artery Vascular Reactivity: Pressure Myography

Control and exposed isolated uterine radial artery response to increasing doses of NE was not different (Fig. 2). Myogenic response was assessed with and without adrenergic stimulation with NE. Control myogenic response compared to control myogenic response with adrenergic stimulation was similar (Fig. 3a) as well as exposed myogenic response compared to exposed myogenic response with adrenergic stimulation (Fig. 3b). Control response without NE compared to exposed response without NE was also not different

(Fig. 4a), nor was control response with NE compared to exposed response with NE (Fig. 4b).

Fetal Aorta Tension Assessment: Wire Myography

Fetal aortic tension generation was assessed following pre-tension generation with U46619. Response to ACh was blunted in the exposure group vessels (Fig. 5a) showing endothelial dependent dysfunction. To assess the smooth muscle response to nitric oxide (NO), the vessels were pretreated with U46619 and treated with increasing doses of SNAP. This showed no impairment in response in the exposure group compared to the control (Fig. 5b), suggesting a functional smooth muscle layer and an intact endothelial independent mechanism. The response to U46619 was also altered at two doses. This data showed that exposed vessels were less responsive to U46619 than the control at the $1x10^{-13}$ and $1x10^{-11}$ doses (Fig. 6).

Discussion

Microvascular adaptation is critical to support a healthy pregnancy, especially within the uterine circulation [16]. One such adaptation is a decrease in myogenic response during late pregnancy [10]. This decrease in myogenic response has been linked to decreased actin polymerization within vascular smooth muscle of uterine arteries. Further, this has been found to be driven by both estrogen and progesterone, which increased during pregnancy [17]. Given that our lab has demonstrated that estrogen is decreased following maternal inhalation exposure to nano-TiO_2 [7], it would be possible that actin polymerization may not be reduced, resulting in no reduction in myogenic response. This study found that myogenic response within the uterine radial arteries was not altered

following maternal inhalation exposure. Myogenic response was not shown to be altered in either group due to adrenergic influence (Fig. 3) nor when comparing control versus exposed group (Fig. 4). This suggests that myogenic responsiveness does not play a role in the vascular dysfunction within the gestational model that leads to poor fetal outcomes [6, 7, 18].

Fetal aortic response was shown to be significantly altered compared to control when evaluating constriction to U46619 at two doses ($1x10^{-13}$ and $1x10^{-11}$). The exposure group had reduced response to U46619 compared to control but was not significantly different at all other concentrations (Fig. 6). Most concern is the reduced vascular response to endothelial dependent vasodilator ACh. While relaxation was significantly blunted within the exposure group to ACh, there was no difference in relaxation with the endothelial independent vasodilator (Fig. 5). This indicates that the endothelial cells are not responding properly while the vascular smooth muscle is capable of responding to nitric oxide (NO), suggesting the dysfunction is stemming from the endothelial cells or bioavailability of NO is decreased. A surprising result within our study was the increase in pup mass following maternal inhalation exposure. This is surprising because all of our data to this point has suggested microvascular dysfunction and poor perfusion to the uterus and fetoplacental unit results in poor nutrient exchange and therefore reduced pup size. It should be noted though that increased pup weight has been reported elsewhere where a group with a single dose of nano-TiO_2 inhalation exposure on GD 12 resulted in larger pups compared to the control group [19]. Moving forward, pup mass should continue to be recorded to assess if the mass is altered with exposure.

A limitation to this study would be the size of the uterine radial arteries assessed. Smaller vessels would have been better to evaluate as vascular resistance is increased in these vessels allowing for minor alterations in response to be identified. Moving forward, smaller resistance vessels should be utilized to fully examine the myogenic response. This is critical as myogenic response should decrease during pregnancy [10] and if not, could lead to increased risk for cardiovascular consequences and reduced fetal weight [20]. Future studies should also examine cardiovascular consequences of offspring into adulthood. While we have evidence of fetal aortic dysfunction, we do not know the ramifications of this dysfunction and if it will persist into adulthood. This would allow us to gain a more complete understanding of the toxicological effects of maternal inhalation exposure to this nano material.

In conclusion, myogenic response does not appear to be altered from inhalation exposure to nano-TiO_2 during gestation. While this was not impaired, fetal aortic response was shown to be altered within the exposure group, suggesting endothelial dysfunction following maternal exposure. This study provides further evidence that toxicological assessment is necessary to advance understand of the toxicological ramifications of exposure as well as to begin to elucidate mechanisms by which these consequences are occurring.

Figure Legends

Fig. 1 Nano-TiO_2 aerosol characterization. Aerosol characterizations were verified and monitored during exposure. Red lines on the size distribution curves represent a log normal fit of the size data. (a) Software controlled aerosol mass concentration over the 6 h exposure paradigm. A feedback system held the mass concentration near the desired 12 mg/m^3 target (red line). (b) Aerosol aerodynamic diameter was assessed using the high-resolution Electrical Low-Pressure Impactor (ELPI) showing a CMD of 167 nm with a geometric standard deviation of 1.92. (c) The diameter was also evaluated using a Scanning Mobility Particle Sizer (SMPS, light gray) and an Aerodynamic Particle Sizer (APS, dark gray) presented a CMD of 118 nm and a geometric standard deviation of 2.09.

Fig. 2 Adrenergic stimulation of radial uterine arteries following maternal inhalation exposure. Increasing doses of NE were added to isolated radial uterine artery preparations to assess adrenergic response. Data are mean ± SE

Fig. 3 Radial uterine artery myogenic responsiveness with and without adrenergic stimulation. Normalized diameter of radial uterine myogenic response and effect of adrenergic stimulation. (a) the effect of adrenergic stimulation on control maternal uterine radial arteries. (b) the effect of adrenergic stimulation on exposed maternal uterine radial arteries. Data are mean ± SE

Fig. 4 Myogenic response with adrenergic stimulation following maternal inhalation exposure. Normalized diameter of radial uterine myogenic response and effect of adrenergic stimulation and exposure. (a) myogenic responsiveness of control and exposed uterine radial arteries. (b) myogenic responsiveness with adrenergic influence of control exposed uterine radial arteries. Data are mean ± SE

Fig. 5 Fetal aortic rings endothelial dependent and independent relaxation. (a). percent maximum tension generation of aortic rings with increasing doses of Ach. This represented endothelial dependent relaxation. (b) percent maximum tension generation of aortic rings with increasing doses of SNAP. This represented endothelial independent relaxation. Data are mean ± SE. *, P ≤ 0.05 vs control

Fig. 6 Fetal aortic rings tension generation with U46619. Percent maximum tension generation of aortic rings with increasing doses of U46619. Data are mean ± SE. *, P ≤ 0.05 vs control

References

1. Palombo, M., et al., *Pharmaceutical and toxicological properties of engineered nanomaterials for drug delivery.* Annu Rev Pharmacol Toxicol, 2014. **54**: p. 581-98.
2. Chong, M.N., et al., *Recent developments in photocatalytic water treatment technology: a review.* Water Res, 2010. **44**(10): p. 2997-3027.
3. Abukabda, A.B., et al., *Group II innate lymphoid cells and microvascular dysfunction from pulmonary titanium dioxide nanoparticle exposure.* Part Fibre Toxicol, 2018. **15**(1): p. 43.
4. Abukabda, A.B., et al., *Heterogeneous Vascular Bed Responses to Pulmonary Titanium Dioxide Nanoparticle Exposure.* Front Cardiovasc Med, 2017. **4**: p. 33.
5. Stapleton, P.A., et al., *Maternal engineered nanomaterial inhalation during gestation alters the fetal transcriptome.* Part Fibre Toxicol, 2018. **15**(1): p. 3.
6. Abukabda, A.B., et al., *Maternal titanium dioxide nanomaterial inhalation exposure compromises placental hemodynamics.* Toxicology and Applied Pharmacology, 2019. **367**: p. 51-61.
7. Bowdridge, E.C., et al., *Maternal Engineered Nanomaterial Inhalation During Gestation Disrupts Vascular Kisspeptin Reactivity.* Toxicol Sci, 2019. **169**(2): p. 524-533.
8. Garner, K.L., Bowdridge, E. C., Griffith, J. A., DeVallance, E., Seman, M. G., Engels, K. J., Groth, C. P., Goldsmith, W. T., Wix, K., Batchelor, T. P., & Nurkiewicz, T. R., *Maternal Nanomaterial Inhalation Exposure: Critical Gestational Period in the Uterine Microcirculation is Angiotensin II Dependent.* Cardiovascular Toxicology, 2022.
9. Davis, M.J.e.a., *Local Regulation of Microvascular Perfusion*, in *Handbook of Physiology: Microcirculation*, R.F. Tuma, et. al, Editor. 2008.
10. Veerareddy, S., et al., *Vascular adaptations to pregnancy in mice: effects on myogenic tone.* Am J Physiol Heart Circ Physiol, 2002. **283**(6): p. H2226-33.

11. Stapleton, P.A., et al., *Maternal engineered nanomaterial exposure and fetal microvascular function: does the Barker hypothesis apply?* Am J Obstet Gynecol, 2013. **209**(3): p. 227.e1-11.

12. Stapleton, P.A., et al., *Estrous cycle-dependent modulation of in vivo microvascular dysfunction after nanomaterial inhalation.* Reprod Toxicol, 2018. **78**: p. 20-28.

13. Nichols, C.E., et al., *Reactive oxygen species damage drives cardiac and mitochondrial dysfunction following acute nano-titanium dioxide inhalation exposure.* Nanotoxicology, 2018. **12**(1): p. 32-48.

14. Nurkiewicz, T.R., et al., *Nanoparticle inhalation augments particle-dependent systemic microvascular dysfunction.* Part Fibre Toxicol, 2008. **5**: p. 1.

15. Yi, J., et al., *Whole-body nanoparticle aerosol inhalation exposures.* J Vis Exp, 2013(75): p. e50263.

16. Mandala, M. and G. Osol, *Physiological Remodelling of the Maternal Uterine Circulation during Pregnancy.* Basic & Clinical Pharmacology & Toxicology, 2012. **110**(1): p. 12-18.

17. Xiao, D., et al., *Pregnancy downregulates actin polymerization and pressure-dependent myogenic tone in ovine uterine arteries.* Hypertension, 2010. **56**(5): p. 1009-15.

18. Hong, F., et al., *Maternal exposure to nanosized titanium dioxide suppresses embryonic development in mice.* Int J Nanomedicine, 2017. **12**: p. 6197-6204.

19. Fournier, S.B., et al., *Effect of Gestational Age on Maternofetal Vascular Function Following Single Maternal Engineered Nanoparticle Exposure.* Cardiovasc Toxicol, 2019. **19**(4): p. 321-333.

20. Hemmings, D.G., et al., *Increased myogenic responses in uterine but not mesenteric arteries from pregnant offspring of diet-restricted rat dams.* Biol Reprod, 2005. **72**(4): p. 997-1003.

Table 1. Dam physical characteristics on GD 20. N represents number of animals. Data are mean ± SE.

	N	Age (d)	Weight (g)	Heart Rate (BPM)	Mean Arterial Pressure (MAP)
Control	29	96±3	374±9	412±12	70±7
Exposed	21	104±3	390±8	398±8	66±4

Table 2. Pup and placental physical characteristics from GD 20. N represents number of animals. Data are mean ± SE. *****, P ≤ vs control

	Litter Size	Wet Pup Mass (g)	Wet Placental Mass (g)	Dry Pup Mass (g)	Dry Placental Mass (g)
Control	10±1	4.51±0.05	0.75±0.02	0.55±0.01	0.11±0.01
Exposed	13±1*****	4.59±0.06	0.77±0.02	0.62±0.02*****	0.11±0.01

Table 3. Isolated microvascular characteristics from GD 20. n represents number of a. Data are mean ± SE. *****, P ≤ vs control

	n	Inner Diameter (µm)	Passive Inner Diameter (µm)	Passive Outer Diameter (µm)	Wall Thickness (µm)	Wall to Lumen Ratio (WLR)	Wall Tension (N/m)	Tone (%)
Control	6	243±28	296±30	367±19	34±6	0.13±0.04	1.58±0.16	18±4
Exposed	6	211±22	287±24	308±29	33±3	0.12±0.02	1.41±0.14	19±5

Fig. 1

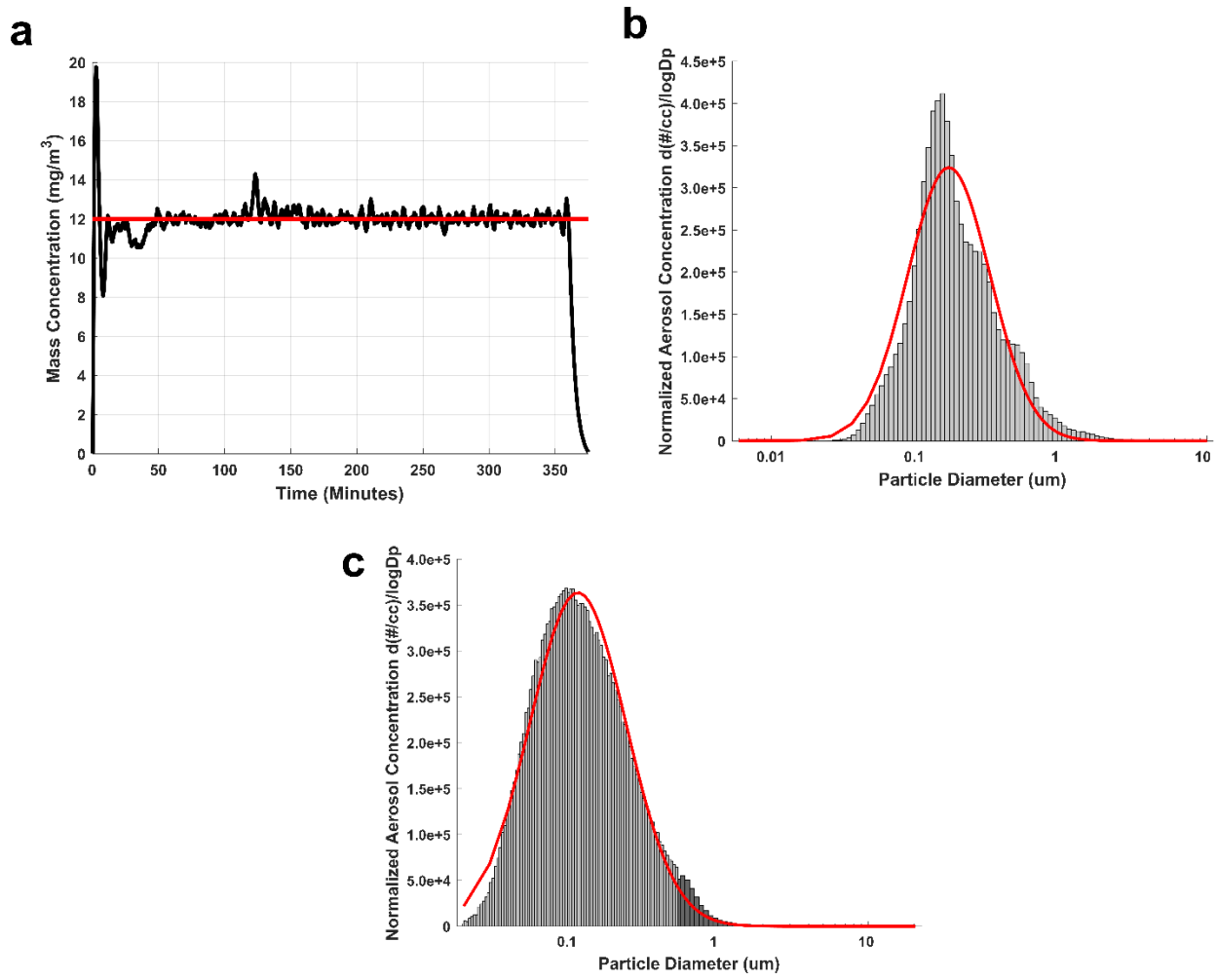
a
Mass Concentration (mg/m3)
Time (Minutes)
b
Normalized Aerosol Concentration d(#/cc)/logDp
Particle Diameter (um)
c
Normalized Aerosol Concentration d(#/cc)/logDp
Particle Diameter (um)

Fig. 2

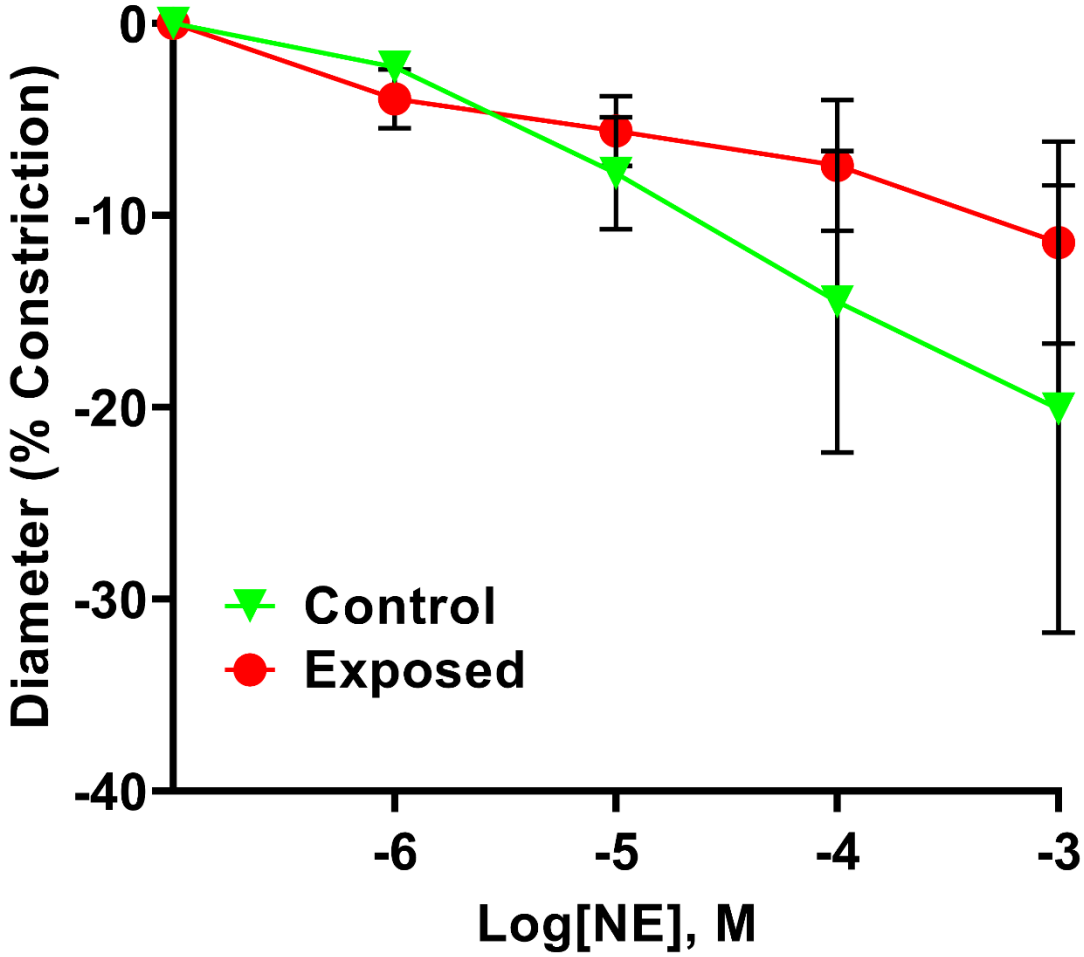
0
-10
-20
-30
-40
Diameter (% Constriction)
Control
Exposed
-6
-5
-4
-3
Log[NE], M

Fig. 3

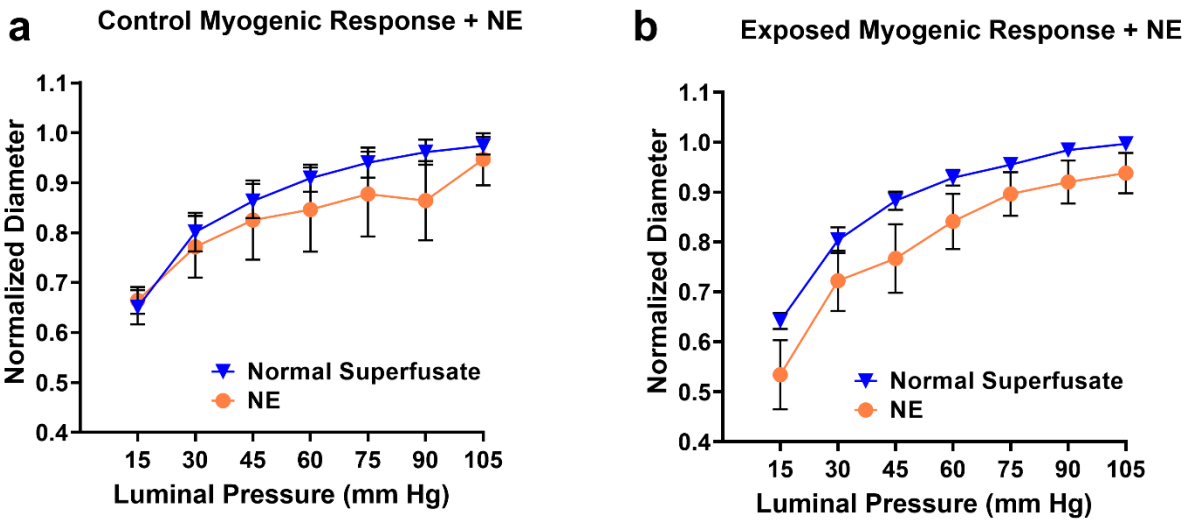
a
Control Myogenic Response + NE
Normalized Diameter
1.1
1.0
0.9
0.8
0.7
0.6
0.5
0.4
15 30 45 60 75 90 105
Luminal Pressure (mm Hg)
Normal Superfusate
NE
b
Exposed Myogenic Response + NE
Normalized Diameter
1.1
1.0
0.9
0.8
0.7
0.6
0.5
0.4
15 30 45 60 75 90 105
Luminal Pressure (mm Hg)
Normal Superfusate
NE

Fig. 4

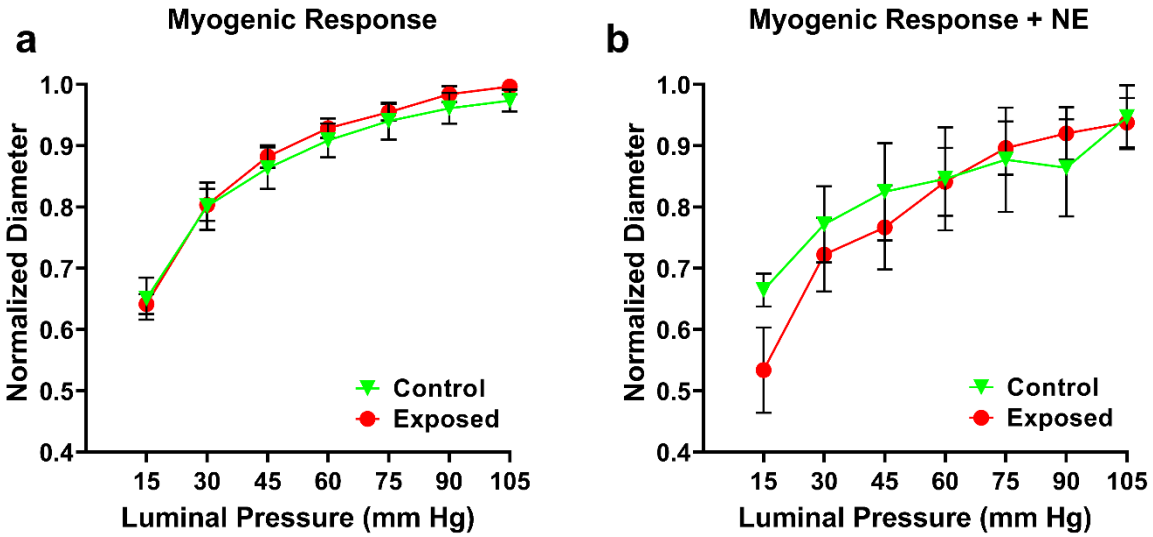
a
Myogenic Response
Normalized Diameter
1.0
0.9
0.8
0.7
0.6
0.5
0.4
15
30
45
60
75
90
105
Luminal Pressure (mm Hg)
Control
Exposed
b
Myogenic Response + NE
Normalized Diameter
1.0
0.9
0.8
0.7
0.6
0.5
0.4
15
30
45
60
75
90
105
Luminal Pressure (mm Hg)
Control
Exposed

Fig. 5

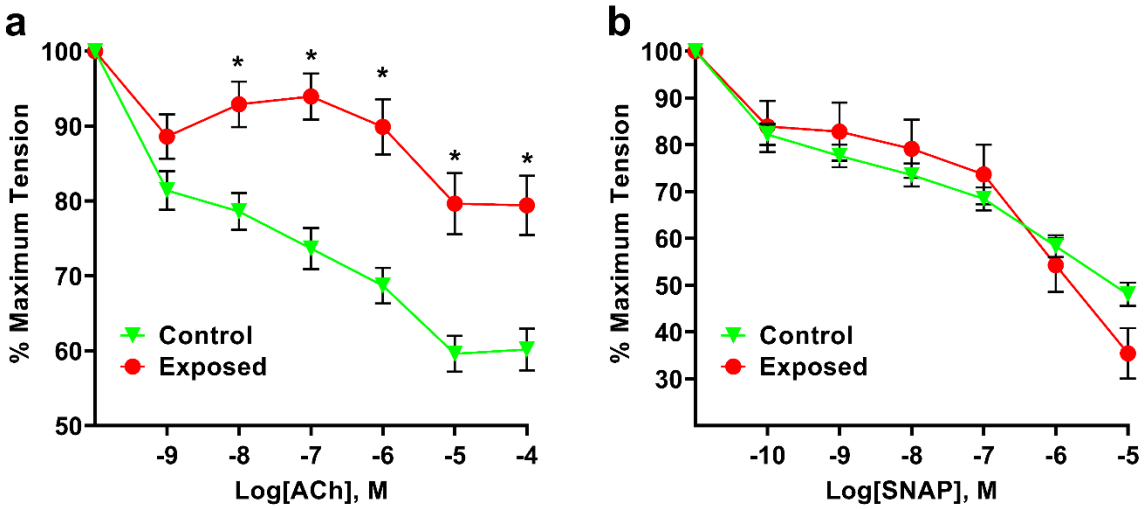
a
100
90
80
70
60
50
% Maximum Tension
*
*
*
*
*
Control
Exposed
-9
-8
-7
-6
-5
-4
Log[ACh], M
b
100
90
80
70
60
50
40
30
% Maximum Tension
Control
Exposed
-10
-9
-8
-7
-6
-5
Log[SNAP], M

Fig. 6

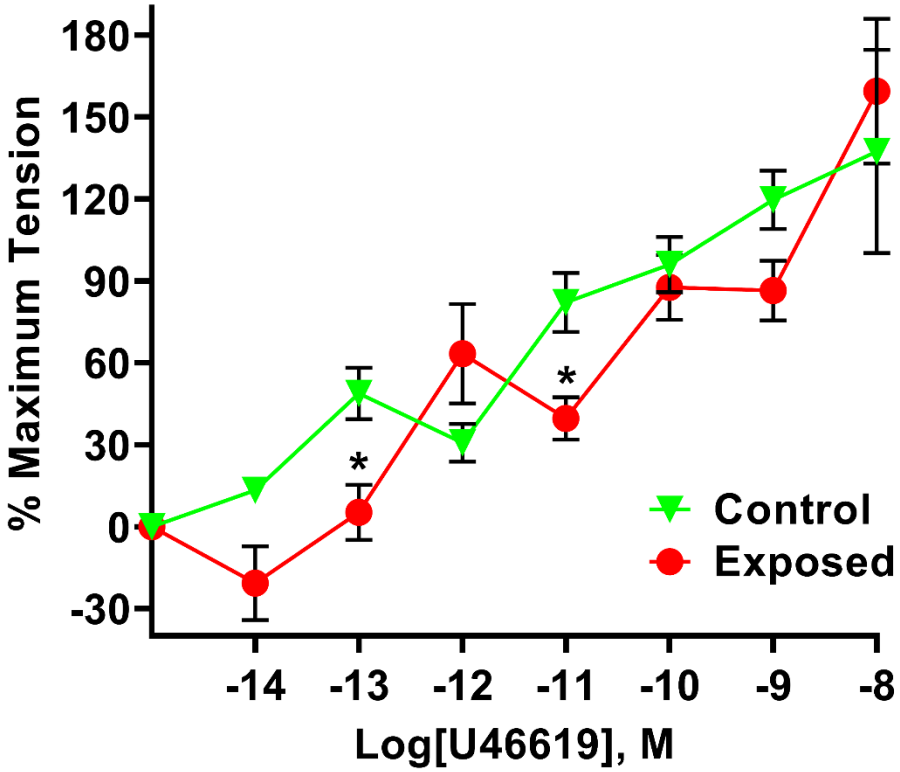
% Maximum Tension
180
150
120
90
60
30
0
-30
-14
-13
-12
-11
-10
-9
-8
Log[U46619], M
Control
Exposed
*
*

III. Chapter 3

Maternal Nanomaterial Inhalation Exposure: Critical Gestational Period in the Uterine Microcirculation is Angiotensin II Dependent

Citation: Garner, K. L., Bowdridge, E. C., Griffith, J. A., DeVallance, E., Seman, M. G., Engels, K. J., Groth, C. P., Goldsmith, W. T., Wix, K., Batchelor, T. P., & Nurkiewicz, T. R. (2022). Maternal Nanomaterial Inhalation Exposure: Critical Gestational Period in the Uterine Microcirculation is Angiotensin II Dependent. *Cardiovascular toxicology*, 10.1007/s12012-021-09712-8. Advance online publication. https://doi.org/10.1007/s12012-021-09712-8

Authors:

Krista L. Garner[1,2]

Elizabeth C. Bowdridge[1,2]

Julie A. Griffith[1,2]

Evan DeVallance[1,2]

Madison G. Seman[3]

Kevin J. Engels[1]

Caroline P. Groth[4]

William T. Goldsmith[1,2]

Kim Wix[1]

Thomas P. Batchelor[1,2]

Timothy R. Nurkiewicz[1,2*]

Affiliations:

[1]Department of Physiology and Pharmacology, West Virginia University School of Medicine, Morgantown, WV

[2]Center for Inhalation Toxicology (iTOX), West Virginia University School of Medicine, Morgantown, WV

[3]Division of Exercise Physiology, West Virginia University School of Medicine, Morgantown, WV

[4]Department of Epidemiology and Biostatistics, West Virginia University School of Public Health, Morgantown, WV

Abstract

Maternal inhalation exposure to engineered nanomaterials (ENM) has been associated with microvascular dysfunction and adverse cardiovascular responses. Pregnancy requires coordinated vascular adaptation and growth is imperative for survival. Key events in pregnancy hallmark distinct periods of gestation such as implantation, spiral artery remodeling, placentation and trophoblast invasion. Angiotensin II (Ang II) is a critical vasoactive mediator responsible for adaptations and is implicated in the pathology of preeclampsia. If perturbations occur during gestation, such as those caused by ENM inhalation exposure, then maternal-fetal health consequences may occur. Our study aimed to identify the period of gestation in which maternal microvascular functional and fetal health are most vulnerable. Additionally, we wanted to determine if Ang II sensitivity and receptor density is altered due to exposure. Dams were exposed to ENM aerosols (nano-titanium dioxide) during three gestational windows: early (EE, gestational day (GD) 2-6), mid (ME, GD 8-12) or late (LE, GD 15-19). Within the EE group dry pup mass decreased by 16.3% and uterine radial artery wall to lumen ratio (WLR) increased by 25.9%. Uterine radial artery response to Ang II sensitivity increased by 40.5% in the EE group. Ang II receptor density was altered in the EE and LE group with decreased levels of AT_2R. We conclude that early gestational maternal inhalation exposures resulted in altered vascular anatomy and physiology. Exposure during this time-period results in altered vascular reactivity and changes to uterine radial artery WLR, leading to decreased perfusion to the fetus and resulting in lower pup mass.

Introduction

Inhalation exposure to engineered nanomaterial (ENM) aerosols, such as nano-titanium dioxide (nano-TiO_2) results in adverse cardiovascular responses and microvascular dysfunction [1-3]. Our lab and others have reported that maternal inhalation exposure to nano-TiO_2 during gestation leads to maternal and fetal microvascular dysfunction and poor fetal health outcomes [4-7]. A successful pregnancy is the result of numerous physiological adjustments that support placental development and fetal growth. Proper cardiovascular adjustments are perhaps the most critical elements of healthy gestation because of their quintessential role in nutrient and waste delivery and end exchange. These are largely characterized by rapid vascular growth, wall remodeling, increased microvascular density, and decreased arteriolar resistance-- all of which concomitantly increase placental blood flow and increasingly match blood flow with fetal growth throughout gestation [8-10]. Various circulating factors and vasoactive mediators signal these elements, such as vascular endothelial growth factor (VEGF), nitric oxide, prostacyclin, endothelin-1 and angiotensin II (Ang II) [11]. Ang II is part of many important processes involved with gestational modifications including placentation [12], spiral artery remodeling [13], trophoblast invasion [13, 14], and maternal blood pressure regulation [15, 16]. Additionally, the actions of Ang II have been implicated in various pathologies of pregnancy including hypertension [15, 17], and fetal growth restriction [18]. If perturbations occur during pregnancy, whether it be hormonal, mediator imbalance, nutrient deficiency, or toxicant exposure, maternal-fetal health consequences may occur, either during pregnancy or later in life [19-24]. While we and others have reported that maternal nanomaterial inhalation exposure during gestation adversely influences uterine

microvascular reactivity and fetal outcomes, our understanding of the critical, or most impactful time-period of exposure on fetal health needs to be further explored [5, 24].

In humans, pregnancy is divided into three trimesters that represent early, mid and late gestation based upon critical periods of growth and development. For Sprague-Dawley rats, gestation spans 21-23 days [25]. For this study we segmented rat gestation into three time periods: early gestation spanning gestational days (GD) 1-7, mid gestation spanning GD 8-13, and late gestation spanning GD 14-21 (Fig. 1). The first week marks the period of implantation and embryonic development [25, 26]. During these early gestational days, rat embryo implantation will begin on GD 5 and the blastocyst will increase in size. The first wave of uterine spiral artery remodeling will occur GD 6.5- 9.5 [27]. This remodeling is essential for proper nutrient delivery and is essential for a healthy pregnancy. During mid gestation, continued embryonic growth occurs and discoid placenta formation is complete by ~GD 11 [28]. Organogenesis continues from GD 5-15 in rats and somite formation begins on GD 9-10 [25, 29]. Late in pregnancy, marks a time-period of rapid fetal growth and trophoblast invasion. This is the second wave of maternal spiral artery remodeling and will occur between GD 15-18 [30, 31]. Gestational windows mark distinct periods of growth and development. Others have reported that the time-period that exposure occurs during pregnancy can lead to varying reproductive and fetal toxicities [32-35] for the rationale for this study. The goal of our study was to determine the critical window of gestation in which maternal microvascular function and fetal health are most vulnerable. Mechanistically we explored if Ang II reactivity was altered by maternal inhalation exposure. We hypothesized that maternal exposure during the first week of gestation would be the most vulnerable period as this is when complex,

foundational events, such as embryonic attachment and initial stimulation of microvascular growth occur. We further hypothesized that because Ang II is ubiquitously involved in microvascular function as well as gestation, that some aspects of this signaling cascade may be affected by maternal nanomaterial inhalation.

Materials and Methods

Animal Characteristics

Female Sprague-Dawley rats were purchased from Hilltop Laboratories (Scottdale, PA) and housed in an AAALAC approved facility at West Virginia University (WVU). Rats were housed under a regulated temperature of 20-26 ˚C, relative humidity of 30-70% and 12:12 h light-dark cycle. Rats were randomly assigned to early exposed (EE), mid exposed (ME), late exposed (LE), early control (EC), mid control (EC), late control (LE) or naive groups. The purpose of the naïve group was to demonstrate that there was no artifact of inhalation exposure to filtered air. Rats had *ad libitum* access to food and water and were acclimated for 48-72 h prior to mating. GD 0 was identified by the presence of sperm following vaginal swab. Dams were euthanized on GD 20. All procedures were approved by the WVU Institutional Animal Care and Use Committee.

Engineered Nanomaterial

Nano-TiO_2 was purchased from Evonik (Aeroxide P25, Parsippany, New Jersey). This powder is composed of anatase (80%) and rutile (20%) TiO_2 and has been shown to have a primary particle size of 21 nm, a surface area of 48.08 m^2/g [36], and a Zeta potential of -56.6 mV [37].

Aerosol Generation

A high-pressure acoustical generator (HPAG, IEStechno, Morgantown, West Virginia) was utilized to generate nano-TiO_2 aerosols. The output of the generator was fed into a Venturi pump (JS-60M, Vaccon, Medway, Massachusetts), causing further de-agglomeration of the particles. The nano-TiO_2 aerosol/air mix then entered the whole-body exposure chamber. A personal DataRAM (pDR-1500; Thermo Environmental Instruments Inc., Franklin, Massachusetts) was used for sampling the exposure chamber air to determine the real-time aerosol mass concentration. The software utilized feed-back loops to automatically adjust the acoustic energy to maintain the targeted, stable mass concentration during the exposure. Exposure chamber air was sampled onto PTFE filters and gravimetric measurements were conducted simultaneously with the DataRAM to obtain a calibration factor for the real-time measurements. The gravimetric mass concentration measurements were reported in this study. Water saturated bedding material was used in the exposure chamber to maintain comfortable humidity (30%-70%). Control animal chambers were held at similar temperature and humidity conditions but were exposed to HEPA-filtered air only.

Aerosol Characterization

To assess the size distribution and mass concentration of the exposure paradigm, various measurements were obtained during the exposure runs. Measurements of the Aerosol size distributions within the exposure chamber were obtained while maintaining a mass concentration target of around 12 mg/m^3 with: a high-resolution electrical low-pressure impactor (ELPI+, Dekati, Tampere, Finland), a scanning mobility particle sizer (SMPS 3938, TSI Inc., St. Paul, Minnesota), an aerodynamic particle sizer (APS 3321, TSI Inc.,

St. Paul, Minnesota) and a Micro-Orifice Uniform Deposit Impactor (MOUDI 115R, MSP Corp, Shoreview, MN).

Exposure Paradigm

All exposure groups were exposed to nano-TiO_2 aerosols in a whole-body chamber at a concentration of 12 mg/m^3 for 3 days, 6 h/day. All control groups were exposed to filtered air at 25 ml/min for 3 days, 6 h/day. Early gestational groups (EE or EC) were exposed on GD 2,4, and 6, mid gestational groups were exposed on GD 8, 10 and 12, and late gestational groups were exposed on GD 15, 17 and 19. While the target mass concentration of the exposure was 12 mg/m^3 variability is expected. Actual mass concentration for EE was 13 ± 1 mg/m^3, for ME was 12 ± 1 mg/m^3 and for LE was 13 ± 1 mg/m^3. Additionally, estimation of lung deposition (D) with nano-TiO_2 [38] was determined using the equation: D=F●V●C●T, in which F is the deposition fraction (10%), V is the minute ventilation (208.3 cc), C is the mass concentration (mg/m^3), and T is the exposure duration (minutes) [39]. This exposure paradigm produced an estimated cumulative lung deposition of 313 ± 19 µg for EE, 291 ± 6 µg for ME and 311 ± 8 µg for LE. These calculations represent cumulative lung deposition and do not account for clearance.

Euthanasia and Tissue Harvest

On GD 20, dams were anesthetized with 5% isoflurane and maintained during surgery under 2.5% isoflurane. Dams were placed on a heating pad to maintain a 37 ˚C body temperature. The trachea was intubated to ensure a patent airway and the right carotid artery was canulated for blood collection. Both uterine horns were surgically excised, and pups and placenta were removed and weighed. The uterus was placed in a dissection

dish containing 4 ˚C physiological salt solution (PSS, in mmol/L: 129.8 NaCl, 5.4 KCl, 0.5 NaH_2PO_4, 0.83 $MgSO_4$, 19.0 $NaHCO_3$, 1.8 $CaCl_2$, 5.5 glucose) and was utilized for vascular assessments as detailed in the Vascular Reactivity section. Uterine arteries were cleared of fat and connective tissue, perfused to remove blood, flash frozen in liquid nitrogen and stored at -80 ˚C until western blot analyses were performed.

Pup/Placental Mass, Placental Efficiency and Sex Determination

To assess reproductive consequences of maternal nano-TiO_2 inhalation exposure, a subset of dams (N = 6-16) were utilized to assess pup mass, placental mass and placental efficiency. Pup and placental wet weights were obtained immediately after dissection. Fetal sex was determined on GD 20 by identifying the uterus or testicles of the pups. Pups and placentas were then dried and weighed again. Placental efficiency was calculated by dividing pup mass by the placental mass.

Vascular Reactivity

Uterine vascular responses were assessed to elucidate alterations in reactivity following inhalation exposure, as blood flow during gestation is paramount for maternal and fetal health. Radial arteries were dissected and transferred to an isolated vessel chamber (Living Systems Instrumentation, Burlington, Vermont) containing PSS. The arteries were cannulated on glass pipette tips (Living Systems Instrumentation, Burlington, Vermont), secured with 6-0 silk suture (AD Surgical, Sunnyvale, California), pressurized to 60 mm Hg, and superfused (rate of 10 ml/min) with PSS warmed to 37 ˚C and oxygenated (21% O_2/5% CO_2). Inner and outer vessel diameter was measured with video calipers (Colorado Video, Boulder, Colorado). The vessels were allowed to develop spontaneous

tone before vascular reactivity was assessed. The degree of constriction by a blood vessel relative to its maximally dilated states is spontaneous tone. Vascular tone ranges from 0% (complete relaxation, maximum dilation) to 100% (complete lumen closure, maximum constriction). Vessels that developed tone ≥20% than initial tone were included in this study.

Radial arteries were treated with increasing doses of endothelium-dependent vasodilator acetylcholine (ACh, 10^{-9} - 10^{-4} M), endothelium-independent vasodilator S-nitroso-N-acetyl-DL-penicillamine (SNAP, 10^{-9} - 10^{-4} M), α_1 adrenergic agonist phenylephrine (PE, 10^{-9} - 10^{-4} M), and Ang II (10^{-13} - 10^{-4} M). The steady state diameter was recorded following the addition of each of these concentrations. Following each dose curve, the vessel was carefully washed with fresh, warmed and oxygenated PSS until the agonist was removed. Once all dose curves were completed, the PSS was removed and replaced with Ca^{2+} - free PSS for 30 minutes to allow maximum passive diameter to be determined.

Pressure Myography Calculations

Spontaneous tone was calculated through the following equation:

$$\boldsymbol{Spontaneous\ Tone}\ (\%) = \left[\frac{(\boldsymbol{Dm} - \boldsymbol{Di})}{(\boldsymbol{Di})}\right] \times \mathbf{100}\%$$

Dm is the maximal diameter and Di is the initial steady-state diameter prior to the experimental treatments. The vasoactive response to ACh and SNAP were calculated using the following equation:

$$\boldsymbol{Diameter}\ (\%\ \boldsymbol{Dilation}) = \left[\frac{(\boldsymbol{Dss} - \boldsymbol{Dcon})}{(\boldsymbol{Dm} - \boldsymbol{Dcon})}\right] \times \mathbf{100}\%$$

Dcon is the diameter prior to starting the treatment and Dss is the steady-state diameter following the addition of each treatment dose. The vasoactive response of PE and Ang II were calculated using the following equation:

$$\boldsymbol{Diameter}\ (\%\ \boldsymbol{Constriction}) = -\left[\frac{(\boldsymbol{Dcon} - \boldsymbol{Dss})}{(\boldsymbol{Dcon})}\right] \times \mathbf{100}\%$$

WT is the wall thickness of the vessel. This is calculated by measuring both the inner (ID) and outer (OD) passive diameters at the end of the Ca^{2+} free wash using the following equation:

$$\boldsymbol{WT} = \frac{(\boldsymbol{OD} - \boldsymbol{ID})}{\mathbf{2}}$$

Wall-to-lumen ratio (WLR) was calculated using the following equation:

$$\boldsymbol{WLR} = \frac{\boldsymbol{WT}}{\boldsymbol{ID}}$$

Circulating Levels of Estradiol

On GD 20 blood was collected from the carotid artery and plasma samples (N= 6-8) were flash frozen and stored at -80 ˚C. An estradiol ELISA was then performed via the manufacturer's instructions (CalBiotech, Spring Valley, CA).

Uterine Artery AT_1R and AT_2R Western Blot

Relative Ang II receptor protein levels were determined via near-infrared western blot (N= 3-6). Uterine artery tissue was homogenized using a bead mill homogenizer and 1.6 mm stainless steel beads (Next Advance, Troy, New York) in RIPA containing 0.1 mM protease and phosphatase inhibitors (Roche, Indianapolis, Indiana). Samples were

prepared with 4x laemeli sample buffer containing β-mercaptoethanol and boiled at 95 ˚C. 30 µg of samples were resolved by SDS-PAGE and transferred to 0.2 µm nitrocellulose membrane. Membranes were blocked with LiCOR Odyssey blocking buffer and probed with primary antibodies against Ang II type 1 receptor (anti-AT1R, sc-515884, Santa Cruz Biotechnology, Inc. Dallas, Texas), Ang II type 2 receptor (anti-AT2R, ab92445, Abcam, Cambridge, Massachusetts) and β-actin (sc-47778, Santa Cruz Biotechnology, Inc. Dallas, Texas). Membranes were then probed with LiCOR near-infrared secondary antibodies and imaged using the LiCOR Odyssey. Secondary antibodies included: goat anti-rabbit (925-68070, LI-COR Biosciences, Lincoln, Nebraska) and goat anti-mouse (925-68071, LI-COR Bioscience, Lincoln, Nebraska). ImageJ software was utilized for optical density, normalized β-actin control and represented as fold change from control group.

Statistics

Two-way repeated measures analysis of variance (ANOVA) was utilized to evaluate point-by-point differences in dose response curves with the Geisser-Greenhouse correction followed by Dunnett's post hoc analysis when significance was found. Dam characteristics were assessed via one-way ANOVA utilizing a Tukey post hoc analysis. EC, MC, LC and naïve pup characteristics, vessel characteristics, maximal response, estradiol concentrations and relative Ang II receptor protein levels were first assessed via one-way ANOVA and a Tukey post hoc analysis. Because no statistical significance was identified, naïve and control groups were combined and then compared to exposure groups using a one-way ANOVA and a Dunnett's post hoc analysis. When equal variance was not met through the Brown-Forsythe test the Welch's ANOVA was utilized and the

Dunnett's T3 post hoc analysis was performed. The combination of naïve, EC, MC and LC groups were denoted as the final "control group." Statistical analyses were calculated via GraphPad Prism 9 (San Diego, California). N represents the number of dams whereas n represents vessel number. The data in this study is reported as the mean ± standard error (SE). Significance was set at $p \leq 0.05$. All p-values are reported after multiple-comparison adjustments.

Results

Nano-TiO_2 Aerosol Characterization

The average real-time aerosol mass concentration during exposures had a target of 12 mg/m^3 (Fig. 2a). Mass concentration for EE was 13 ± 1 mg/m^3, for ME was 12 ± 1 mg/m^3 and for LE was 13 ± 1 mg/m^3. The aerosol aerodynamic diameter (assessed via the ELPI) had a count median diameter (CMD) of 157 nm with a standard deviation of 1.73 (Fig. 2b). Aerosol diameter was also assessed via the SMPS and APS and had a combined CMD of 118 nm with a standard deviation of 2.11 (Fig. 2c). The size distribution (assessed via the MOUDI) had a mass median aerodynamic diameter (MMAD) of 1.03 µm with a geometric standard deviation of 2.57 (Fig. 2d). We have extensively characterized morphology of the agglomerates via electron microscopy [4, 5].

Animal Characteristics

Dams in all groups showed no significant difference in age or GD 20 weight (Table 1). EC, MC, LC and naïve pup and placental masses were not statistically different and can be found within Online Resource Table 1. ME and LE were not statistically different from the control group. EE wet pup weight (3.87 ± 0.14 g), dry pup weight (0.44 ± 0.02 g), wet

placental efficiency (4.68 ± 0.30), and dry placental efficiency (3.63 ± 0.27) were all significantly decreased compared to the control group (wet pup weight: 4.21 ± 0.07 g; dry pup weight: 0.53 ± 0.01 g; wet placental efficiency: 5.86 ± 0.20; dry placental efficiency: 5.15 ± 0.26). However, EE placental weights were not significantly different from the control (Fig. 3a-f). Sex ratio of the pups were not significantly different between the naïve and control groups (Online Resource Table 2) or between the control group and the exposure groups (Table 2). This data indicates that maternal exposure during the first trimester resulted in decreased pup size and lower placental efficiency which may suggest poor nutrient delivery to the pups and therefore resulting in smaller offspring.

Uterine Radial Artery Characteristics

Uterine radial arteries from the naïve and control groups displayed similar diameter, wall thickness, wall to lumen ratio (WLR), wall tension and % tone (Online Resource Table 3). All radial artery characteristics were similar when comparing the control verses exposure groups, except WLR. The EE radial arteries had significantly increased WLR (0.12 ± 0.01) compared to the control (0.10 ± 0.01), which could result from a thicker vascular wall or smaller luminal space (Table 3). This suggests that vascular growth is altered in the EE group and could contribute to poor blood perfusion through the radial arteries and therefore decreased nutrient delivery.

Vascular Reactivity

Uterine radial artery reactivity between all control groups and the naïve group to ACh, SNAP, PE or Ang II was not different (Fig. 4a-h). Due to this, the naïve, EC, MC, and LC

groups were combined and were denoted as the “control group” for comparison to the exposure groups. Endothelium-dependent vasodilation (ACh) was significantly decreased in all exposure groups (Fig. 5a). The maximal response to ACh across all concentrations was also significantly decreased in all exposure groups (control: 54 ± 3 %; EE: 29 ± 5 %; ME: 23 ± 5 %; LE: 31 ± 6%) (Fig. 5b). Endothelium-independent vasodilation (SNAP) was not significantly altered between the groups (Fig. 5c-d) nor was adrenergic vasoconstriction (Fig. 5e-f). The point-by-point response to Ang II was not different among the groups (Fig. 5g), but when assessing the maximal Ang II response, EE reactivity was augmented (control: -46 ± 3 %; EE: -64 ± 6 %) (Fig. 5h). These findings suggest that endothelium-dependent vasodilation is altered within the uterine microcirculation, independent of gestational period of maternal nano-TiO_2 inhalation exposure. In contrast, Ang II reactivity is only altered during early gestation, showing an increased maximal response. Exposure at any point during gestation results in decreased response to vasodilation and if exposed during early pregnancy, may additionally result in increased sensitivity to Ang II, which could collectively contribute to poor perfusion and nutrient delivery.

Uterine Vascular AT1R/AT2R Protein Concentration

To determine if the altered Ang II reactivity in the EE group maybe due to receptor subtype density, Ang II receptor type protein levels (AT_1R and AT_2R) were assessed in uterine vasculature by Western blot analysis. There were no differences between the EC, MC, or LC groups (data not shown), therefore representative controls from these groups were run with the exposure groups. Relative AT_1R protein levels, which stimulate

vasoconstriction were not significantly altered in the exposure groups compared to the control (Fig. 6a). Relative AT_2R protein levels, which stimulate vasodilation, were significantly reduced in both EE and LE groups (Fig. 6b). These findings support the augmented vascular reactivity results in the EE group to Ang II.

Circulating Levels of Estradiol on GD 20

Estradiol (E_2) has been shown to upregulate uterine artery AT_2R during pregnancy [16]. Additionally, our lab has shown that nano-TiO_2 exposure during pregnancy can result in decreased circulating levels of E_2 [5]. Based on these finding we assessed if the decreased presence of AT_2R within the uterine vasculature of the EE and LE groups could be the result of decreased circulating E_2. E_2 concentration between all control groups was not significantly different (Fig. 7a) and were combined. E_2 concentrations between the combined control and the exposure groups were found to not be statistically different (Fig. 7b). These results suggest that either E_2 is not altered under this exposure paradigm or alterations that occur due to exposure during early or mid-gestation may return to normal following time without exposure prior to assessment of E_2 on GD 20.

Discussion

This novel study demonstrates that maternal nano-TiO_2 inhalation exposure during the early period of gestation resulted in lower pup mass, decreased placental efficiency, and increased Ang II-induced vasoconstriction within the radial uterine arteries which may be due to the observed Ang II receptor imbalance. While the uterine radial arteries in all exposure groups showed decreased endothelium-dependent vasodilation compared to

control, only the EE group showed augmented vasoconstriction to Ang II. Ang II receptor protein levels were found to be altered within the uterine arteries of early and late exposed dams with a decrease in AT_2R protein levels (Fig. 6b), which are responsible for vasodilation via Ang II signaling. Additionally, we found that the WLR of the EE radial arteries was significantly increased compared to control, suggestive of inappropriate anatomic adaptation to pregnancy (Table 3).

Endothelium-dependent vasodilation was significantly decreased in all exposure groups (Fig. 5a-b) independent of time-period of exposure. This is consistent with endothelial dysfunction that has been reported after maternal nano-TiO_2 inhalation exposure [4, 5]. In contrast, EE group was the only time-period to show a functional change in response to Ang II (Fig. 5h). Ang II is a key hormone involved in pregnancy, a potent vasoconstrictor, with most of its action due to binding of AT_1R, that must decrease in sensitivity during pregnancy to allow for proper fetal perfusion and to accommodate increased blood volume [40]. The EE group shares similarities with preeclampsia, as Ang II sensitivity is heightened and vascular resistance is increased, which may result in smaller fetal weight [15, 41-43]. Decreased fetal weight can result when nutrient availability or delivery is impaired and may account for the poor fetal outcomes observed in this study and others from our lab (Fig. 3) [5] and could potentially lead to health complications later in life [44]. Additionally, the increased WLR could indicate inward eutrophic growth or inward hypertrophic growth, which is associated with hypertension and a decrease in blood flow (Table 3) [8, 45]. Together, the augmented Ang II response, diminished endothelium-dependent dilation and increased WLR suggests nano-TiO_2 exposure early in gestation impairs uterine perfusion. Through this mechanism the

placenta and fetus would not receive adequate blood flow, reducing the delivery of nutrients resulting in the observed lower pup mass.

To further explore this mechanism, Ang II receptor densities were assessed to see if the increased Ang II response was due to alterations in uterine artery AT_1R and AT_2R relative protein levels. AT_1R activation is associated with vasoconstriction, cellular growth and migration, and inflammation whereas AT_2R is associated with vasodilation, cellular differentiation and anti-inflammatory effects [46, 47]. Decreased AT_1R sensitivity to Ang II is associated with a healthy pregnancy and pathologies such as preeclampsia have been tied to increased sensitivity to Ang II vasoconstriction during pregnancy [47]. AT_2R was decreased in the maternal uterine arteries on GD 20 in EE and LE groups (Fig. 6b). This may explain the increased maximum vasoconstrictive response to Ang II in the EE group. AT_2R is expected to increase during pregnancy, which would aid in decreased vascular resistance and increased fetal blood flow [16]. If the AT_2R is decreased, then an increased sensitivity to allow for vasoconstriction may occur leading to decreased placental and fetal perfusion.

A relationship between E_2 and AT_2R has been established in research within the kidney [48] as well as uterine arteries during pregnancy [16] where E_2 can induce increased levels of AT_2R. Additionally, our lab has shown that maternal inhalation exposure to nano-TiO_2 may result in decreased circulating levels of E_2 [5]. To assess if E_2 may be responsible for the decrease in AT_2R in the EE and LE groups E_2 levels were assessed at GD 20. Our results showed no significant differences in E_2 (Fig. 7). While this could indicate that Ang II sensitivity is altered by a different mechanism, it is important to note

the possibility of E_2 levels recovering post exposure. Further research needs to assess E_2 levels across gestation and not only at GD 20 when E_2 levels naturally begin to fall.

Limitations with this study include that the Ang II receptor density was assessed within uterine arteries and not radial uterine arteries, which was the site where vascular reactivity was assessed. This was due to the inadequate mass of the radial arteries for western blot analysis. Reactivity within vascular beds can vary widely depending on the artery/arteriole level and therefore receptor protein levels may be different in the larger uterine arteries versus the smaller, resistant radial arteries. Another limitation of this study, as stated earlier, was we only assessed E_2 levels at GD 20 of pregnancy, where levels of E_2 begin to fall prior to parturition. E_2 levels may have fallen following the maternal exposure during the early or mid-period of exposure but may have recovered by GD 20 and would not be reflected in this study. Additionally, we assumed assumptions of ANOVA/linear regression including normality, equal variances, linearity and independence.

Once hormone levels across gestation are fully identified, further understanding of the effects of maternal inhalation exposure, during various periods of growth and development, can be achieved. Additionally, due to Ang II's role in placentation and vascular growth further studies on the alteration of Ang II response specifically within the placenta are of interest. Past studies have shown that maternal nano-TiO_2 inhalation exposure across gestation results in increased vascular resistance within placental units as well as increased Ang II sensitivity [4]. Additionally, Ang II has been linked to regulating placental vascular tone in the pathology of preeclampsia [49].

We conclude that maternal nano-TiO_2 inhalation exposure is strongly associated with alterations in vascular reactivity, decreased fetal weight and decreased placental

efficiency that are dependent on the gestational time-period in which the exposure occurs. Our findings strongly suggest that inhalation exposure during early gestation robustly alters vascular response during a critical time period normally hallmarked by decreased vascular resistance and increased blood flow. These adjustments are imperative to nutrient delivery and waste exchange. When reactivity is altered, endothelium-dependent vasodilation is impaired and increased vasoconstrictor sensitivity to Ang II occurs. Vascular resistance is subsequently increased, and blood flow is compromised. This impaired blood flow, nutrient delivery and vascularization may lead to poor fetal health outcomes, such as the poor placental efficiency and decreased pup size. EE, representing exposure during embryonic development, and LE, representing exposure during fetal development, both showed decreased uterine artery AT_2R density and altered endothelial dependent response, but only EE showed altered Ang II response and poor fetoplacental characteristics. It is therefore entirely possible that these deficits may be due to different underlying mechanisms dependent upon the period of gestation in which they were exposed. Future studies should focus on developing further understanding of these mechanisms.

Declarations

Funding: This work was supported by the following sources: National Institutes of Health: R01-ES015022 (TRN), U54-GM104942 (ECB), F32-HL152534 (ED), T32-AG52375 (KLG)

Conflicts of Interest/ Competing interests: The authors have no relevant financial or non-financial interests to disclose.

Availability of Data and Material: The data sets generated and analyzed during the current study are available from the corresponding author on reasonable request.

Code Availability: Not Applicable

Ethics Approval: Animal studies were reviewed and approval by the Animal Care and Use Committee at West Virginia University (#160200621)

Consent to Participate: Not Applicable

Figure Legends

Fig. 1 Gestational exposure paradigm. Experimental design depicting the three exposure groups and the representation of the gestational periods.

Fig. 2 Nano-TiO_2 aerosol real-time characterizations. Aerosol characterizations were monitored and verified during exposure. Red lines on the size distribution curves represent a log normal fit of the size data. (a) Software controlled aerosol mass concentration over the 6 h exposure paradigm. A feedback system held the mass concentration near the desired 12 mg/m^3 target (red line). (b) Aerosol aerodynamic diameter was assessed using the high-resolution Electrical Low-Pressure Impactor (ELPI) showing a CMD of 157 nm with a geometric standard deviation of 1.73. (c) The diameter was also evaluated using a Scanning Mobility Particle Sizer (SMPS, light gray) and an Aerodynamic Particle Sizer (APS, dark gray) revealing a CMD of 118 nm with a geometric standard deviation of 2.11. (d) A Nano Micro-Orifice Uniform Deposit Impactor (MOUDI) indicated a MMAD of 1.03 µm with a geometric standard deviation of 2.57

Fig. 3 Pup and placental mass and placental efficiency. Combined control weights and placental efficiency versus exposure groups on GD 20 pups. (a) Wet pup mass. (b) Wet placental mass. (c) Wet placental efficiency. (d) Dry pup mass. (e) Dry placental mass. (f) Dry placental efficiency. EE = Early Exposed, ME = Mid Exposed, LE = Late Exposed. *, $P \leq 0.05$ vs control

Fig. 4 Vascular reactivity of naïve and sham-control uterine radial arteries. Dose response curves were generated to assess if vascular reactivity of uterine radial arteries was altered between naïve and control groups. (a) Vascular reactivity following increasing

doses of ACh. (b) Maximum response to ACh across the dose response curve. (c) Vascular reactivity following increasing doses of SNAP. (d) Maximum response to SNAP across the dose response curve. (e) Vascular response following increasing doses of PE. (f) Maximum response to PE across the dose response curve. (g) Vascular response following increasing doses of Ang II. (h) Maximum response to Ang II across the dose response curve. EC = Early Control, MC = Mid Control, LC = Late Control

Fig. 5 Alteration of vascular reactivity following various time-periods of exposure. Dose response curves were generated to assess if vascular reactivity of uterine radial arteries was altered. (a) Vascular reactivity following increasing doses of ACh. (b) Maximum response to ACh across the dose response curve. (c) Vascular reactivity following increasing doses of SNAP. (d) Maximum response to SNAP across the dose response curve. (e) Vascular response following increasing doses of PE. (f) Maximum response to PE across the dose response curve. (g) Vascular response following increasing doses of Ang II. (h) Maximum response to Ang II across the dose response curve. EE = Early Exposed, ME = Mid Exposed, LE = Late Exposed. a, $P \leq 0.05$ EE vs control; b, $P \leq 0.05$ ME vs control; c, $P \leq 0.05$ LE vs control; *, $P \leq 0.05$ vs control

Fig. 6 AT_1R and AT_2R protein concentration in uterine vasculature following nano-TiO_2 inhalation exposure. (a) Representative image of Western blot for protein concentration of AT_1R in control, early exposed (EE), mid exposed (ME), late exposed (LE) uterine vascular tissue and the average relative protein density of AT_1R protein among exposed groups. (b) Representative image of Western blot protein concentration of AT_2R in control, EE, ME, LE uterine vascular tissue and the average relative protein density of AT_2R protein among exposed groups

Fig. 7 Circulating estradiol (E_2) plasma concentration. Circulating levels of E_2 in pg/ml. (a) E_2 concentration in control groups. (b) E_2 concentration in combined control group and exposure groups. EC = Early Control, MC = Mid Control, LC = Late Control. EE = Early Exposed, ME = Mid Exposed, LE = Late Exposed

References

1. Abukabda, A.B., McBride, C.R., Batchelor, T.P., Goldsmith, W.T., Bowdridge, E.C., Garner, K.L., Friend, S., and Nurkiewicz, T.R. (2018). Group II innate lymphoid cells and microvascular dysfunction from pulmonary titanium dioxide nanoparticle exposure. *Part Fibre Toxicol*, *15*(1), 43. DOI: 10.1186/s12989-018-0280-2.

2. Abukabda, A.B., Stapleton, P.A., McBride, C.R., Yi, J., and Nurkiewicz, T.R. (2017). Heterogeneous Vascular Bed Responses to Pulmonary Titanium Dioxide Nanoparticle Exposure. *Front Cardiovasc Med*, *4*, 33. DOI: 10.3389/fcvm.2017.00033.

3. Rossi, S., Savi, M., Mazzola, M., Pinelli, S., Alinovi, R., Gennaccaro, L., Pagliaro, A., Meraviglia, V., Galetti, M., Lozano-Garcia, O., Rossini, A., Frati, C., Falco, A., Quaini, F., Bocchi, L., Stilli, D., Lucas, S., Goldoni, M., Macchi, E., Mutti, A., and Miragoli, M. (2019). Subchronic exposure to titanium dioxide nanoparticles modifies cardiac structure and performance in spontaneously hypertensive rats. *Part Fibre Toxicol*, *16*(1), 25. DOI: 10.1186/s12989-019-0311-7.

4. Abukabda, A.B., Bowdridge, E.C., McBride, C.R., Batchelor, T.P., Goldsmith, W.T., Garner, K.L., Friend, S., and Nurkiewicz, T.R. (2019). Maternal titanium dioxide nanomaterial inhalation exposure compromises placental hemodynamics. *Toxicology and Applied Pharmacology*, *367*, 51-61. DOI: https://doi.org/10.1016/j.taap.2019.01.024.

5. Bowdridge, E.C., Abukabda, A.B., Engles, K.J., McBride, C.R., Batchelor, T.P., Goldsmith, W.T., Garner, K.L., Friend, S., and Nurkiewicz, T.R. (2019). Maternal Engineered Nanomaterial Inhalation During Gestation Disrupts Vascular Kisspeptin Reactivity. *Toxicol Sci*, *169*(2), 524-533. DOI: 10.1093/toxsci/kfz064.

6. Stapleton, P.A., Nichols, C.E., Yi, J., McBride, C.R., Minarchick, V.C., Shepherd, D.L., Hollander, J.M., and Nurkiewicz, T.R. (2015). Microvascular and mitochondrial dysfunction in the female F1

generation after gestational TiO2 nanoparticle exposure. *Nanotoxicology*, *9*(8), 941-951. DOI: 10.3109/17435390.2014.984251.

7. Kunovac, A., Hathaway, Q.A., Pinti, M.V., Goldsmith, W.T., Durr, A.J., Fink, G.K., Nurkiewicz, T.R., and Hollander, J.M. (2019). ROS promote epigenetic remodeling and cardiac dysfunction in offspring following maternal engineered nanomaterial (ENM) exposure. *Part Fibre Toxicol*, *16*(1), 24. DOI: 10.1186/s12989-019-0310-8.

8. Osol, G. and Mandala, M. (2009). Maternal uterine vascular remodeling during pregnancy. *Physiology (Bethesda, Md.)*, *24*, 58-71. DOI: 10.1152/physiol.00033.2008.

9. Rennie, M.Y., Rahman, A., Whiteley, K.J., Sled, J.G., and Adamson, S.L. (2015). Site-Specific Increases in Utero- and Fetoplacental Arterial Vascular Resistance in eNOS-Deficient Mice Due to Impaired Arterial Enlargement1. *Biology of Reproduction*, *92*(2). DOI: 10.1095/biolreprod.114.123968.

10. Cipolla, M. and Osol, G. (1994). Hypertrophic and hyperplastic effects of pregnancy on the rat uterine arterial wall. *American Journal of Obstetrics & Gynecology*, *171*(3), 805-811. DOI: 10.5555/uri:pii:0002937894901023.

11. Sheppard, S.J. and Khalil, R.A. (2010). Risk factors and mediators of the vascular dysfunction associated with hypertension in pregnancy. *Cardiovasc Hematol Disord Drug Targets*, *10*(1), 33-52. DOI: 10.2174/187152910790780096.

12. Walther, T., Jank, A., Heringer-Walther, S., Horn, L.C., and Stepan, H. (2008). Angiotensin II type 1 receptor has impact on murine placentation. *Placenta*, *29*(10), 905-909. DOI: 10.1016/j.placenta.2008.07.006.

13. Morgan, T., Craven, C., and Ward, K. (1998). Human spiral artery renin-angiotensin system. *Hypertension*, *32*(4), 683-687. DOI: 10.1161/01.hyp.32.4.683.

14. Hering, L., Herse, F., Geusens, N., Verlohren, S., Wenzel, K., Staff, A.C., Brosnihan, K.B., Huppertz, B., Luft, F.C., Muller, D.N., Pijnenborg, R., Cartwright, J.E., and Dechend, R. (2010). Effects of circulating and local uteroplacental angiotensin II in rat pregnancy. *Hypertension*, *56*(2), 311-318. DOI: 10.1161/HYPERTENSIONAHA.110.150961.

15. Takeda-Matsubara, Y., Iwai, M., Cui, T.X., Shiuchi, T., Liu, H.W., Okumura, M., Ito, M., and Horiuchi, M. (2004). Roles of angiotensin type 1 and 2 receptors in pregnancy-associated blood pressure change. *Am J Hypertens*, *17*(8), 684-689. DOI: 10.1016/j.amjhyper.2004.03.680.

16. Mishra, J.S., Gopalakrishnan, K., and Kumar, S. (2018). Pregnancy upregulates angiotensin type 2 receptor expression and increases blood flow in uterine arteries of rats. *Biol Reprod*, *99*(5), 1091-1099. DOI: 10.1093/biolre/ioy130.

17. Anton, L., Merrill, D.C., Neves, L.A., Stovall, K., Gallagher, P.E., Diz, D.I., Moorefield, C., Gruver, C., Ferrario, C.M., and Brosnihan, K.B. (2008). Activation of local chorionic villi angiotensin II levels but not angiotensin (1-7) in preeclampsia. *Hypertension*, *51*(4), 1066-1072. DOI: 10.1161/HYPERTENSIONAHA.107.103861.

18. Delforce, S.J., Lumbers, E.R., Ellery, S.J., Murthi, P., and Pringle, K.G. (2019). Dysregulation of the placental renin-angiotensin system in human fetal growth restriction. *Reproduction*, *158*(3), 237-245. DOI: 10.1530/REP-18-0633.

19. Ghosh, A., Freestone, N.S., Anim-Nyame, N., and Arrigoni, F.I.F. (2017). Microvascular function in pre-eclampsia is influenced by insulin resistance and an imbalance of angiogenic mediators. *Physiol Rep*, *5*(8). DOI: 10.14814/phy2.13185.

20. Pintican, D., Poienar, A.A., Strilciuc, S., and Mihu, D. (2019). Effects of maternal smoking on human placental vascularization: A systematic review. *Taiwan J Obstet Gynecol*, *58*(4), 454-459. DOI: 10.1016/j.tjog.2019.05.004.

21. Zhang, Y., Tu, B., Jiang, X., Xu, G., Liu, X., Tang, Q., Bai, L., Meng, P., Zhang, L., Qin, X., Zou, Z., and Chen, C. (2019). Exposure to carbon black nanoparticles during pregnancy persistently damages the cerebrovascular function in female mice. *Toxicology*, *422*, 44-52. DOI: 10.1016/j.tox.2019.04.014.

22. Santos-Rocha, J., Lima-Leal, G.A., Moreira, H.S., Ramos-Alves, F.E., de Sa, F.G., Duarte, G.P., and Xavier, F.E. (2019). Maternal high-sodium intake affects the offspring' vascular renin-angiotensin system promoting endothelial dysfunction in rats. *Vascul Pharmacol*, *115*, 33-45. DOI: 10.1016/j.vph.2019.02.001.

23. Morales-Rubio, R.A., Alvarado-Cruz, I., Manzano-Leon, N., Andrade-Oliva, M.D., Uribe-Ramirez, M., Quintanilla-Vega, B., Osornio-Vargas, A., and De Vizcaya-Ruiz, A. (2019). In utero exposure to ultrafine particles promotes placental stress-induced programming of renin-angiotensin system-related elements in the offspring results in altered blood pressure in adult mice. *Part Fibre Toxicol*, *16*(1), 7. DOI: 10.1186/s12989-019-0289-1.

24. Stapleton, P.A., Minarchick, V.C., Yi, J., Engels, K., McBride, C.R., and Nurkiewicz, T.R. (2013). Maternal engineered nanomaterial exposure and fetal microvascular function: does the Barker hypothesis apply? *Am J Obstet Gynecol*, *209*(3), 227.e221-211. DOI: 10.1016/j.ajog.2013.04.036.

25. *Sprague Dawley Rat: Preferred for Safety and Efficacy, Surgical Modification and Reproductive Studies*, I. Taconic Biosciences, Editor. p. 7-8.

26. Lee, K.Y. and DeMayo, F.J. (2004). Animal models of implantation. *Reproduction*, *128*(6), 679-695. DOI: 10.1530/rep.1.00340.

27. Soares, M.J., Chakraborty, D., Karim Rumi, M.A., Konno, T., and Renaud, S.J. (2012). Rat placentation: an experimental model for investigating the hemochorial maternal-fetal interface. *Placenta*, *33*(4), 233-243. DOI: 10.1016/j.placenta.2011.11.026.

28. Silva, J.F. and Serakides, R. (2016). Intrauterine trophoblast migration: A comparative view of humans and rodents. *Cell Adh Migr*, *10*(1-2), 88-110. DOI: 10.1080/19336918.2015.1120397.

29. Hill, M.A. *Rat Development Stages*. Embryology 2020; Available from: https://embryology.med.unsw.edu.au/embryology/index.php/Rat_Development_Stages.

30. de Rijk, E.P., van Esch, E., and Flik, G. (2002). Pregnancy dating in the rat: placental morphology and maternal blood parameters. *Toxicol Pathol*, *30*(2), 271-282. DOI: 10.1080/019262302753559614.

31. Vercruysse, L., Caluwaerts, S., Luyten, C., and Pijnenborg, R. (2006). Interstitial trophoblast invasion in the decidua and mesometrial triangle during the last third of pregnancy in the rat. *Placenta*, *27*(1), 22-33. DOI: 10.1016/j.placenta.2004.11.004.

32. Fournier, S.B., Kallontzi, S., Fabris, L., Love, C., and Stapleton, P.A. (2019). Effect of Gestational Age on Maternofetal Vascular Function Following Single Maternal Engineered Nanoparticle Exposure. *Cardiovasc Toxicol*, *19*(4), 321-333. DOI: 10.1007/s12012-019-09505-0.

33. Percy, Z., DeFranco, E., Xu, F., Hall, E.S., Haynes, E.N., Jones, D., Muglia, L.J., and Chen, A. (2019). Trimester specific PM2.5 exposure and fetal growth in Ohio, 2007-2010. *Environ Res*, *171*, 111-118. DOI: 10.1016/j.envres.2019.01.031.

34. Cauley, M., Hall, B.J., Abreu-Villaca, Y., Junaid, S., White, H., Kiany, A., Slotkin, T.A., and Levin, E.D. (2018). Critical developmental periods for effects of low-level tobacco smoke exposure on behavioral performance. *Neurotoxicology*, *68*, 81-87. DOI: 10.1016/j.neuro.2018.07.012.

35. Blum, J.L., Chen, L.C., and Zelikoff, J.T. (2017). Exposure to Ambient Particulate Matter during Specific Gestational Periods Produces Adverse Obstetric Consequences in Mice. *Environ Health Perspect*, *125*(7), 077020. DOI: 10.1289/EHP1029.

36. Stapleton, P.A., McBride, C.R., Yi, J., Abukabda, A.B., and Nurkiewicz, T.R. (2018). Estrous cycle-dependent modulation of in vivo microvascular dysfunction after nanomaterial inhalation. *Reprod Toxicol*, *78*, 20-28. DOI: 10.1016/j.reprotox.2018.03.001.

37. Nichols, C.E., Shepherd, D.L., Hathaway, Q.A., Durr, A.J., Thapa, D., Abukabda, A., Yi, J., Nurkiewicz, T.R., and Hollander, J.M. (2018). Reactive oxygen species damage drives cardiac and mitochondrial dysfunction following acute nano-titanium dioxide inhalation exposure. *Nanotoxicology*, *12*(1), 32-48. DOI: 10.1080/17435390.2017.1416202.

38. Nurkiewicz, T.R., Porter, D.W., Hubbs, A.F., Cumpston, J.L., Chen, B.T., Frazer, D.G., and Castranova, V. (2008). Nanoparticle inhalation augments particle-dependent systemic microvascular dysfunction. *Part Fibre Toxicol*, *5*, 1. DOI: 10.1186/1743-8977-5-1.

39. Yi, J., Chen, B.T., Schwegler-Berry, D., Frazer, D., Castranova, V., McBride, C., Knuckles, T.L., Stapleton, P.A., Minarchick, V.C., and Nurkiewicz, T.R. (2013). Whole-body nanoparticle aerosol inhalation exposures. *J Vis Exp*(75), e50263. DOI: 10.3791/50263.

40. Irani, R.A. and Xia, Y. (2011). Renin angiotensin signaling in normal pregnancy and preeclampsia. *Semin Nephrol*, *31*(1), 47-58. DOI: 10.1016/j.semnephrol.2010.10.005.

41. Xiong, X., Demianczuk, N.N., Buekens, P., and Saunders, L.D. (2000). Association of preeclampsia with high birth weight for age. *Am J Obstet Gynecol*, *183*(1), 148-155. DOI: 10.1067/mob.2000.105735.

42. Visser, W. and Wallenburg, H.C. (1991). Central hemodynamic observations in untreated preeclamptic patients. *Hypertension*, *17*(6 Pt 2), 1072-1077. DOI: 10.1161/01.hyp.17.6.1072.

43. Ananth, C.V., Peedicayil, A., and Savitz, D.A. (1995). Effect of hypertensive diseases in pregnancy on birthweight, gestational duration, and small-for-gestational-age births. *Epidemiology*, *6*(4), 391-395. DOI: 10.1097/00001648-199507000-00011.

44. Barker, D.J. (1990). The fetal and infant origins of adult disease. *Bmj*, *301*(6761), 1111. DOI: 10.1136/bmj.301.6761.1111.

45. Renna, N.F., de Las Heras, N., and Miatello, R.M. (2013). Pathophysiology of vascular remodeling in hypertension. *Int J Hypertens*, *2013*, 808353. DOI: 10.1155/2013/808353.

46. Matavelli, L.C. and Siragy, H.M. (2015). AT2 receptor activities and pathophysiological implications. *J Cardiovasc Pharmacol*, *65*(3), 226-232. DOI: 10.1097/FJC.0000000000000208.

47. Yang, J., Shang, J., Zhang, S., Li, H., and Liu, H. (2013). The role of the renin-angiotensin-aldosterone system in preeclampsia: genetic polymorphisms and microRNA. *J Mol Endocrinol*, *50*(2), R53-66. DOI: 10.1530/JME-12-0216.

48. Armando, I., Jezova, M., Juorio, A.V., Terron, J.A., Falcon-Neri, A., Semino-Mora, C., Imboden, H., and Saavedra, J.M. (2002). Estrogen upregulates renal angiotensin II AT(2) receptors. *Am J Physiol Renal Physiol*, *283*(5), F934-943. DOI: 10.1152/ajprenal.00145.2002.

49. Gao, Q., Tang, J., Li, N., Zhou, X., Li, Y., Liu, Y., Wu, J., Yang, Y., Shi, R., He, A., Li, X., Zhang, Y., Chen, J., Zhang, L., Sun, M., and Xu, Z. (2017). A novel mechanism of angiotensin II-regulated placental vascular tone in the development of hypertension in preeclampsia. *Oncotarget*, *8*(19), 30734-30741. DOI: 10.18632/oncotarget.15416.

Table 1. Dam physical characteristics on GD 20. EC = Early Control, EE = Early Exposed, MC = Mid Control, ME = Mid Exposed, LC = Late Control, LE = Late Exposed. N represents number of animals. Data are mean ± SE

	N	Age (d)	Weight (g)
Naïve	14	88±9	363±11
EC	17	105±7	369±7
EE	19	94±8	343±8
MC	16	79±5	363±8
ME	19	85±6	365±7
LC	17	83±9	372±9
LE	17	74±6	353±6

Table 2. Pup sex distribution assessed on GD 20. EE= Early Exposed, ME = Mid Exposed, LE = Late Exposed. Data are mean ± SE

	Litter Size	% Female	% Male
Control	11±1	54±2	46±2
EE	9±1	59±5	41±5
ME	13±1	59±5	41±5
LE	11±1	51±4	49±4

Table 3. Uterine radial artery characteristics on GD 20. EE = Early Exposed, ME = Mid Exposed, LE = Late Exposed. n represents number of vessels assessed. Data are mean ± SE. *, P ≤ 0.05 vs control

	n	Inner Diameter (µm)	Passive Inner Diameter (µm)	Passive Outer Diameter (µm)	Wall Thickness (WT)	Wall to Lumen Ratio (WLR)	Wall Tension (N/m)	Tone (%)
Control	70	106±7	149±9	177±11	14±1	0.10±0.01	0.80±0.05	31±2
EE	13	90±12	133±15	135±18	16±3	0.12±0.01*	0.72±0.10	33±3
ME	17	102±12	151±15	179±18	14±1	0.10±0.01	0.80±0.08	35±3
LE	18	109±18	166±24	197±28	15±2	0.09±0.01	1.02±0.13	38±5

Fig. 1

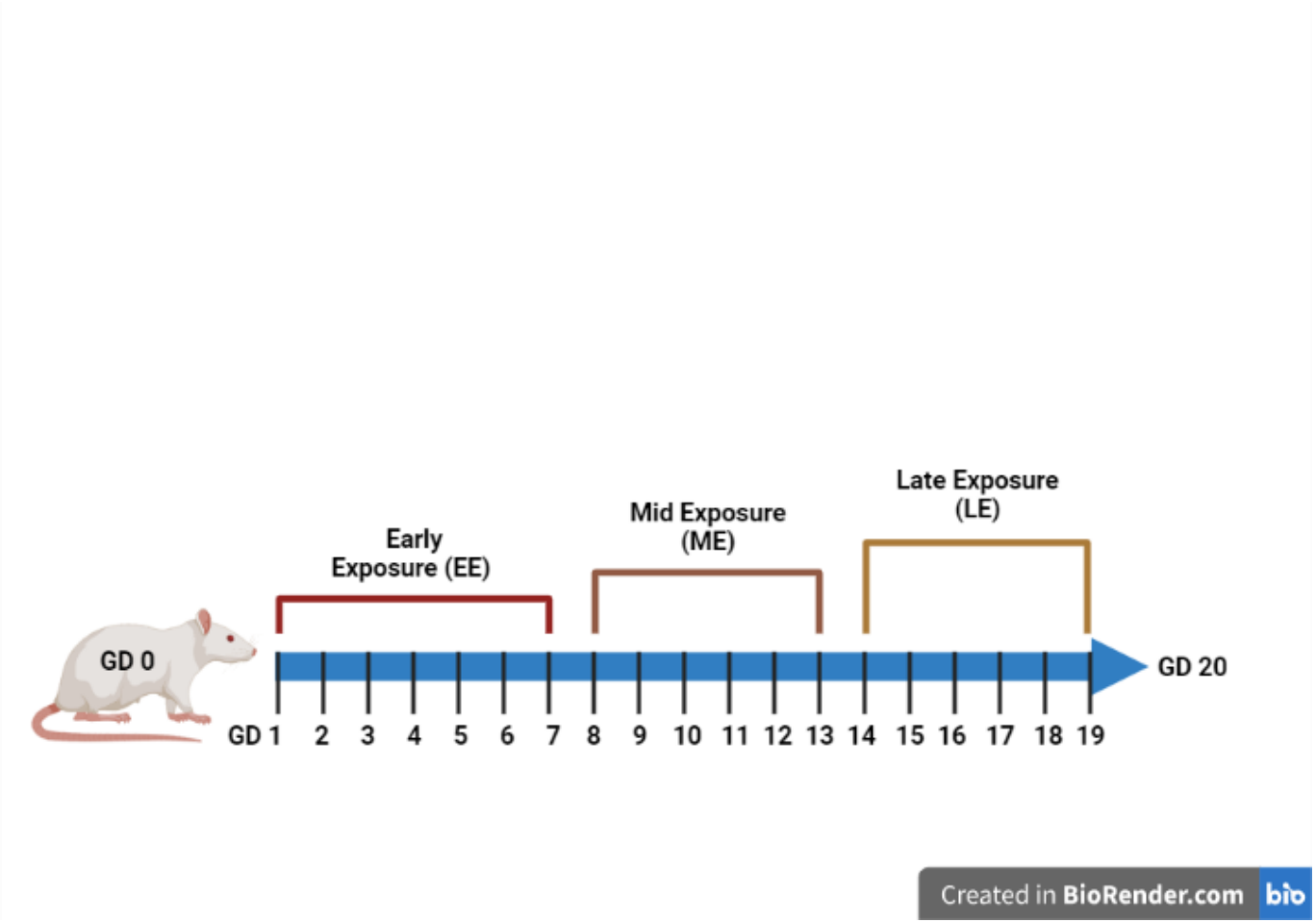
Late Exposure
(LE)
Mid Exposure
(ME)
Early
Exposure (EE)
GD 0
GD 20
GD 1 2 3 4 5 6 7 8 9 10 11 12 13 14 15 16 17 18 19
Created in BioRender.com
bio

Fig. 2

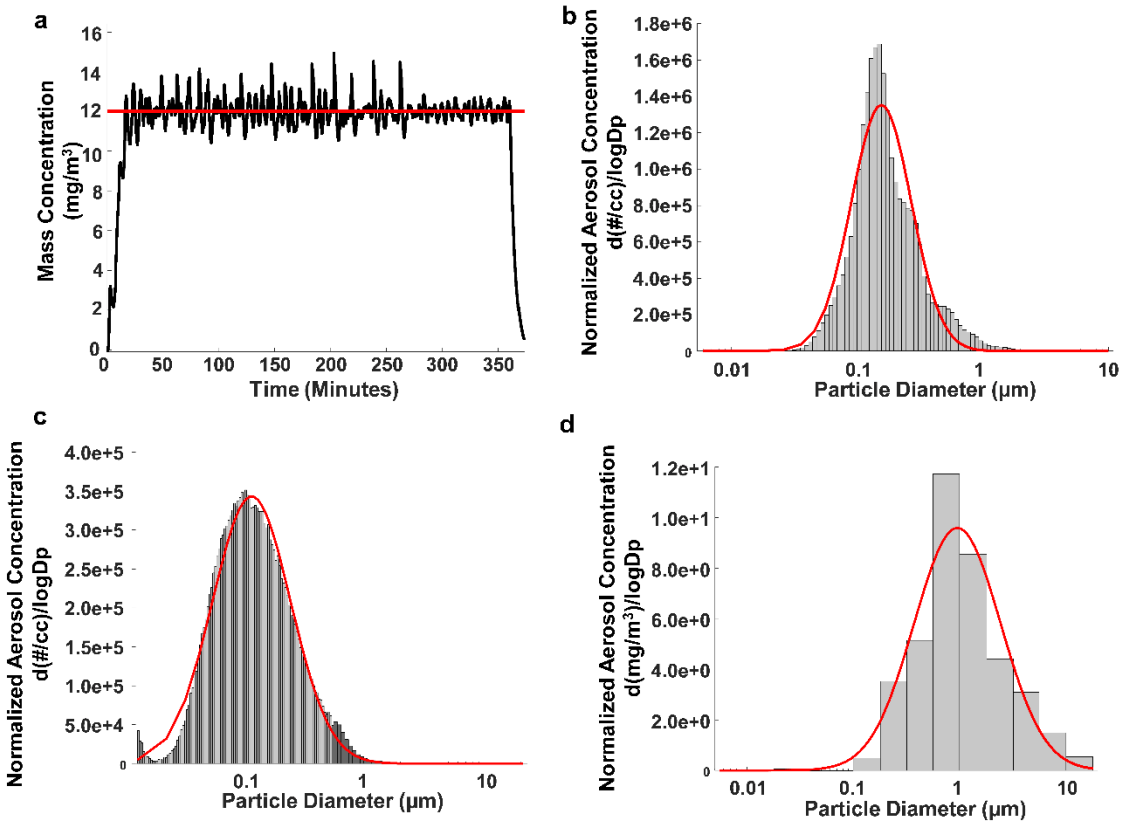
a
Mass Concentration (mg/m³)
Time (Minutes)
b
Normalized Aerosol Concentration d(#/cc)/logDp
Particle Diameter (µm)
c
Normalized Aerosol Concentration d(#/cc)/logDp
Particle Diameter (µm)
d
Normalized Aerosol Concentration d(mg/m³)/logDp
Particle Diameter (µm)

Fig. 3

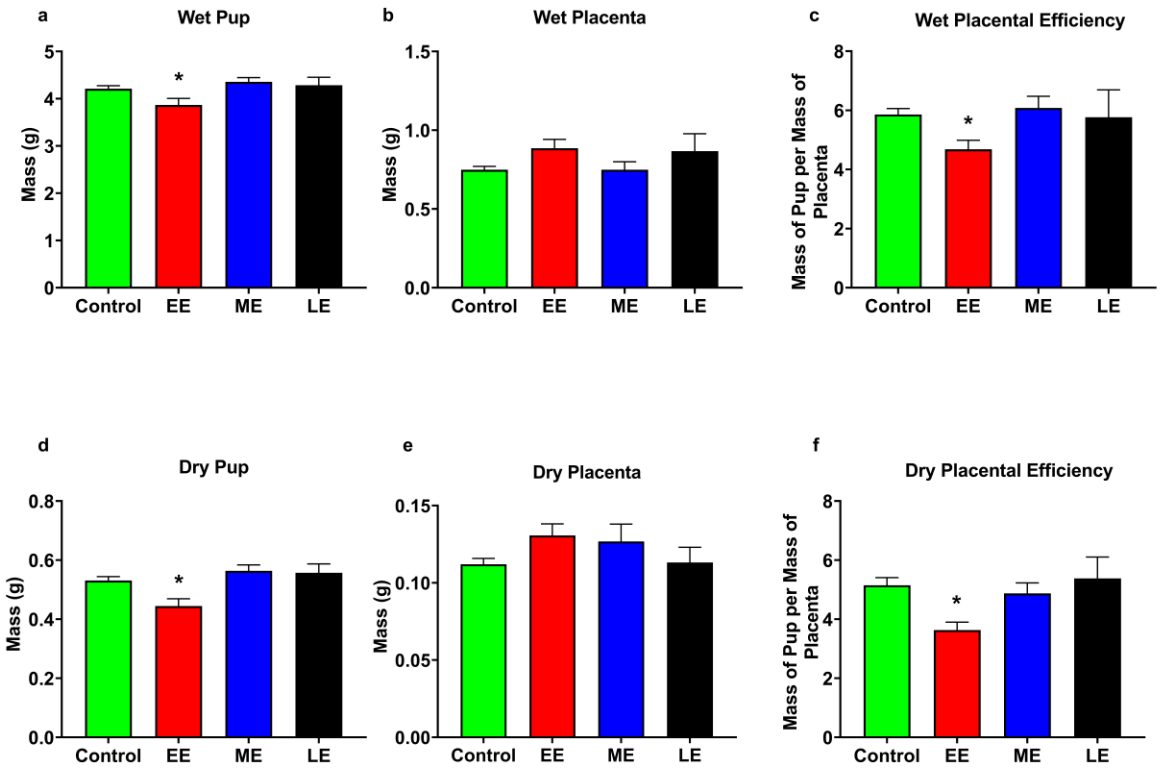
a
Wet Pup
Mass (g)
5
4
3
2
1
0
*
Control
EE
ME
LE
b
Wet Placenta
Mass (g)
1.5
1.0
0.5
0.0
Control
EE
ME
LE
c
Wet Placental Efficiency
Mass of Pup per Mass of Placenta
8
6
4
2
0
*
Control
EE
ME
LE
d
Dry Pup
Mass (g)
0.8
0.6
0.4
0.2
0.0
*
Control
EE
ME
LE
e
Dry Placenta
Mass (g)
0.15
0.10
0.05
0.00
Control
EE
ME
LE
f
Dry Placental Efficiency
Mass of Pup per Mass of Placenta
8
6
4
2
0
*
Control
EE
ME
LE

Fig. 4

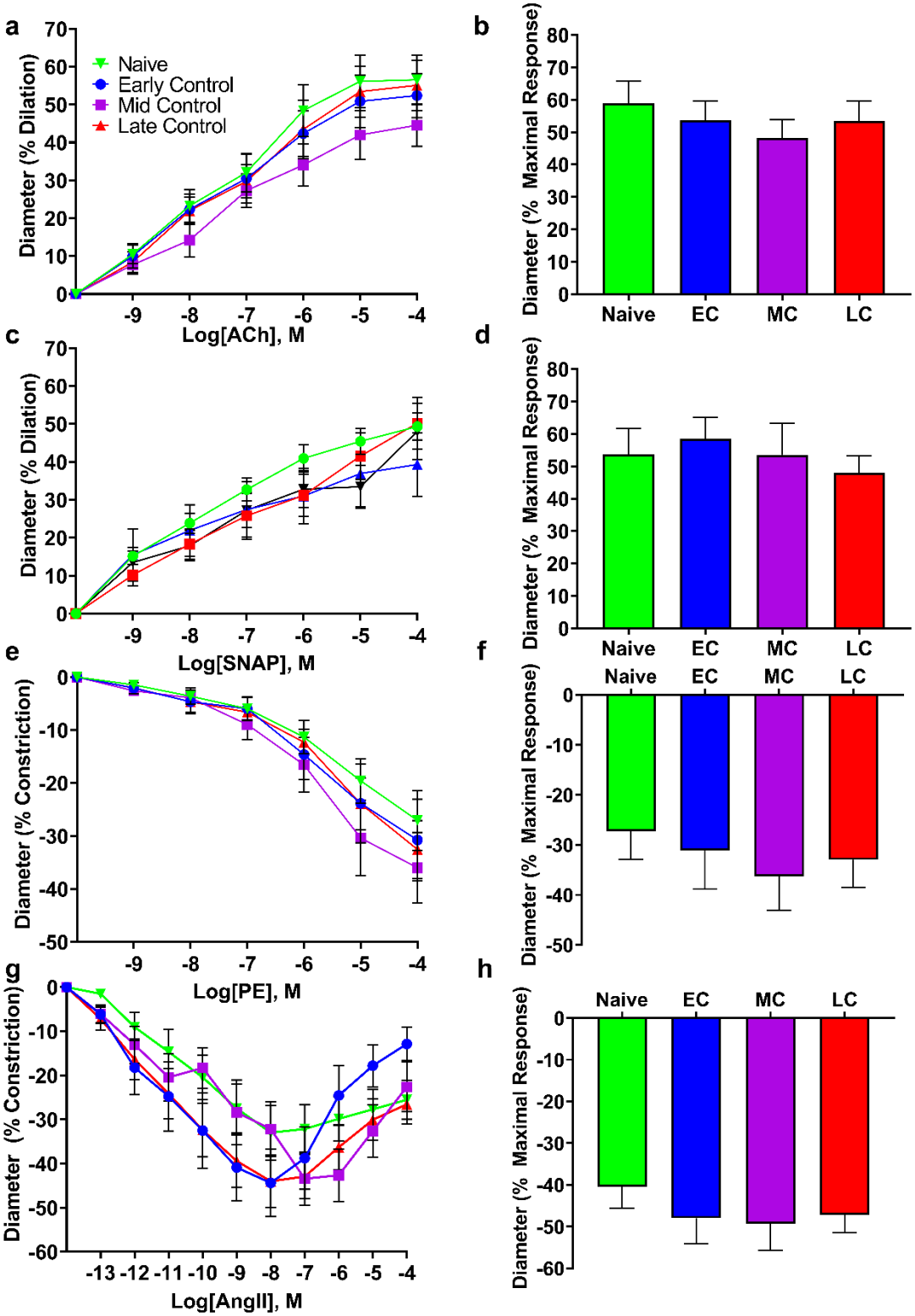
a
Naive
Early Control
Mid Control
Late Control
Diameter (% Dilation)
Log[ACh], M
b
Diameter (% Maximal Response)
Naive
EC
MC
LC
c
Diameter (% Dilation)
Log[SNAP], M
d
Diameter (% Maximal Response)
e
Diameter (% Constriction)
Log[PE], M
f
Diameter (% Maximal Response)
g
Diameter (% Constriction)
Log[AngII], M
h
Diameter (% Maximal Response)

Fig. 5

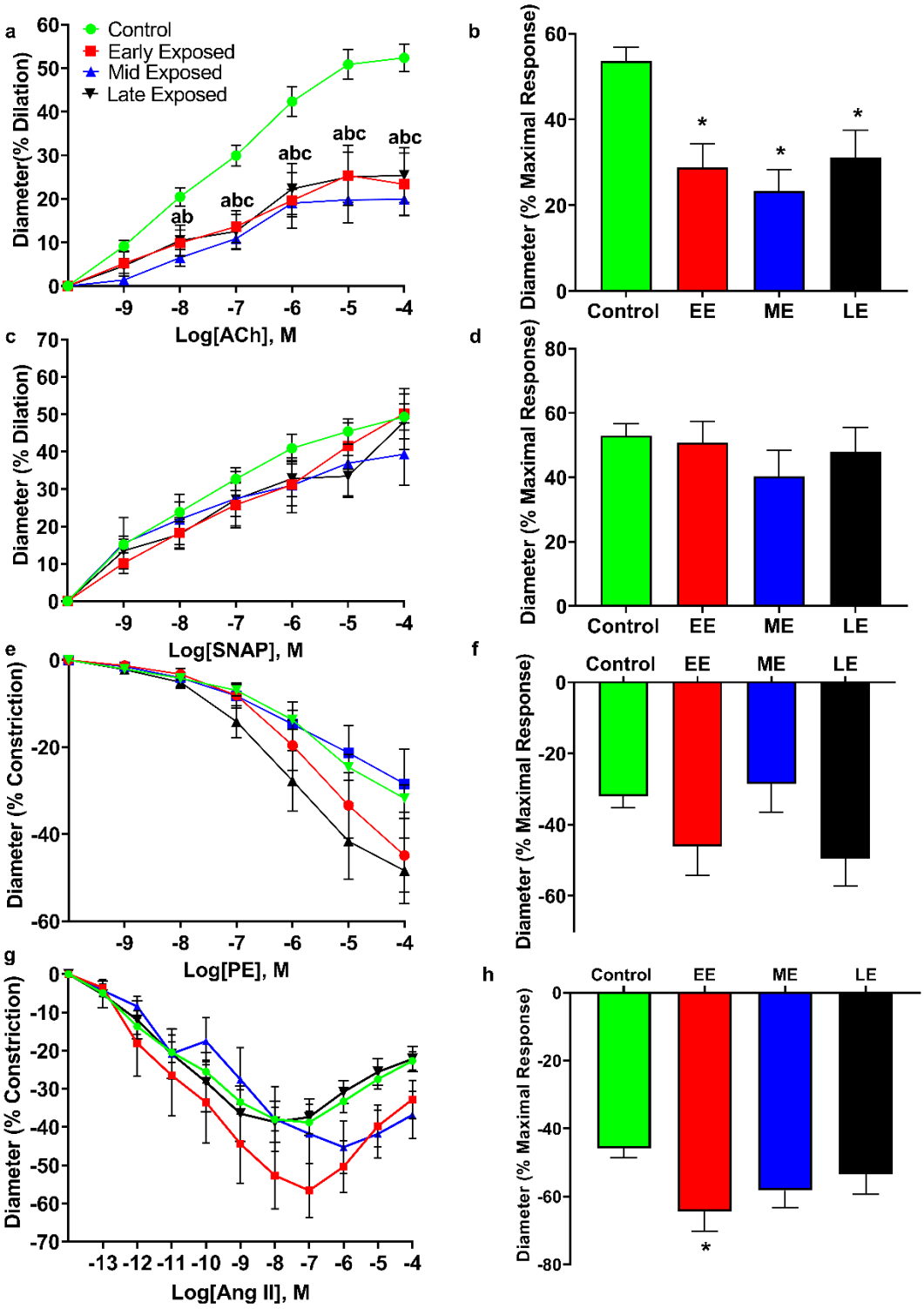
a
Control
Early Exposed
Mid Exposed
Late Exposed
Diameter(% Dilation)
Log[ACh], M
ab
abc
abc
abc
abc
b
Diameter (% Maximal Response)
Control
EE
ME
LE
c
Diameter (% Dilation)
Log[SNAP], M
d
Diameter (% Maximal Response)
Control
EE
ME
LE
e
Diameter (% Constriction)
Log[PE], M
f
Diameter (% Maximal Response)
Control
EE
ME
LE
g
Diameter (% Constriction)
Log[Ang II], M
h
Diameter (% Maximal Response)
Control
EE
ME
LE

Fig. 6

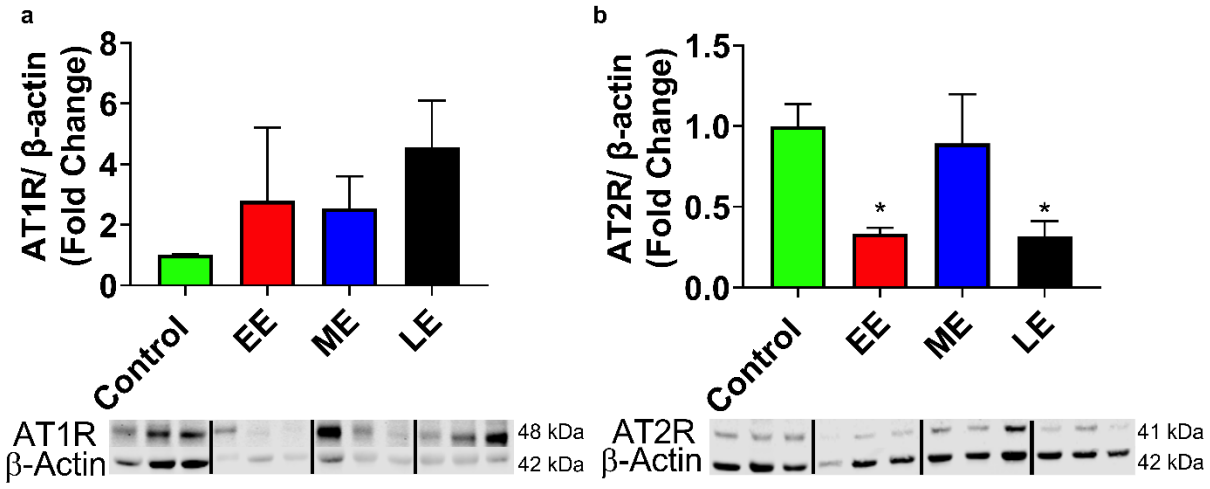
a
AT1R/ β-actin (Fold Change)
8
6
4
2
0
Control
EE
ME
LE
AT1R
β-Actin
48 kDa
42 kDa
b
AT2R/ β-actin (Fold Change)
1.5
1.0
0.5
0.0
*
*
Control
EE
ME
LE
AT2R
β-Actin
41 kDa
42 kDa

Fig. 7

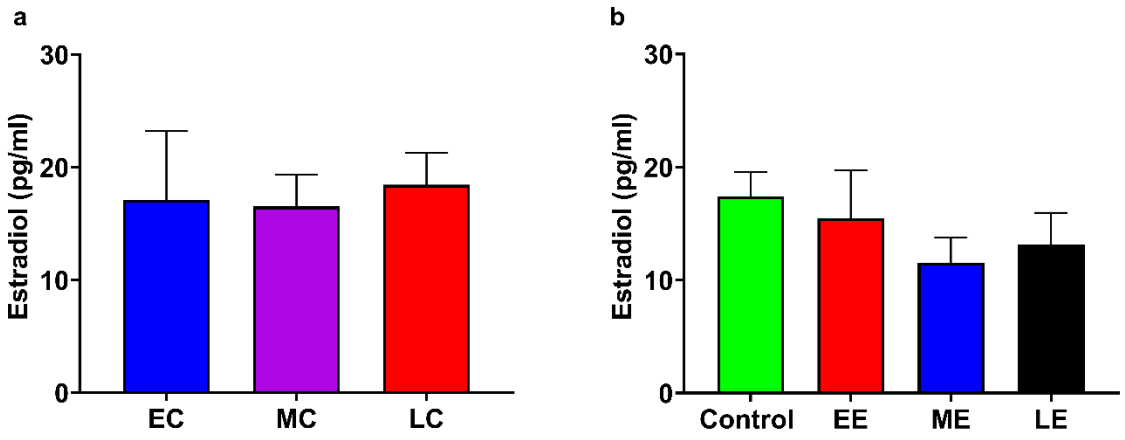
a
Estradiol (pg/ml)
30
20
10
0
EC
MC
LC
b
Estradiol (pg/ml)
30
20
10
0
Control
EE
ME
LE

Supplementary Information

Article Title: Maternal Nanomaterial Inhalation Exposure: Critical Gestational Period in the Uterine Microcirculation is Angiotensin II Dependent

Journal: Cardiovascular Toxicology

Authors: Krista L. Garner[1,2], Elizabeth C. Bowdridge[1,2], Julie A. Griffith[1,2], Evan DeVallance[1,2], Madison G. Seman[3], Kevin J. Engels[1], Caroline P. Groth[4], William T. Goldsmith[1,2], Kim Wix[1], Thomas P. Batchelor[1,2], and Timothy R. Nurkiewicz[1,2*]

Affiliation:

[1]Department of Physiology and Pharmacology, West Virginia University School of Medicine, Morgantown, WV

[2]Center for Inhalation Toxicology (iTOX), West Virginia University School of Medicine, Morgantown, WV

[3]Division of Exercise Physiology, West Virginia University School of Medicine, Morgantown, WV

[4]Department of Epidemiology and Biostatistics, West Virginia University School of Public Health, Morgantown, WV

Declarations

Funding: This work was supported by the following sources: National Institutes of Health R01 ES015022 (TRN), WV-CTSI U54 GM104942-05 (ECB), NHLBI F32 HL152534-01 (ED), 5 T32 AG 52375-3 (KLG)

Conflicts of Interest/ Competing interests: The authors have no relevant financial or non-financial interests to disclose.

Availability of Data and Material: The data sets generated and analyzed during the current study are available from the corresponding author on reasonable request.

Code Availability: Not Applicable

Ethics Approval: Animal studies were reviewed and approval by the Animal Care and Use Committee at West Virginia University (#160200621)

Consent to Participate: Not Applicable

Supplemental Table 1 Pup and placental physical characteristics from GD 20 collection for all control and naïve groups. EC = Early Control, MC = Mid Control, LC= Late Control. Data are mean ± SE

	Wet Pup Weight (g)	Wet Placental Weight (g)	Placental Efficiency (grams fetus/grams placenta)	Dry Pup Weight (g)	Dry Placental Weight (g)	Placental Efficiency (grams fetus/grams placenta)
Naïve	4.27±0.23	0.77±0.04	6.88±0.13	0.48±0.04	0.114±0.005	4.30±0.33
EC	4.02±0.09	0.78±0.04	5.32±0.26	0.52±0.01	0.108±0.008	5.25±0.58
MC	4.26±0.08	0.78±0.04	5.74±0.43	0.57±0.03	0.121±0.009	5.01±0.46
LC	4.26±0.15	0.78±0.13	6.23±0.63	0.54±0.02	0.116±0.011	5.45±0.59

Supplemental Table 2 Pup sex distribution assessed on GD 20 for all control and naïve groups. EC = Early Control, MC = Mid Control, LC= Late Control. Data are mean ± SE

	Litter Size	% Female	% Male
Naïve	12±1	54±3	46±3
EC	10±1	54±6	46±6
MC	11±1	52±3	48±3
LC	12±1	52±3	48±3

Supplemental Table 3 Uterine radial artery characteristics on GD 20 for all control and naïve groups. EC = Early Control, MC = Mid Control, LC= Late Control. n represents number of vessels assessed. Data are mean ± SE

	n	Inner Diameter (µm)	Passive Inner Diameter (µm)	Passive Outer Diameter (µm)	Wall Thickness (WT)	Wall to Lumen Ratio (WLR)	Wall Tension (N/m)	Tone (%)
Naïve	20	110±14	153±18	180±20	14±1	0.10±0.01	0.98±0.09	30±2
EC	15	109±15	146±19	171±22	12±2	0.10±0.01	0.78±0.10	28±4
MC	17	109±14	150±17	180±21	15±2	0.10±0.01	0.89±0.09	29±3
LC	18	98±15	147±20	174±24	14±2	0.09±0.01	0.86±0.11	34±3

IV. Chapter 4

Using the Isolated Rat Placenta to Assess Fetoplacental Hemodynamics

Citation: Garner, K. L., Bowdridge, E. C., DeVallance, E., Griffith, J. A., Kelley, E. E., & Nurkiewicz, T. R. (2022). Using the Isolated Rat Placenta to Assess Fetoplacental Hemodynamics. *Frontiers in toxicology*, *4*, 814071. https://doi.org/10.3389/ftox.2022.814071

Authors:

Garner, K.L.

Bowdridge, E.C.

DeVallance, E.

Griffith, J.A.

Kelley, E.E.

Nurkiewicz, T.R.

Affiliations:

Department of Physiology and Pharmacology, West Virginia University School of Medicine, Morgantown, WV

Center for Inhalation Toxicology (iTOX), West Virginia University School of Medicine, Morgantown, WV

Abstract

Placental health is critical to fetal growth and maternal health during gestation. However, investigating placental flow in an ex-vivo isolated system where inflow is independently controlled has yet to be developed in the rat. Here, we describe a novel technique, isolated perfused placenta technique that allows for analysis of placental pressure outflow pressure, placental flow in rats at gestational day 20. Using this method, we successfully perfused placentas from dams and were able to observe increases in outflow pressure and flow as the inflow pressure to the placenta was increased in a step wise fashion. This method will help to advance the functional analysis of placental flow and therefore placental resistance and efficiency.

Introduction

The rat has been long established as an ideal animal model to study both pregnancy and the fetoplacental interface due to its similarities with the human. Despite the fact that some differences exist between the two species, the function of the discoid placenta and the lineage of the cells comprising the maternal-fetal interface are overwhelmingly comparable [1]. Additionally, the rat and human both have a hemochorial placenta in which only two fetal cell layers are crossed in the exchange of molecules between the dam and fetus [1]. However, it should be noted that the rat has one layer of cytotrophoblast compared to two layers of syncytiotrophblast cells, whereas the human placenta has one only layer of each trophoblast cells type separating the maternal and fetal blood systems [2]. Given the similarities between the species, this model provides scientists with the opportunity to study physiological processes and challenges to homeostasis that would otherwise be ethically impossible in humans.

Fetal and placental weights at or near birth are positively correlated and are often used as an indicator of the ability of the placenta to provide the appropriate amount of nutrients to the fetus [3]. Placental efficiency (gram of pup per gram of placenta [4]), is often used as a metric of pregnancy health. Placental efficiency ranges from 5 g/g in humans to 20 g/g in horses [3]. Decreased placental efficiency is usually an indicator of poor placental vascularization that has occurred during gestation and/or insufficient maternal blood flow to the placenta. Conversely, deprivation of caloric or protein intake reduces oxidation substrates and may contribute to increased placental efficiency. Ultimately, a decrease in maternal blood flow or improper placental vascularization, lead to decreased placental

transport of nutrients and oxygen exchange through flow-limited passive diffuse processes [5]. This may potentially contribute to smaller fetuses at term.

Environmental factors may also lead to decreased efficiency within the placenta, one of which being toxicant exposure during critical windows of gestational development. Considering the growing number of toxicants humans are exposed to throughout our lifetime, safety assessment of these known toxicants, the doses and discovery of new toxicants, is critical to improving fetal and maternal health. Therefore, a need exists to be able to discreetly study placental physiology under tightly controlled conditions. We have developed a rat model of gestational toxicant exposure, through which placental flow can be assessed. This model is unique in regard to assessment of hemodynamics within the placenta proper and does so without the involvement of any maternal vascular inputs. Other groups have successfully used an ex vivo placental perfusion model to study the transfer of chemical compounds from dam to fetus in rats [6] and in humans [7]. Placental flow and pressure are assessed by manipulating input pressure over the physiological range via the umbilical artery and measuring the output flow pressure delivered to the umbilical vein. Dissipation of pressure and flow rate across this circuit is a function of vascular resistance, which has active (umbilical artery and vein tone) and passive elements (anatomical structure within the placenta, vessel bifurcation). Both these elements can be assessed with this model. Using a modified pressure myography chamber, inflow pressure to the placental unit is independently controlled, and outflow pressure and placental flow are recorded. Further, this model allows for assessment of multiple placentas from the same dam and characterization of placental hemodynamics as determined by sex of the fetus, placement within the uterine horn, and many other

factors. We present data herein that demonstrate our ability to modify this chamber, and reliability and successfully measure placental flow in rats.

Materials and Equipment

Equipment- Isolated vessel chamber (CH-1; Living Systems; St. Albans, VT), pressure servo pump (PS-200-P; Living Systems; St. Albans, VT), pressure monitor (PS-200-S; Living Systems; St. Albans, VT), peristaltic pump (Masterflex L/S 77200-60; Living Systems Instrumentation, St. Albans, VT), size matched glass pipettes (~300 µm; Living Systems; St. Albans, VT), dissecting dish, forceps, scissors, silk braided suture (9-0; Unify #S-S918R13), LabChart software (AD Instruments, Colorado Springs, CO). Livings Systems chambers were selected as this is a complete integrated system that can be easily adapted to the isolated placenta. CH-1 chambers were selected because the entire chamber can be enclosed and pressurized, and temperature controlled. LabChart Software was chosen because it has the ability to record the digital data output from the Living Systems equipment (pressure, flow, vessel diameter).

Solutions- Physiological salt solution (PSS, in mmol/L: 129.8 NaCl, 5.4 KCl, 0.5 NaH_2PO_4, 0.83 $MgSO_4$, 19.0 $NaHCO_3$, 1.8 $CaCl_2$, 5.5 glucose), Calcium free-PSS (Ca^{2+} -free).

Methods

Pregnant Sprague Dawley rats (Hilltop, Scottdale, PA) at gestational day (GD) 20 are anesthetized under general anesthesia (isoflurane gas, 5% induction, and 2% maintenance) and placed on a heating pad to maintain at 37 ºC rectal temperature. The uterus is harvested and placed in Ca^{2+} -free PSS (4 ºC) in a chilled circulation dish

(Preparatory Tissue Bath, #158401; Radonti; Covina, CA) and maintained at this temperature with a circulating chiller (IsoTemp 3016D; Fisher Scientific). The left and right uterine horns are pinned out. A tissue section containing the fetus, placenta, uterine wall and supplying vasculature are surgically excised and transferred to a clean dissection dish. The uterine wall is cut longitudinally, and the umbilical cord is cut as close to the fetus as possible immediately prior to mounting the placenta in the chamber. All uterine vascular conduits are ligated with 9-0 silk suture to contain perfusate flow exclusively to the fetal side of the placenta and maintain intervillous volume/pressure (Fig. 1a-c). Ligating all the maternal vascular inputs is one unique aspect of this placenta flow model and assures that any changes in flow that are observed are due to hemodynamic alterations within the placenta. The vitelline artery is removed, and the umbilical cord is opened to reveal the paired umbilical artery and vein. The umbilical artery and vein are gently dissected away from one another from the umbilical stalk of the fetus (Fig. 1a) up to the insertion point of the vessels into the placenta (Fig. 1c). A magnified view of the distinction between the umbilical artery and vein compared to the vitelline artery and chorionic vessels can be seen in Fig. 2. Connective tissue is gently dissected/cleaned, and the artery is mounted on a size-matched pipette (~300 µm). The umbilical artery is placed onto the inflow pipette and securely tied with 9-0 silk braided suture (Fig. 3). The umbilical vein is left unmounted so that residual blood within the placenta can be gently flushed under low pressure prior to starting the experiment (Fig. 4a). This step is critical to obtain accurate flow readings throughout the experiment. Once the blood has been removed from the placenta the umbilical vein is securely tied to the outflow pipette (Fig 4b). The tissue preparation is now ready for study using the Living Systems chambers

(St. Albans, VT) and measurement of inflow and outflow pressure as well as placental flow using LabChart software (Colorado Springs, CO). The completed preparation is presented in Fig. 4c. The chamber is maintained at 37 ºC, and the perfusate and superfusate are continuously bubbled with 21% O2 - 5% CO2. To begin the experiment, inflow pressure within the umbilical artery is increased in a stepwise fashion by 5 mm Hg, starting at 0 mm Hg, until maximum pressure is reached (~40-60 mm Hg). At each incremental increase in pressure a steady state outflow pressure is reached (approximately 2 minutes) prior to the subsequent increase in pressure. We typically experience resistance across the placenta where outflow pressure is approximately half of inflow pressure under normal superfusate conditions in control placentas. Any treatment administered to the dam prior to tissue harvest, or pharmacological treatment within the bath can affect this resistance. Once the initial pressure with PSS has been established as the baseline the bath is washed and treatment of the placenta with pharmacological agents of interest can be added and the incremental increase in inflow pressure repeated. The successfully prepared placental unit once dissected is viable for up to 4 hours when kept on ice from the time of tissue removal from the dam. Viability is assessed as the ability to cannulate the umbilical artery and vein without tissue degradation as well as pressurize the placenta with resultant outflow measurements. Because maternal/fetal placental integrity begins to drop at the time of tissue harvest it is imperative to verify pressurization is being held in the preparation throughout the duration of the experiment. Observing an inability to maintain this indicates the experiment should be ended and the placenta is no longer viable. This has been repeatedly measured in our laboratory over the last 4 years when we began using this fetoplacental preparation in a

variety of treatment groups at GD 20, and 4 hours has been shown to be the maximum viability time to start an experiment from the time of euthanasia of the dam and removal of tissue. From the time of tissue removal to the end of an experiment, an experienced technician would be able to complete this procedure in 1.5-2 hours. Therefore, the examination of multiple placentas from the same dam is possible once the technique is mastered allowing for more biological repetition and repeatability. Importantly, endothelium-dependent, endothelium-independent relaxation, and vascular smooth muscle contractility as well as mechanotransduction (flow/shear stress and transmural pressure/myogenic responsiveness) are all able to be assessed within this isolated placenta system. Additionally, the influence of local metabolic factors may be assessed by altering [O2], [CO2] and/or temperature.

Results

Analysis Techniques and Preliminary Studies with Isolated Perfused Placenta: In Fig. 5, raw data tracings are provided that establish our proficiency with this novel approach. Perfusate flow (placental input pressure) is manipulated with servo pumps in a stepwise fashion as mentioned above, umbilical artery and vein diameter can be measured simultaneously. Note that changes in pressure and flow can occur independently or in tandem. The critical functional measurements are vascular diameters, perfusate flow, and umbilical vein pressure. Umbilical vein pressure is of greatest interest as it represents placental resistance, post-placental hemodynamic conditions, and blood flow rate returning to the fetus. The placental pressure drop (pressure delta between Fig. 5a-b) is an index of vascular resistance, and therefore placental health. The potential also exists to measure permeability and many fluorescently labeled biomarkers in the vascular wall,

placental unit, effluent, and eluate. Increasing inflow pressure in the setup increases both outflow pressure (Fig. 6a) and flow (Fig. 6b) through the placenta. Additionally, we have previously shown that a pressure drop is observed in nano-TiO_2 placentas (n = 8) compared to controls (n = 10) when placed in Ca^{2+} -free PSS. This reflects increased resistance from an anatomical perspective (altered passive elements/structural changes) due to maternal inhalation exposure during gestation [8]. This is important to note because increased placental resistance is inversely correlated with placental efficiency due to a decrease in vascular density and/or length within the placental circulation. Additionally, we showed decreased outflow pressure in nano-TiO_2 placentas with normal superfusate, acetylcholine and angiotensin II treatment. Overall, we were able to conclude that maternal nano-TiO_2 exposure during gestation impairs fetoplacental hemodynamics.

Discussion

The data presented here reflect our ability to develop a unique, reliable and efficient system to assess placental physiology within the isolated rat placenta. The content of this protocol was presented to demonstrate the utilitarian nature of isolated vessel chambers and repeated three times herein. We have also demonstrated the reliability of this model in previous publications [8]. Placental health is inextricably linked to maternal and fetal health throughout gestation. Perturbations in placental development and/or blood flow throughout gestation leads to poor health outcomes for both the dam and the fetus such as preeclampsia [9], intrauterine growth restriction [5] and gestational diabetes [10]. Examining and understanding how disturbances in adaptations during critical windows of gestation affect fetal and maternal health is essential to improving pre- and postnatal care.

The maintenance of hemodynamic resistance is fundamental in all tissues for the healthy exchange of nutrients and wastes, and preservation of homeostasis. The fetal-placental unit is no exception. We hypothesize that toxicant exposure during gestation disturbs mechanisms of placental vascular resistance and reactivity. Specifically, impairment of endothelium-dependent reactivity would lead to an increased placental resistance, which would appear as lower post placental pressure and flow rate. The health interpretation of this outcome would be that the fetal-placental unit is unable to efficiently remove wastes and gain nutrients leading to placental insufficiency and a smaller pup. It is equally plausible that toxicant exposure during gestation abolishes placental resistance. In that case, uterine artery and vein pressures would closely match, and again, the effective exchange of nutrients and wastes would be impaired, leading to the similar outcome of decreased pup size due to placental insufficiency. Further, the maintenance of extravascular nutrient gradients would be disturbed in the placental interstitium. Utilizing the isolated placenta as a tool to assess fetal and placental health is incredibly valuable because measuring these endpoints after specific gestational insults would advance our understanding, independent of the outcome, of the materno-fetal consequences that follow.

We anticipate two potential challenge areas. First, because the placenta is not fully developed after GD 7, the necessary umbilical vasculature for cannulation may not be present, and in our experience, it is not be possible to perfuse the placenta prior to GD 15 due to fragility and underdevelopment of the umbilical artery and vein. Second, because the placenta begins to slough cells and deteriorate rapidly after delivery, great effort must be made to prevent or slow this process. The placenta is viable for the

experimental protocol for 1.5-2 hours from when it is mounted in the chamber and therefore this technique must be performed rapidly. This is in comparison to the four hours mentioned earlier, which refers to the maximum amount of time after tissue collection that a placenta can be mounted in the chamber for experimentation. The single most important variable in doing this is to avoid a hypoxic environment that stimulates glycolysis. This can be achieved by rapid dissection, temporary placement/preparation in Ca^{2+}- free PSS (4 ºC); and constant bubbling with 21% O2 - 5% CO2. In the event that this is insufficient for all the measurements proposed, the individual components can easily be separated. Additionally, these measurements could also be made in a murine model, as the model has already been established [11]. Independent of animal model, multiple placentas are present per animal, histology and fluorescence measurements, and effluent and eluate collections can be made or prepared rapidly in individual units. Lastly, caution should be taken when directly extrapolating data from this rodent model to human health given the difference in trophoblast cells at the fetal-maternal interface between the rat and human. The isolated placenta holds the potential to examine multiple mechanisms that impair placental efficiency during gestation. Fetal size, sex, placement within the uterus, gestational age, toxicant exposure, blood flow restriction, and treatment of the placenta with circulating gestational or other factors are future areas of research that hold tremendous potential. Our data validate that this model enables the assessment of multiple endpoints within the same placenta. Additionally, by optimizing this technique we report that multiple placentas within the same dam can be utilized for experimentation.

Data Availability Statement

The original contributions presented in the study are included in the article and further inquires can be directed to the corresponding author.

Ethics Statement

Female Sprague Dawley (SD rats) were purchased from Hilltop Laboratories (Scottdale, Pennsylvania), and housed in an Assessment and Accreditation of Laboratory Animal Care (AAALAC) approved facility at West Virginia University (WVU) under a regulated temperature and 12:12 h light-dark cycle. Animal studies were reviewed and approved by the Animals Care and Use Committee at WVU (#160200621). Rats had ad libitum access to food and water throughout the acclimation period. All procedures were approved by the WVU Institutional Animal Care and Use Committee.

Author Contribution

Study design: EB/KG/TN. Data collection: KG. Data interpretation: EB/KG/TN/ED/JG/EK. Manuscript draft: EB/KG. Critical revisions and final decision to submit: all authors. The authors read and approved the final manuscript.

Funding

These studies were supported by the following sources: National Institutes of Health R01 ES015022 (TRN) and U54 GM104942 (ECB),F32 HL152534 (ERD), T32 AG52375 (JAG).

Conflict of Interest

The authors have no conflict(s) of interest to declare.

Publisher's Note

All claims expressed in this article are solely those of the authors and do not necessarily represent those of their affiliated organizations, or those of the publisher, the editors and the reviewers. Any product that may be evaluated in this article, or claim that may be made by its manufacturer, is not guaranteed, or endorsed by the publisher.

Acknowledgments

The author would like to thank WV-CTSI for the support to the authors in funding and the iTOX facility vivarium in which animals were housed.

Figure Legends

Fig. 1 Dissection of umbilical artery and vein. (a) isolated fetoplacental unit with the umbilical artery and vein completely intact. (b) dissection of the umbilical artery (white vessel located on the left) and vein (red vessel on the right) beginning at the insertion int the fetus. (c) umbilical artery and vein completely separated from the fetus to the placenta and ready for transfer to the chamber

Fig. 2 Dissection of placental and chorionic vessels. (a) from left to right: umbilical vein; umbilical artery; vitelline artery and other chorionic vessels. Amnionic membranes can also be seen surrounding the vessels prior to removal. Black arrow indicated the umbilical artery and vein pair while the white arrow shows the vitelline artery and chorionic vessels. (b) placental unit with membranes removed and umbilical artery and vein isolated. Note the chorionic vessels with the white arrow at the top of the figure indicating how closely these two are prior to dissection. Vessel insertion and branching into the placenta can also be seen

Fig. 3 Chamber set up for isolated placenta perfusion. The placental unite with separated umbilical artery and view is placed into the Living Systems chamber with PSS. The umbilical artery is cannulated onto the inflow glass pipette while the umbilical vein is cannulated onto the outflow pipette and tied with braided silk suture. Red arrows indicated the inflow (left, 1) and outflow (right, 2) pipettes

Fig. 4 Preparation of the placental unit prior to starting an experiment. (a) the umbilical artery is cannulated onto the inflow pressure cannula while the umbilical vein is left untied in order to clear the blood from the placenta. Note the pooling blood in the

bottom of the chamber as PSS is flowing through the placenta. (b) both umbilical artery and vein are placed onto and tied to the inflow and outflow cannulas, respectively. No pressure is being applied to the system. (c) the placental is fully pressurized. Note the increase in size and volume of the vessels within the chamber. Again, red arrows indicated inflow (left, 1) and outflow (right, 2) pipettes

Fig. 5 Representative trace of placental flow. (a) input (umbilical artery) perfusion pressure is increased in a stepwise fashion to measure placental resistance. (b) output pressure is measured and a drop in pressure across the placenta is expected and indicative of placental health. (c) alterations in placenta flow (µl/min) can be seen concomitantly with the change in inflow and outflow pressure, indicating placental resistance

Fig. 6 Outflow pressure and flow rate across the inflow pressures. (a) as inflow pressure is increased in a stepwise fashion outflow pressure increases with normal superfusate. (b) alternatively, flow rate can be measured as the result of increasing inflow pressure. (n=3 placentas)

Fig. 7 Graphical representation of the isolated rat placenta model and perfusion pathways. Numbering in the figure represent the following: 1- input pressure pipette; 2- umbilical artery; 3- arteriolar waste delivery network; 4- venular nutrient network return; 5- umbilical vein; 6- output pressure pipette. Arrows show direction of perfusate flow

References

1. Soares, M.J., et al., *Rat placentation: an experimental model for investigating the hemochorial maternal-fetal interface.* Placenta, 2012. **33**(4): p. 233-43.
2. Furukawa, S., N. Tsuji, and A. Sugiyama, *Morphology and physiology of rat placenta for toxicological evaluation.* J Toxicol Pathol, 2019. **32**(1): p. 1-17.
3. Fowden, A.L., et al., *Placental efficiency and adaptation: endocrine regulation.* J Physiol, 2009. **587**(Pt 14): p. 3459-72.
4. Wilson, M.E. and S.P. Ford, *Comparative aspects of placental efficiency.* Reprod Suppl, 2001. **58**: p. 223-32.
5. Fowden, A.L., et al., *Programming placental nutrient transport capacity.* J Physiol, 2006. **572**(Pt 1): p. 5-15.
6. Fournier, S.B., et al., *Nanopolystyrene translocation and fetal deposition after acute lung exposure during late-stage pregnancy.* Part Fibre Toxicol, 2020. **17**(1): p. 55.
7. Conings, S., et al., *Integration and validation of the ex vivo human placenta perfusion model.* J Pharmacol Toxicol Methods, 2017. **88**(Pt 1): p. 25-31.
8. Abukabda, A.B., et al., *Maternal titanium dioxide nanomaterial inhalation exposure compromises placental hemodynamics.* Toxicology and Applied Pharmacology, 2019. **367**: p. 51-61.
9. Brosens, J.J., R. Pijnenborg, and I.A. Brosens, *The myometrial junctional zone spiral arteries in normal and abnormal pregnancies: a review of the literature.* Am J Obstet Gynecol, 2002. **187**(5): p. 1416-23.
10. Holemans, K., et al., *Diet-induced obesity in the rat: a model for gestational diabetes mellitus.* Am J Obstet Gynecol, 2004. **190**(3): p. 858-65.
11. Goeden, N. and A. Bonnin, *Ex vivo perfusion of mid-to-late-gestation mouse placenta for maternal-fetal interaction studies during pregnancy.* Nat Protoc, 2013. **8**(1): p. 66-74.

Fig. 1

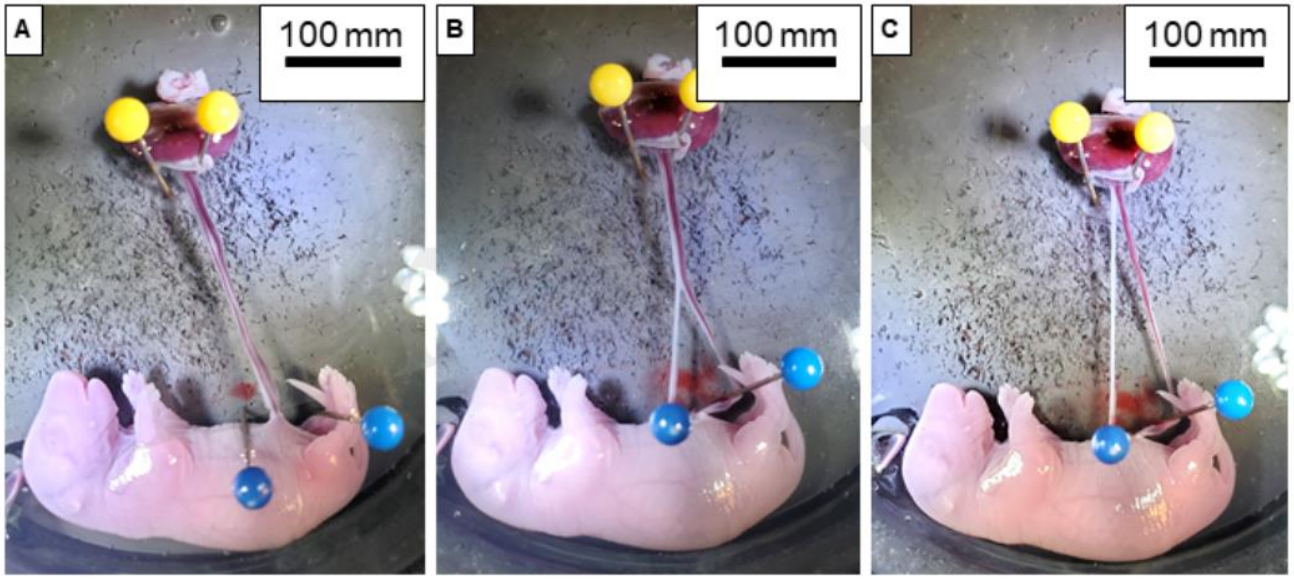

Fig. 2

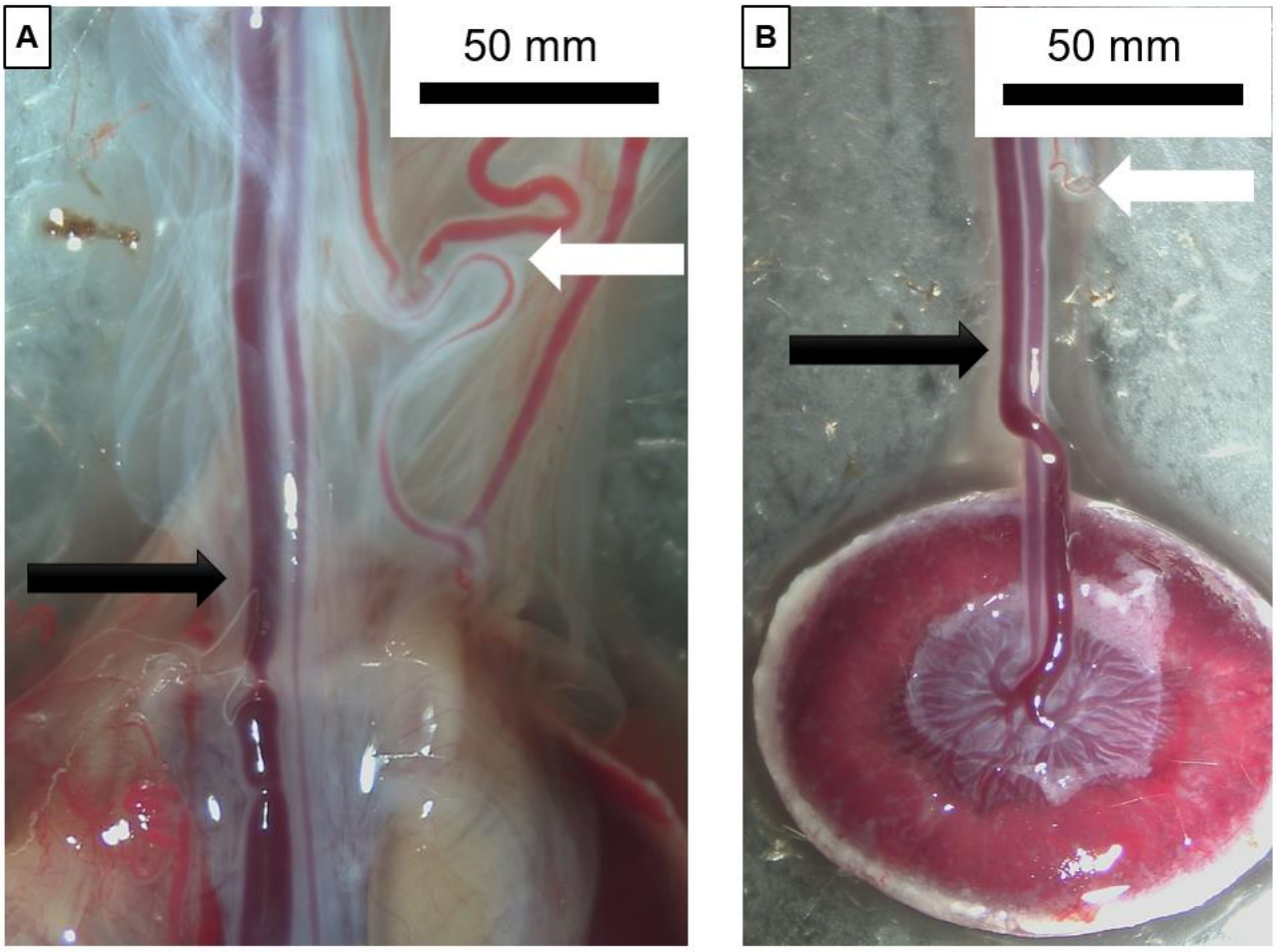

Fig. 3

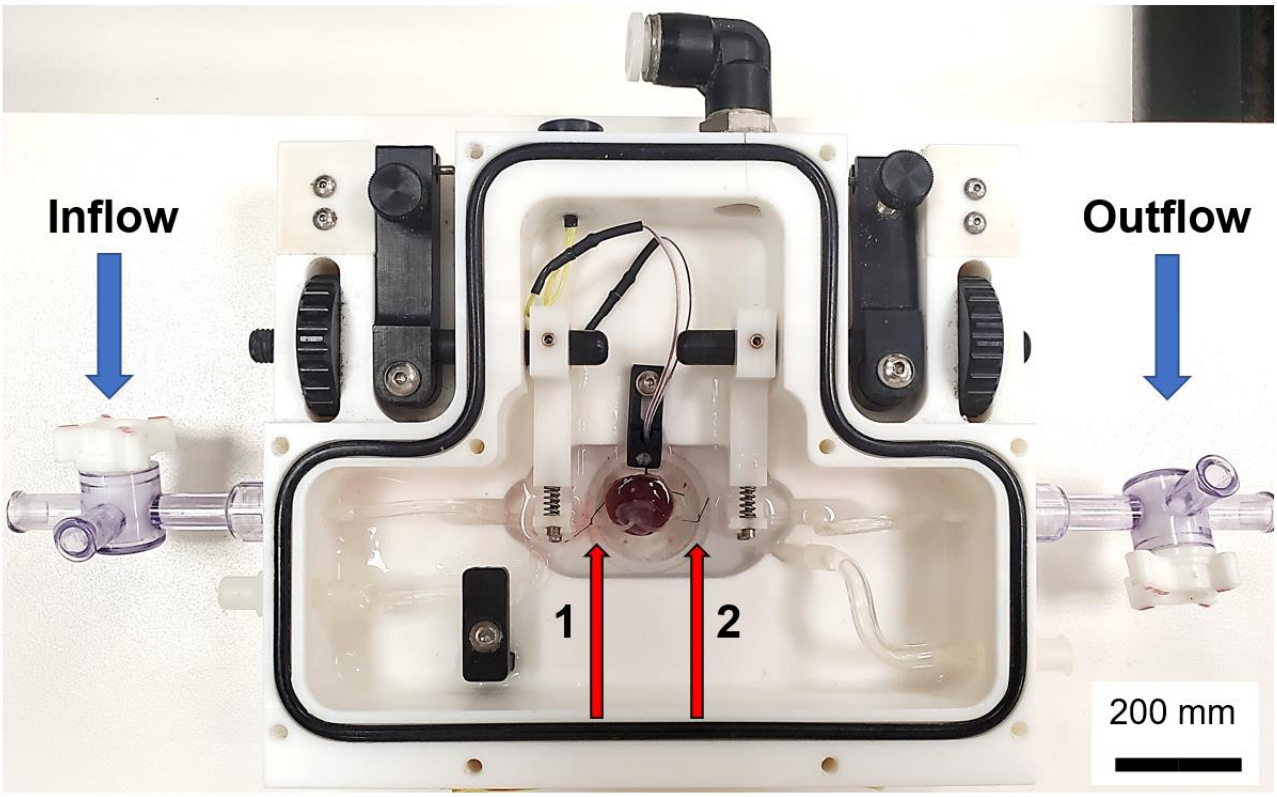

Fig. 4

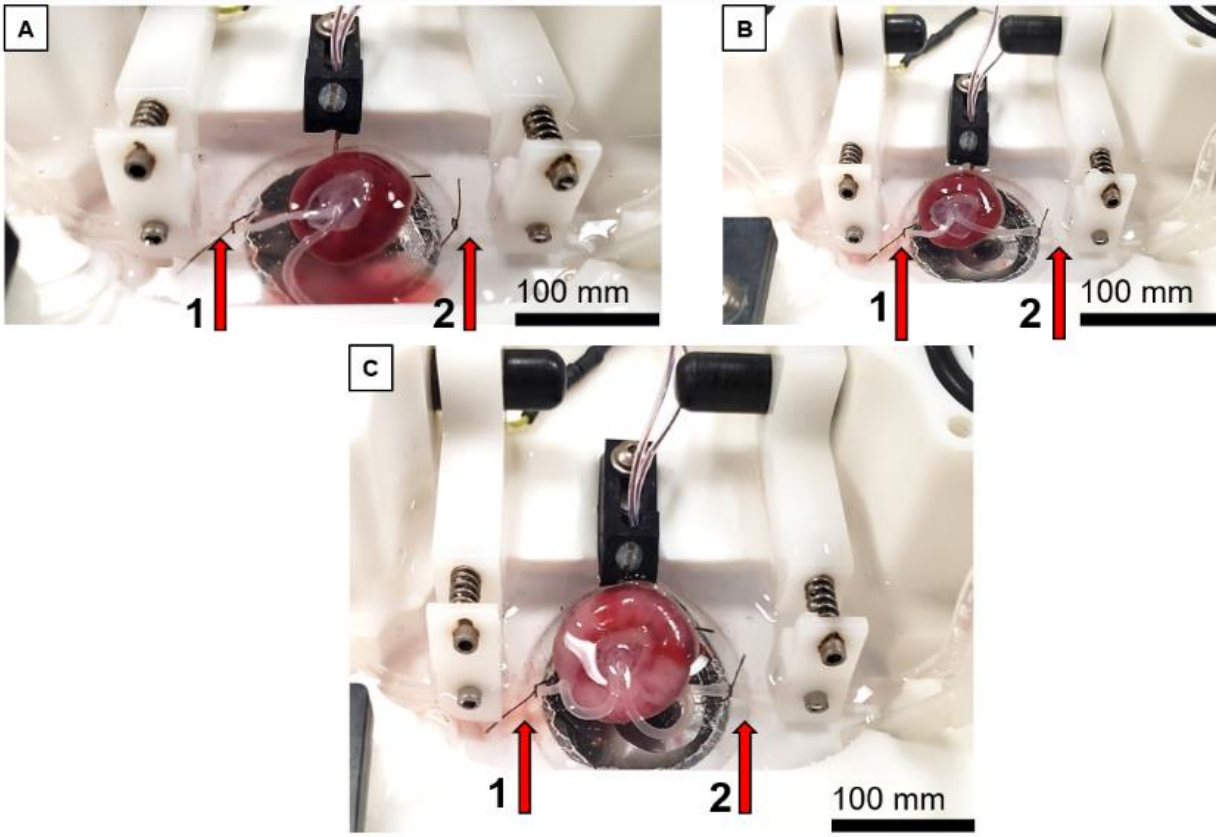

Fig. 5

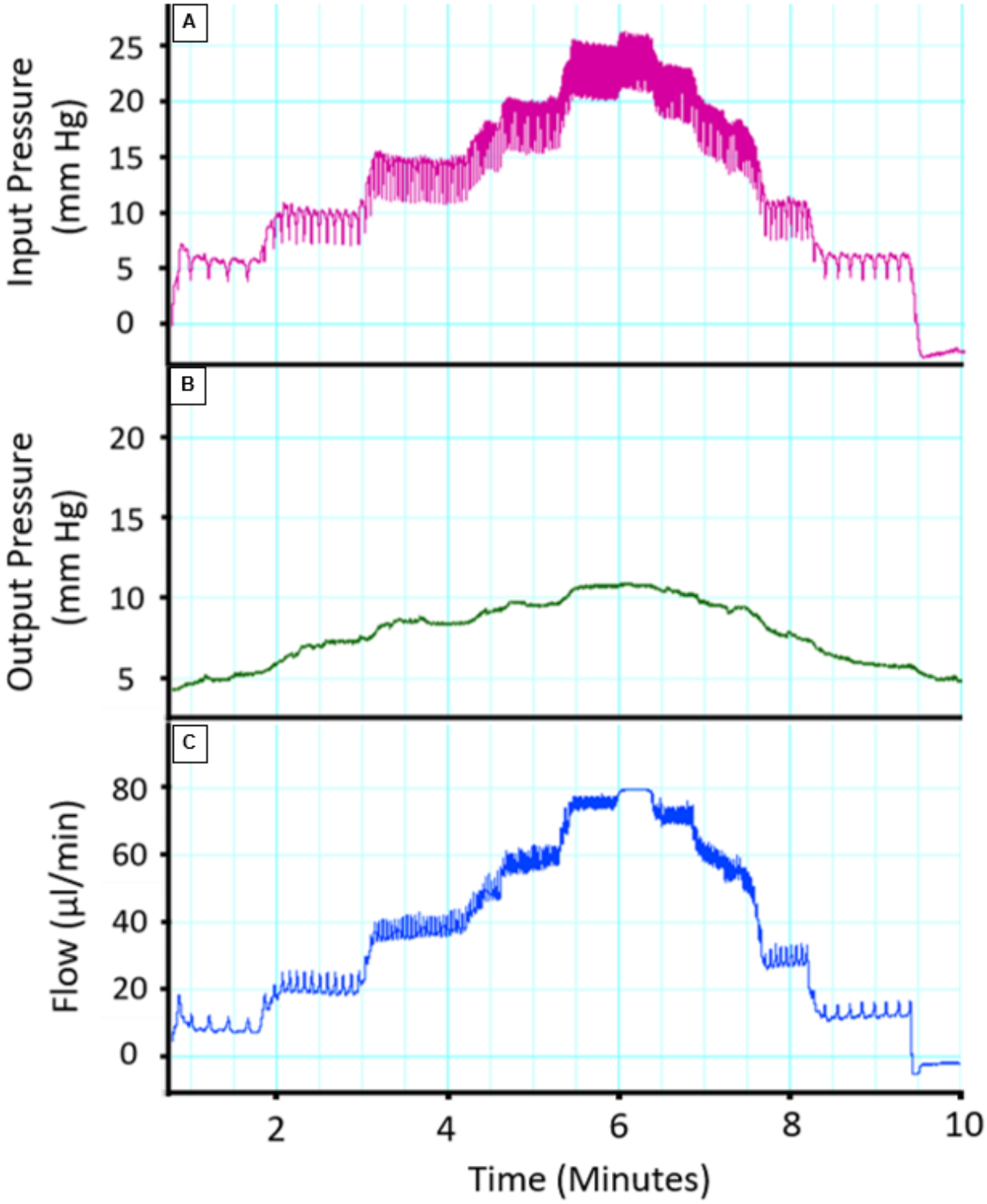
A
Input Pressure (mm Hg)
25
20
15
10
5
0
B
Output Pressure (mm Hg)
20
15
10
5
C
Flow (µl/min)
80
60
40
20
0
2
4
6
8
10
Time (Minutes)

Fig. 6

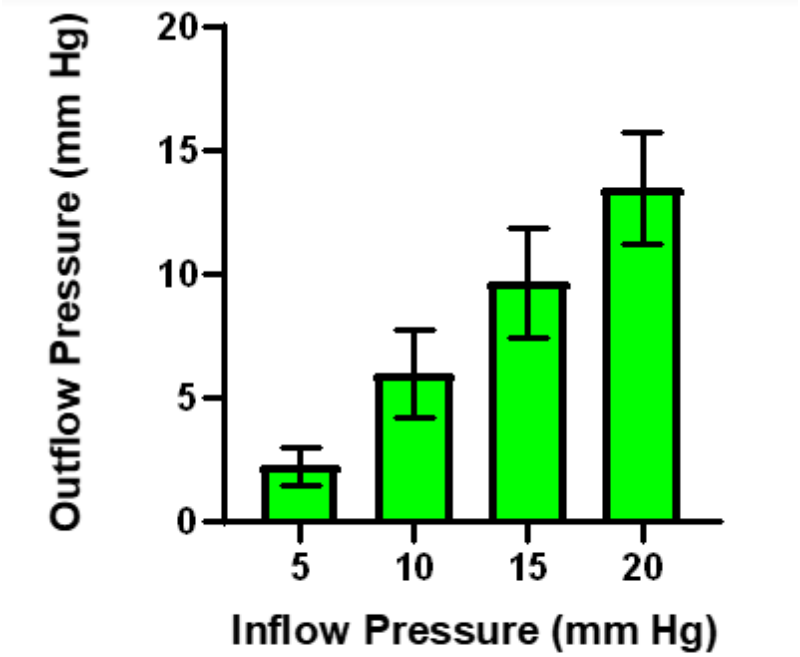
Outflow Pressure (mm Hg)
20
15
10
5
0
5
10
15
20
Inflow Pressure (mm Hg)

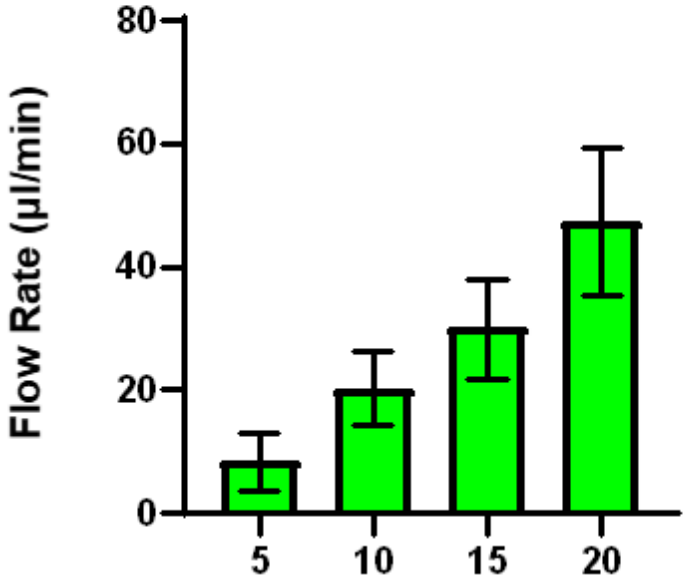
Flow Rate (µl/min)
80
60
40
20
0
5
10
15
20

Fig. 7

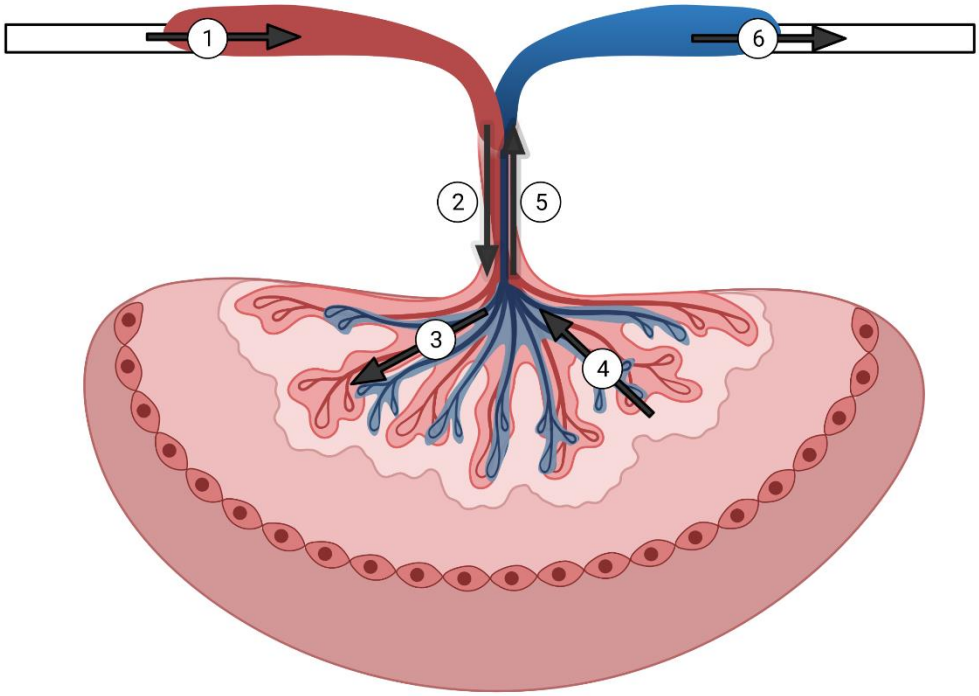

V. Chapter 5

Maternal Inhalation Exposure to Nano Titanium Dioxide does not Alter Placental Hemodynamics Regardless of Period of Gestational Exposure

Authors:

Garner, K.L.

Bowdridge, E.C.

Griffith, J.A.

DeVallance, E.

Schafner, K.

Goldsmith, W.T.

Engels, K.J.

Wix, K.

Batchelor, T.P.

Nurkiewicz, T.R.

Affiliations:

Department of Physiology and Pharmacology, West Virginia University School of Medicine, Morgantown, WV

Center for Inhalation Toxicology (iTOX), West Virginia University School of Medicine, Morgantown, WV

Abstract

Advanced materials consisting of engineered nanomaterials (ENM) are found ubiquitously throughout our day to day lives, yet cardiovascular and reproductive consequences associated with exposure have not been thoroughly examined. The placenta, a critical organ to support fetal health and fetal nutrient demands, is a toxicological target that affects fetal health outcomes. This study assessed placental hemodynamics and structural consequences associated with maternal inhalation exposure during distinct gestational time-points. Dams were exposed to ENM aerosols (nano-titanium dioxide) during three gestational time-points: early (EE, gestational day (GD) 2-6), mid (ME, GD 8-12) or late (LE, GD 15-19). Dry pup mass (0.39 ± 0.03 g) was significantly decreased in the EE group compared to controls (0.51 ± 0.01 g). There were no differences found in placental hemodynamics, umbilical artery function, placental angiotensin II receptor density, or placental zone surface area. We conclude that while early gestational exposure results in poor fetal outcomes, placental dysfunction that persists into GD 20 does not play a significant role in these findings.

Introduction

Pregnancy is a complex process that requires anatomical and physiological adaptation to support both maternal and fetal health. When perturbations occur during these adaptive processes this can lead to poor fetal health outcomes, and even death. One such critical adaptive component of pregnancy is the formation of the placenta. Abnormal placentation and placental development have been implicated in many gestational complications including preeclampsia, intrauterine growth restriction and miscarriage [1-4]. Various environmental exposures have been known to play a role in altering placental function and development. Engineered nanomaterials (ENM) are one such environmental exposure that is understudied and may play a role in uterine microvascular, placental and reproductive maternal and fetal consequences. Our lab and others have shown how maternal inhalation exposure to nano-titanium dioxide (nano-TiO_2) may affect maternal microvascular response and lead to fetal consequences [5-9], but few studies have assessed placental consequences associated with this exposure [10, 11]. Additionally, few studies have focused on the consequences of maternal nano-TiO_2 exposure in regard to the specific gestational time-points, which was shown to alter maternal vascular consequences in pregnant dams [8, 9]. Therefore, this study aimed to identify if placental dysfunction played a role in the fetal consequence observed in our previous study, Garner et al., 2022 [9]. Additionally, we examined if the period of gestational exposure resulted in varying degrees of placental vascular dysfunction as previously reported in uterine radial arteries [9].

Based on the length of gestation in the rat, which spans approximately 21-23 gestational days (GD), our study was broken down into three time-points: early exposure (EE), mid

exposure (ME) and late exposure (LE) [12]. EE represented GD 1-7, ME GD 8-13 and LE GD 14-21. These time-points represent implantation, attachment, spiral artery remodeling and embryonic development within the EE group. In the ME group embryonic growth will continue and discoid placental formation will be complete by approximately GD 11 [13]. In the LE group fetal growth is rapid and must occur for the fetus to survive after parturition. Many vasoactive components play a critical role during gestation for proper adaptation, including angiotensin II (Ang II), which plays a role in blood pressure regulations, maternal vascular remodeling, and placentation [14-17]. Ang II is also known to play a negative role in pregnancy when unregulated and may contribute to the pathology of preeclampsia [18, 19]. We have also shown in past studies that Ang II uterine radial artery, umbilical artery and placental reactivity may be altered following maternal exposure [9, 10]. Due to this, we hypothesized that maternal inhalation exposure during the early time-point of gestation would cause the most detriment to placental development, which would contribute to the decreased pup size reported in past studies. Additionally, we believed that Ang II sensitivity would be significantly increased and contribute to an increased placental resistance and an alteration in nutrient delivery to the pup.

Toxicant exposure during gestation has been implicated in alterations to critical zones of the placenta [20]. Exposure with known endocrine disruptors, such as bisphenol A and S, arsenic [21, 22] and cancer drugs have been shown to alter the labyrinth zone and even the junctional zone of murine placentas [23, 24]. The labyrinth zone in murine placentas, or the placental villi in humans, acts as the placental barrier. This is where the exchange of nutrients and waste take place between mother and fetus. If this zone decreases in

size, resistance could increase and decreased nutrient exchange may occur, leading to decreased fetal size or fatality. Therefore, we wanted to assess if placentas underwent anatomical changes due to our exposure paradigm ultimately leading to decreased function. Given that our lab has seen a decrease in pup size with nano-TiO_2 exposure [5, 9], as well as decreased estradiol production [5, 7], we believed that the labyrinth zone may be altered, specifically in the early exposure group.

Materials and Methods

Animal Characteristics

Female Sprague-Dawley rats were purchased from Hilltop Laboratories (Scottdale, PA) and housed in an AAALAC approved facility at West Virginia University (WVU). Rats were housed under a regulated temperature of 20-26 ˚C, relative humidity of 30-70% and 12:12 h light-dark cycle. Rats were assigned randomly to early exposed (EE), mid exposed (ME), late exposed (LE), early control (EC), mid control (EC), or late control (LE). Rats had *ad libitum* access to food and water and were acclimated for 48-72 h prior to mating. GD 0 was identified by the presence of sperm following vaginal swab. Dams were euthanized on GD 20. All procedures were approved by the WVU Institutional Animal Care and Use Committee.

Engineered Nanomaterial

Nano-TiO_2 was purchased from Evonik (Aeroxide P25, Parsippany, New Jersey). The powder is composed of anatase (80%) and rutile (20%) TiO_2 with a primary particle size of 21 nm, a surface area of 48.08 m^2/g [7], and a Zeta potential of -56.6 mV [25].

Aerosol Generation

A high-pressure acoustical generator (HPAG, IEStechno, Morgantown, West Virginia) was utilized to generate nano-TiO_2 aerosols. Output of the generator was fed into a Venturi pump (JS-60M, Vaccon, Medway, Massachusetts), causing further de-agglomeration of the particles. The nano-TiO_2 aerosol/air mix then entered the whole-body exposure chamber. A personal DataRAM (pDR-1500; Thermo Environmental Instruments Inc., Franklin, Massachusetts) was used for sampling the exposure chamber air to determine the real-time aerosol mass concentration. The software utilized feed-back loops to automatically adjust the acoustic energy to maintain the targeted, stable mass concentration during the exposure. Exposure chamber air was sampled onto PTFE filters and gravimetric measurements were conducted simultaneously with the DataRAM to obtain a calibration factor for the real-time measurements. The gravimetric mass concentration measurements were reported in this study. Water saturated bedding material was used in the exposure chamber to maintain comfortable humidity (30%-70%). Control animal chambers were held at similar temperature and humidity conditions but were exposed to HEPA-filtered air only.

Aerosol Characterization

Size distribution and mass concentration of the exposure paradigm were assessed through various measurements obtained during the exposure runs. Aerosol size distributions within the exposure chamber were obtained while maintaining a mass concentration target of around 12 mg/m^3 with: a high-resolution electrical low-pressure impactor (ELPI+, Dekati, Tampere, Finland), a scanning mobility particle sizer (SMPS 3938, TSI Inc., St. Paul, Minnesota), an aerodynamic particle sizer (APS 3321, TSI Inc.,

St. Paul, Minnesota) and a Micro-Orifice Uniform Deposit Impactor (MOUDI 115R, MSP Corp, Shoreview, MN).

Exposure Paradigm

All exposure groups were exposed to nano-TiO_2 aerosols in a whole-body chamber at a concentration of 12 mg/m^3 for 3 days, 6 h/day. All control groups were exposed to filtered air at 25 ml/min for 3 days, 6 h/day. Early gestational groups (EE or EC) were exposed during GD 2-6, mid gestational groups were exposed on GD 8-12, and late gestational groups were exposed on GD 15-19. Estimation of lung deposition (D) with nano-TiO_2 [26] was determined using the equation: D=F●V●C●T, in which F is the deposition fraction (10%), V is the minute ventilation (208.3 cc), C is the mass concentration (mg/m^3), and T is the exposure duration (minutes) [27]. This exposure paradigm produced an estimated cumulative lung deposition of 268± 11µg for EE, 286± 12 µg for ME and 296± 19 µg for LE. These calculations represent cumulative lung deposition and do not account for clearance.

Euthanasia and Tissue Harvest

On GD 20, dams were anesthetized with 5% isoflurane and maintained during surgery under 2.5% isoflurane. Dams were placed on a heating pad to maintain a 37 ˚C body temperature. The trachea was intubated to ensure a patent airway and the right carotid artery was canulated for blood collection. Both uterine horns were surgically excised, and pups and placenta were removed. The placental/pup units were placed in a dissection dish containing 4 ˚C physiological salt solution (PSS, in mmol/L: 129.8 NaCl, 5.4 KCl, 0.5 NaH_2PO_4, 0.83 $MgSO_4$, 19.0 $NaHCO_3$, 1.8 $CaCl_2$, 5.5 glucose) and was utilized for

placental hemodynamic assessment [28]. An additional placental/pup unit was used for umbilical artery assessment via wire myography. Additional placentas were perfused to remove blood, flash frozen in liquid nitrogen and stored at -80 ˚C until western blot analyses were performed or were used for placental histology.

Pup/Placental Mass, Placental Efficiency and Sex Determination

To assess reproductive consequences of maternal nano-TiO_2 inhalation exposure pup mass, placental mass and placental efficiency were assessed. Pup and placental wet weights were obtained immediately after dissection. Fetal sex was determined on GD 20 by identifying the uterus or testicles of the pups. Pups and placentas were then dried and weighed again. Placental efficiency was calculated by dividing pup mass by the placental mass.

Placental Histology

On GD 20 placentas were perfused and drop fixed with 4 % paraformaldehyde at 4 ˚C overnight. Placental tissue was then transferred to phosphate buffer solution (PBS) overnight. Tissue was then flash frozen and stored at -80 ˚C. Using a cryostat at -24 ˚C, placentas were sectioned at 10 µm thickness at the center of the placenta. Sections were placed on slides and stained with hematoxylin and eosin (H&E) following protocol instructions (Vector Laboratories, Burlingame, California). Tissue sections were incubated with hematoxylin for 3 minutes and eosin for 4 minutes. Slide were imaged at 10x objective and were analyzed using ImageJ. Total placental area and percent total area of the junctional and labyrinth zones were determined.

Placental AT_1R and AT_2R Western Blot

Using near-infrared western blot, relative Ang II receptor protein levels were assessed. Placentas were homogenized using 1.6 mm stainless steel beads (Next Advance, Troy, New York) in RIPA containing 0.1 mM protease and phosphatase inhibitors (Roche, Indianapolis, Indiana). Samples were prepared with 4x laemeli sample buffer containing β-mercaptoethanol and boiled at 95 ˚C. 30 µg of samples were resolved by SDS-PAGE and transferred to 0.2 µm nitrocellulose membrane. Membranes were blocked with LiCOR Odyssey blocking buffer and probed with primary antibodies against Ang II type 1 receptor (anti-AT1R, sc-515884, Santa Cruz Biotechnology, Inc. Dallas, Texas), Ang II type 2 receptor (anti-AT2R, ab92445, Abcam, Cambridge, Massachusetts) and β-actin (sc-47778, Santa Cruz Biotechnology, Inc. Dallas, Texas). Membranes were then probed with LiCOR near-infrared secondary antibodies and imaged using the LiCOR Odyssey. Secondary antibodies included: goat anti-rabbit (925-68070, LI-COR Biosciences, Lincoln, Nebraska) and goat anti-mouse (925-68071, LI-COR Bioscience, Lincoln, Nebraska). ImageJ software was utilized for optical density, normalized β-actin control and represented as fold change from control.

Placental Hemodynamics

Placenta and pup were removed, still connected, from the uterus and placed in a dissecting dish containing 4 ˚C PSS. The umbilical cord was opened, and the umbilical artery and vein were separated. Once cleaned of the amniotic sac, the umbilical vessels were severed as close to the pup as possible, and the placenta was transferred to an isolated vessel chamber (Living Systems Instrumentation, Burlington, Vermont) containing oxygenated (21% O_2/5% CO_2) 37 ˚C PSS. The umbilical artery and vein were cannulated on glass pipette tips and secured with 6-0 silk suture (AD Surgical, Sunnyvale,

California). This protocol is presented in the technical manuscript Garner and Bowdridge et. al 2022 [28]. The placenta was pressurized from 0-20 mm Hg in 5 mm Hg increments. Outflow pressure and flow were assessed following the addition of vasoactive drugs to assess vascular hemodynamics. Acetylcholine (ACh, $1x10^{-2}$ M), used to assess endothelium-dependent response, S-nitroso-N-acetyl-DL-penicillamine (SNAP, $1x10^{-2}$ M), used to assess endothelium-independent response, and Ang II ($1x10^{-2}$ M) were added to the bath individually to assess outflow pressure. Washes were performed between each drug. Once all drug responses were assessed PSS was removed and replaced with Ca^{2+} - free PSS.

Uterine Artery Tension Generation

The umbilical artery was dissected and isolated as described above. 2-3 mm sections were then mounted on wire myography pins. The wire myography chamber (AD Instruments- DMT 620 M) contained 5 mL of PSS (119 mM NaCl, 4.7 mM KCl, 1.18 mM KH2PO4, 1.17 mM MgSO4, 2.5 mM, CaCl2, 25 mM NaHCO3, 0.027 mM EDTA, and 5.5 mM glucose) bubbled with 95% O_2/ 5% CO_2 at 37 ˚C. Vessels were equilibrated for 30 minutes at 2.0 mN and then maximum tension generation was determined using high-potassium PSS (K+PSS, 123.7 mM KCl, 1.18 mM KH2PO4, 1.17 mM MgSO4, 2.5 mM, CaCl2, 25 mM NaHCO3, 0.027 mM EDTA, and 5.5 mM glucose). Vessels were washed with PSS until baseline relaxion was achieved. Contractile responses were then assessed via cumulative doses of Ang II ($1x10^{-9}$ -$1x10^{-4}$ M) and α1 adrenergic agonist phenylephrine (PE, $1x10^{-9}$ -$1x10^{-4}$ M), washing between each drug. Relaxation responses were determined via cumulative doses of ACh ($1x10^{-9}$ -$1x10^{-4}$ M) or SNAP ($1x10^{-9}$ -$1x10^{-4}$ M), following pretreatment of thromboxane memetic U46619 ($1x10^{-7}$ M).

Wire Myography Calculations

The tension developed by the vessels with K+PSS represent maximum tension. Tension with agonists were recorded and the percent of maximum tension generation was calculated using the formula below:

$$\boldsymbol{Percent\ Maximum\ Tension}\ (\%) = \left(\frac{\boldsymbol{Tension\ with\ agonist}\ (\boldsymbol{mN})}{\boldsymbol{Maximum\ tension}\ (\boldsymbol{mN})}\right)\boldsymbol{x}\ \mathbf{100}\%$$

Statistics

Dam characteristics were assessed by one-way analysis of variance (ANOVA) utilizing a Tukey post hoc analysis when statistical significance was found. EC, MC and LC pup/placental characteristics, relative Ang II receptor protein levels, and % total area of placental zones were first assessed via one-way ANOVA with a Tukey post hoc analysis when significance was found. If no statistical significance was identified control groups were combined into one group and then compared to the exposure groups utilizing a one-way ANOVA and a Dunnett's post hoc analysis when significance was found. If equal variance was not met the Welch's ANOVA was utilized and the Dunnett's T3 post hoc analysis was utilized. A t test was utilized to assess differences among sexes within their own experimental group. Two-way repeated measures ANOVA was utilized to assess point-by-point differences in dose response curves and mixed effects model was utilized to assess differences between groups with increasing pressure curves. A Tukey post hoc test was utilized when differences were indicated between controls, if no differences were identified these values were combined. A Dunnett's post hoc analysis was then utilized when significance was found between the combined control group and treatment groups. All data is reported as mean ± SE. Significance was set as $p \leq 0.05$.

Results

Nano-TiO_2 Aerosol Characterization

The average real-time aerosol mass concentration during exposures had a target of 12 mg/m^3 (Fig. 1a). While the target mass concentration of the exposure was 12 mg/m^3 variability is expected. Actual mass concentration for EE was 11.45± 0.45 mg/m^3, for ME was 12.23± mg/m^3 and for LE was 12.67± mg/m^3. The aerosol aerodynamic diameter (assessed via the ELPI) had a count median diameter (CMD) of 162 nm with a standard deviation of 1.88 (Fig. 1b). Aerosol diameter was also assessed via the SMPS and APS and had a combined CMD of 119 nm with a standard deviation of 2.09 (Fig. 1c). The characterization of agglomerate morphology has been extensively characterized via electron microscopy [5, 10].

Animal Characteristics

The age and mass of dams at GD 20 were not statistically different between any of the groups (Table 1). The litter size and sex distribution between the control groups (EC, MC and LC) were statistically similar (Table 2) and therefore were combined into one control group. The exposure groups were then compared to the combined control. Table 3 shows that there were no differences between exposure groups and the control group in litter size or sex distributions.

Pup/Placental Characteristics and Sex Differences

When assessing wet and dry pup and placental mass and placental efficiency it was found that the control groups were not statistically different from each other, because of this the groups were combined to form one control group (Table 4). When compared to the exposure groups, dry pup mass was significantly decreased within the EE group; with EE

pups weighing 0.39 ± 0.03 g and control 0.51 ± 0.01 g. Additionally, the placental efficiency was trending towards significance (p-value = 0.0699) within the EE group (3.72 ± 0.17) compared to the control (4.62 ± 0.20), suggesting EE caused a decreased placental efficiency (Fig. 2). This decreased placental efficiency could suggest placental vascular dysfunction, which may lead to the smaller pup mass.

Due to evidence of altered male-to-female sex ratios in various toxicological exposures [29-31] assessment of pup characteristics between sexes were examined. Pup and placental mass and placental efficiency between males and females in the control groups were not statistically different (Table 5), therefore they were combined into the male control or female control group. Male and female comparisons were assessed within each group. There were no significant differences except between the control male versus female dry pup mass, with females (0.47 ± 0.01 g) being significantly smaller than males (0.52 ± 0.01 g). Male and female controls were then compared to the same sex exposure groups. Female control (0.47 ± 0.01 g) and EE (0.39 ± 0.01 g) dry pup mass was significantly different as was placental efficiency between the female control group (4.87 ± 0.23) and late exposure group (5.28 ± 0.10) (Fig. 3).

Placental Hemodynamics

The outflow pressure of the placental units was measured to assess resistance of the tissue. The assessment of outflow pressure was performed on the control groups with PSS, ACh, SNAP, Ang II and Ca^{2+}-free PSS (Fig. 4a-e) and no differences were found within these groups. Due to this, the groups were combined into one control group and compared to the exposure treatment groups. Outflow pressure at various inflow pressures where not statistically different from the control when incubated in PSS, ACh, SNAP, Ang

II or Ca^{2+}-free PSS (Fig. 4f-j). This suggests that placental function was not altered with exposure and did not contribute to the altered fetal outcomes within the EE group as shown in Fig. 2d.

Umbilical Artery Vascular Reactivity

To further assess the potential role of the placenta in poor fetal outcomes due to exposure, the vascular response of the umbilical arteries was assessed via wire myography. Firstly, the control groups were compared with treatments of increasing doses of ACh, SNAP, PE and Ang II. There was no statistical difference identified between these control groups (Fig. 5a-d), therefore there were combined into one control group and compared to the exposure groups. Statistical differences were identified between EE vs control and ME vs control with the endothelial independent agonist SNAP at the 1×10^{-7} M dose, with a decrease in tension in these exposure groups compared to control (Fig.5e-h). No other statistical differences were identified between the groups.

Placental AT_1R and AT_2R Western Blot

An increased expression of AT_1R within the EE group was trending towards significance compared to the control ($p=0.059$), but no groups were shown to be significantly altered compared to the control (Fig. 6a). AT_2R was not shown to be significantly altered in any of the exposure groups compared to the control (Fig. 6b).

Placental Histology

Placental histology was utilized to assess if placental anatomy was altered due to exposure, which could contribute to decreased placental efficiency and pup size in the EE group (Fig. 2). Fig. 7a is a representative image of a placental unit. Percent total area

for the junctional and labyrinth zone were not statistically different between the control groups (Fig. 7b-c) and were combined into a single control group. Exposures did not alter the junctional or labyrinth zone size as compared to control placentas (Fig. 7d-e).

Discussion

Our novel study assessed how maternal inhalation exposure to nano-TiO_2 during distinct gestation periods may affect placental function and thus fetal health outcomes. From this study we determined that exposure did not alter litter size, reabsorption site occurrence or pup sex ratio (Table 3). We also determine that the EE group exposure treatment resulted in smaller pup mass and decreased placental efficiency compared to controls (Fig. 2). This data was further supported by our past gestation study, which found the EE group most susceptible to poor fetal outcomes from exposure [9]. To assess if one sex was more susceptible to exposure than the other, female and male placental mass and efficiency were compared between exposure groups. We found that male and female dry pup mass was significantly different from one and another, however exposure did not affect mass between sexes. Additionally, the EE females were significantly smaller than control females, but this difference was not observed in males (Fig. 3). This could indicate that the decrease in female weights may be driving the reduced pup size reported, suggesting females may be more significantly impacted by exposure.

Placental hemodynamics were assessed through our novel isolated placental method to examine placental resistance [28]. There were no differences found between the control group or any exposure groups (Fig. 4). Additionally, there were no differences observed in umbilical artery vascular function except for a single concentration of endothelium independent agonist SNAP (1×10^{-7} M) between EE and control and ME and control (Fig.

5). EE and ME showed decreased tension generation compared to the control, suggesting increased sensitivity to SNAP at that dose. This could show how exposure during early and mid-gestation may alter umbilical artery response to nitric oxide that may lead to vasodilation and increased blood flow to the placenta. With this being altered one could hypothesis that umbilical artery and vein pressures would be too close, resulting in overperfusion and perturbations to nutrient and waste exchange which may results in fetal consequences.

Although Ang II responses were not altered by exposure, we wanted to examine the relative receptor concentrations for AT_1R and AT_2R, as receptor density naturally changes throughout gestation due to estrogen levels [17] and receptor density can affect vascular function [9]. We found that neither AT_1R nor AT_2R density was altered following exposure (Fig. 6) which supports the vascular results of this study. Interestingly though, AT_1R levels within the EE were shown to be trending towards significance with a p value of 0.059. An increase in vasoconstrictive AT_1R without alteration to placental hemodynamics or AT_2R could suggest that additionally RAS components, such as the MAS receptor (MASR) may be altered, which is also known to balance out the effects of AT_1R [32]. If MASR levels were simultaneously increased, then the effects of AT_1R may have been balanced out. Future research should investigate additional arms of RAS following exposure. It is also important to highlight the effects of overactivation of AT_1R in trophoblast cells. If AT_1R were upregulating early in pregnancy AT_1R activation results in increased anti-angiogenic factors, such as soluble fms-like tyrosine kinase-1 (sFLT-1) [33], which can bind proangiogenic factors such as vascular endothelial growth factor (VEGF) and placental growth factor (PlGF). The decrease in VEGF and PlGF will result in poor trophoblast

invasion and reduced spiral artery remodeling which will reduce placental perfusion from the maternal tissue [34]. This will result in an increasingly hypoxic environment, further reinforcing a negative loop with increase AT_1R, as prolonged hypoxia has been shown to enhance angiotensin II receptor expression as well as inhibit PlGF expression in trophoblast cells [35]. The EE group may have experienced reduced spiral artery remodeling and invasions which could explain the reduced pup size. Previously we have shown that AT_2R density is altered as well as uterine microvascular Ang II sensitivity within our EE group [9], but perhaps due to the placenta development not being completed within GD 2-6 these alterations were not observed within the placenta.

Finally, because correct anatomical formation of the placental zones is imperative for healthy physiology and derivation from this has been reported in toxicant exposure [20], we wanted to assess the junctional and labyrinth zone areas of placentas. Regardless of exposure paradigm, there was no effect on either placental zone area between treatment groups (Fig. 7). These data indicate that the outcomes observed in EE pup size and placental efficiency are not due to placental dysfunction but seem to be linked to maternal vascular dysfunction associated with exposure [9].

This exposure paradigm yielded fetal outcomes consistent with past experiments [9], further supporting that the EE group is most sensitive to maternal nano-TiO_2 inhalation exposure. This new data, though, does suggest that placental dysfunction does not play a role in these fetal outcomes. This does not fit with past studies were maternal exposure caused alterations of placental hemodynamics, leading to an increase in placental resistance and increased sensitivity to Ang II [10]. It is important to consider that this study's exposure paradigm is considerably shorter, which may result in the discrepancies

seen with these results. If exposure, starting from early gestation, lasted 6 days instead of 3, we may have seen placental consequences and perhaps even greater alterations to fetal health. Given that women typically remain in the workforce well into pregnancy, it would be of importance to assess vascular and fetal consequences of exposure starting in early gestation continuing into late.

One limitation to the study may have been that the N was rather low and some of the differences may not have been pronounced between the groups. This may be seen in the EE with PE and Ang II umbilical artery response compared to the control (Fig. 5g-h). While the tension generation appeared to be slightly increasing, the variability between groups prevented this from reaching statistical significance. Additionally, issues occurred with increasing the placental pressure beyond 20 mm Hg. Due to this some of the physiological range of the placenta is missing from the evaluation and this is another consequence of a smaller N. Future studies will want to increase this N as well as assess consequences of longer exposures as stated above.

Our group has demonstrated that exposure during early gestation may lead to significantly smaller pups, which also lead to decreased placental efficiency. Furthermore, our data does not suggest that placental dysfunction, due to anatomical or physiological alterations, plays a role in fetal health outcomes, regardless of the window of gestational exposure.

Figure Legends

Fig. 1 Real-time characterizations of nano-TiO_2. Verification of aerosol characterization during exposure. (a) 6 h exposure paradigm was monitored with feedback system controlling aerosol mass concentration. Mass concentration was held near desired 12 mg/m^3 target. (b) High-resolution Electrical Low-Pressure Impactor (ELPI) assessed aerosol aerodynamic diameter showing a CMD of ___ nm with a geometric standard deviation of 1.73. (c) The Scanning Mobility Particle Sizer (SMPS) and Aerodynamic Particle Sizer (APS) assessed aerosol mobility diameter revealing a CMD of 119 nm with a geometric standard deviation of 2.09

Fig. 2 Pup and placental characteristics. Pup and placental mass and placental efficiency assessed on GD 20 between combined control group and exposure groups. (a) Wet pup mass. (b) Wet placental mass. (c) Wet placental efficiency. (d) Dry pup mass. (e) Dry placental mass. (d) Dry placental efficiency. EE = Early Exposed, ME = Mid Exposed, LE = Late Exposed. Data are mean ± SE. *, P ≤ 0.05 vs control; #, P ≤ 0.07 vs control

Fig. 3 Sex-based pup and placental characteristics. Pup and placental mass and placental efficiency assessed on GD 20 between combined control group and exposure groups. Analysis performed assessed difference within each sex. (a) Wet pup mass. (b) Wet placental mass. (c) Wet placental efficiency. (d) Dry pup mass. (e) Dry placental mass. (d) Dry placental efficiency. EE = Early Exposed, ME = Mid Exposed, LE = Late Exposed. Data are mean ± SE. *, P ≤ 0.05 vs male control/female control; a, P ≤ 0.05 vs male/female characteristics within the same experimental group

Fig. 4 Placental hemodynamics following maternal inhalation exposure. Outflow pressure readings with increasing pressure input. (a) Outflow pressure with PSS between control groups. (b) Outflow pressure with ACh between control groups. (c) Outflow pressure with SNAP between control groups. (d) Outflow pressure with Ang II between control groups. (e) Outflow pressure with Ca^{2+}-free between control groups. (f) Outflow pressure with PSS between combine control and exposure groups. (g) Outflow pressure with ACh between combine control and exposure groups. (h) Outflow pressure with SNAP between combine control and exposure groups. (i) Outflow pressure with Ang II between combine control and exposure groups. (j) Outflow pressure with Ca^{2+}-free between combine control and exposure groups. EC = Early Control, MC = Mid Control, LC = Late Control. EE = Early Exposed, ME = Mid Exposed, LE = Late Exposed. Data are mean ± SE

Fig. 5 Umbilical artery vascular reactivity following maternal inhalation exposure. Dose response curves to assess umbilical artery vascular function. (a) % maximum tension of increasing doses of ACh between control groups. (b) % maximum tension of increasing doses of SNAP between control groups. (c) % maximum tension of increasing doses of PE between control groups. (d) % maximum tension of increasing doses of Ang II between control groups. (e) % maximum tension of increasing doses of ACh between combined control group and exposure treatment groups. (f) % maximum tension of increasing doses of SNAP between combined control group and exposure treatment groups. (g) % maximum tension of increasing doses of PE between combined control group and exposure treatment groups. (h) % maximum tension of increasing doses of Ang II between combined control group and exposure treatment groups. EC = Early

Control, MC = Mid Control, LC = Late Control. EE = Early Exposed, ME = Mid Exposed, LE = Late Exposed. Data are mean ± SE. a, P ≤ 0.05 comparing EE to control; b ≤ 0.05 comparing ME to control

Fig. 6 AT_1R and AT_2R protein concentration in placental tissue. (a) Western blot representative image for protein concentration of AT_1R in control, early exposed (EE), mid exposed (ME), late exposed (LE) placental tissue and the average relative protein density of AT_1R protein among exposed groups. (b) Representative image of Western blot protein concentration of AT_2R in control, EE, ME, LE placental tissue and the average relative protein density of AT_2R protein among exposed groups. EC = Early Control, MC = Mid Control, LC = Late Control. EE = Early Exposed, ME = Mid Exposed, LE = Late Exposed. Data are mean ± SE. #, P ≤ 0.07 vs control

Fig. 7 Placental histology of GD 20 Pups. Quantification of placental zones within GD 20 placenta. (a) Hematoxylin and eosin staining of placental tissue at 10x. Scale bar represents 1 mm. The yellow arrow indicates myometrial tissue. Black arrow shows decidua. Red arrow indicates junctional zone of the placenta. Blue arrow indicates the labyrinth zone. Purple arrow shows remanence of the yolk sac. Asterisk shows umbilical cord location. (b) Junctional zone as % of total area of the placenta for control groups. (c) Labyrinth zone as % total area of placenta for control groups. (d) Junctional zone as % total area of placenta for control vs exposure groups. (e) Labyrinth zone as % total area of placenta for control vs exposure groups. EC = Early Control, MC = Mid Control, LC = Late Control. EE = Early Exposed, ME = Mid Exposed, LE = Late Exposed.

References

1. Rana, S., et al., *Preeclampsia: Pathophysiology, Challenges, and Perspectives.* Circ Res, 2019. **124**(7): p. 1094-1112.
2. Brosens, I., et al., *The "Great Obstetrical Syndromes" are associated with disorders of deep placentation.* Am J Obstet Gynecol, 2011. **204**(3): p. 193-201.
3. Tang, Q., et al., *Downregulation of miR-424 in placenta is associated with severe preeclampsia.* Pregnancy Hypertens, 2019. **17**: p. 109-112.
4. Atia, T.A., *Placental apoptosis in recurrent miscarriage.* Kaohsiung J Med Sci, 2017. **33**(9): p. 449-452.
5. Bowdridge, E.C., et al., *Maternal Engineered Nanomaterial Inhalation During Gestation Disrupts Vascular Kisspeptin Reactivity.* Toxicol Sci, 2019. **169**(2): p. 524-533.
6. Abukabda, A.B., et al., *Group II innate lymphoid cells and microvascular dysfunction from pulmonary titanium dioxide nanoparticle exposure.* Part Fibre Toxicol, 2018. **15**(1): p. 43.
7. Stapleton, P.A., et al., *Estrous cycle-dependent modulation of in vivo microvascular dysfunction after nanomaterial inhalation.* Reprod Toxicol, 2018. **78**: p. 20-28.
8. Fournier, S.B., et al., *Effect of Gestational Age on Maternofetal Vascular Function Following Single Maternal Engineered Nanoparticle Exposure.* Cardiovasc Toxicol, 2019. **19**(4): p. 321-333.
9. Garner, K.L., Bowdridge, E. C., Griffith, J. A., DeVallance, E., Seman, M. G., Engels, K. J., Groth, C. P., Goldsmith, W. T., Wix, K., Batchelor, T. P., & Nurkiewicz, T. R., *Maternal Nanomaterial Inhalation Exposure: Critical Gestational Period in the Uterine Microcirculation is Angiotensin II Dependent.* Cardiovascular Toxicology, 2022.
10. Abukabda, A.B., et al., *Maternal titanium dioxide nanomaterial inhalation exposure compromises placental hemodynamics.* Toxicology and Applied Pharmacology, 2019. **367**: p. 51-61.

11. Zhang, L., et al., *Gestational exposure to titanium dioxide nanoparticles impairs the placentation through dysregulation of vascularization, proliferation and apoptosis in mice.* Int J Nanomedicine, 2018. **13**: p. 777-789.

12. *Sprague Dawley Rat: Preferred for Safety and Efficacy, Surgical Modification and Reproductive Studies*, I. Taconic Biosciences, Editor. p. 7-8.

13. Silva, J.F. and R. Serakides, *Intrauterine trophoblast migration: A comparative view of humans and rodents.* Cell Adh Migr, 2016. **10**(1-2): p. 88-110.

14. Walther, T., et al., *Angiotensin II type 1 receptor has impact on murine placentation.* Placenta, 2008. **29**(10): p. 905-9.

15. Morgan, T., C. Craven, and K. Ward, *Human spiral artery renin-angiotensin system.* Hypertension, 1998. **32**(4): p. 683-7.

16. Hering, L., et al., *Effects of circulating and local uteroplacental angiotensin II in rat pregnancy.* Hypertension, 2010. **56**(2): p. 311-8.

17. Mishra, J.S., K. Gopalakrishnan, and S. Kumar, *Pregnancy upregulates angiotensin type 2 receptor expression and increases blood flow in uterine arteries of rats.* Biol Reprod, 2018. **99**(5): p. 1091-1099.

18. Takeda-Matsubara, Y., et al., *Roles of angiotensin type 1 and 2 receptors in pregnancy-associated blood pressure change.* Am J Hypertens, 2004. **17**(8): p. 684-9.

19. Anton, L., et al., *Activation of local chorionic villi angiotensin II levels but not angiotensin (1-7) in preeclampsia.* Hypertension, 2008. **51**(4): p. 1066-72.

20. Furukawa, S., N. Tsuji, and A. Sugiyama, *Morphology and physiology of rat placenta for toxicological evaluation.* J Toxicol Pathol, 2019. **32**(1): p. 1-17.

21. Mao, J., et al., *Bisphenol A and bisphenol S disruptions of the mouse placenta and potential effects on the placenta-brain axis.* Proc Natl Acad Sci U S A, 2020. **117**(9): p. 4642-4652.

22. Patel, B., et al., *Evaluation of vascular effect of arsenic using in vivo assays.* Environ Sci Pollut Res Int, 2017. **24**(18): p. 15521-15527.

23. Furukawa, S., et al., *Effect of cisplatin on rat placenta development.* Exp Toxicol Pathol, 2013. **65**(1-2): p. 211-7.

24. Taki, K., et al., *6-Mercaptopurine-induced histopathological changes and xanthine oxidase expression in rat placenta.* J Toxicol Sci, 2012. **37**(3): p. 607-15.

25. Nichols, C.E., et al., *Reactive oxygen species damage drives cardiac and mitochondrial dysfunction following acute nano-titanium dioxide inhalation exposure.* Nanotoxicology, 2018. **12**(1): p. 32-48.

26. Nurkiewicz, T.R., et al., *Nanoparticle inhalation augments particle-dependent systemic microvascular dysfunction.* Part Fibre Toxicol, 2008. **5**: p. 1.

27. Yi, J., et al., *Whole-body nanoparticle aerosol inhalation exposures.* J Vis Exp, 2013(75): p. e50263.

28. Garner, K.L., et al., *Using the Isolated Rat Placenta to Assess Fetoplacental Hemodynamics.* Frontiers in Toxicology, 2022. **4**.

29. Mocarelli, P., et al., *Change in sex ratio with exposure to dioxin.* Lancet, 1996. **348**(9024): p. 409.

30. Chiang, C., et al., *Late-life consequences of short-term exposure to di(2-ethylhexyl) phthalate and diisononyl phthalate during adulthood in female mice.* Reprod Toxicol, 2020. **93**: p. 28-42.

31. Liu, G.X., et al., *Effect of chronic sublethal exposure of major heavy metals on filtration rate, sex ratio, and gonad development of a bivalve species.* Bull Environ Contam Toxicol, 2014. **92**(1): p. 71-4.

32. Povlsen, A.L., et al., *The Vasoactive Mas Receptor in Essential Hypertension.* J Clin Med, 2020. **9**(1).

33. Irani, R.A. and Y. Xia, *Renin angiotensin signaling in normal pregnancy and preeclampsia.* Semin Nephrol, 2011. **31**(1): p. 47-58.

34. Yart, L., et al., *Role of the Uteroplacental Renin-Angiotensin System in Placental Development and Function, and Its Implication in the Preeclampsia Pathogenesis.* Biomedicines, 2021. **9**(10).

35. Bdolah, Y., V.P. Sukhatme, and S.A. Karumanchi, *Angiogenic imbalance in the pathophysiology of preeclampsia: newer insights.* Semin Nephrol, 2004. **24**(6): p. 548-56.

Table 1. Dam physical characteristics on GD 20. EC = Early Control, MC = Mid Control, LC = Late Control, EE = Early Exposed, ME = Mid Exposed, LE = Late Exposed. N represents number of animals. Data are mean ± SE

	N	Age (d)	Mass (g)
EC	3	98±4	362±26
MC	3	80±4	342±21
LC	3	85±6	364±5
EE	5	92±4	339±18
ME	4	115±8	328±10
LE	3	87±10	389±36

Table 2. Litter characteristics assessed on GD 20 between control groups. EC = Early Control, MC = Mid Control, LC = Late Control. Data are mean ± SE

	Litter Size	Reabsorption Sites	% Female	% Male
EC	13±1	0.7±0.3	43±11	57±11
MC	10±1	0.3±0.3	48±2	52±2
LC	13±1	1.3±0.3	50±7	50±7

Table 3. Litter characteristics assessed on GD 20 between combined control group and exposure groups. EE = Early Exposed, ME = Mid Exposed, LE = Late Exposed. Data are mean ± SE

	Litter Size	Reabsorption Sites	% Female	% Male
Control	12±1	0.8±0.2	47±4	53±4
EE	9±3	1.2±0.4	51±9	49±9
ME	8±2	0.8±0.3	58±15	42±15
LE	10±4	0.3±0.3	31±16	69±16

Table 4. Pup and placental mass and placental efficiency of control groups on GD 20.

EC = Early Control, MC = Mid Control, LC = Late Control. Data are mean ± SE

	Wet Pup Mass (g)	Wet Placental Mass (g)	Wet Placental Efficiency	Dry Pup Mass (g)	Dry Placental Mass (g)	Dry Placental Efficiency
EC	4.03±0.11	0.75±0.11	5.65±0.63	0.52±0.04	0.11±0.01	4.80±0.32
MC	3.38±.45	0.94±0.01	4.16±0.35	0.51±0.01	0.12±0.01	4.14±0.11
LC	3.54±0.34	0.78±0.12	4.94±1.11	0.50±0.02	0.11±0.02	4.75±0.42

Table 5. Pup and placental mass and placental efficiency assessed on GD 20 between combined control groups assessing differences within each sex. EC = Early Control, MC = Mid Control, LC = Late Control. M and F denote Male and Female, respectively. Data are mean ± SE

	Wet Pup Mass (g)	Wet Placental Mass (g)	Wet Placental Efficiency	Dry Pup Mass (g)	Dry Placental Mass (g)	Dry Placental Efficiency
EC-M	4.13±0.10	0.76±0.14	5.75±0.81	0.51±0.03	0.11±0.01	4.52±0.14
EC-F	3.91±0.10	0.73±0.08	5.52±0.49	0.49±0.03	0.11±0.01	4.72±0.39
MC-M	3.48±0.55	0.94±0.02	4.38±0.12	0.54±0.01	0.12±0.01	4.47±0.28
MC-F	3.23±0.36	0.95±0.01	3.84±0.28	0.47±0.03	0.13±0.01	3.74±0.26
LC-M	3.72±0.38	0.78±0.13	5.18±1.24	0.52±0.01	0.10±0.01	5.05±0.47
LC-F	3.31±0.27	0.78±0.11	4.51±0.82	0.47±0.02	0.11±0.01	4.31±0.28

Fig. 1

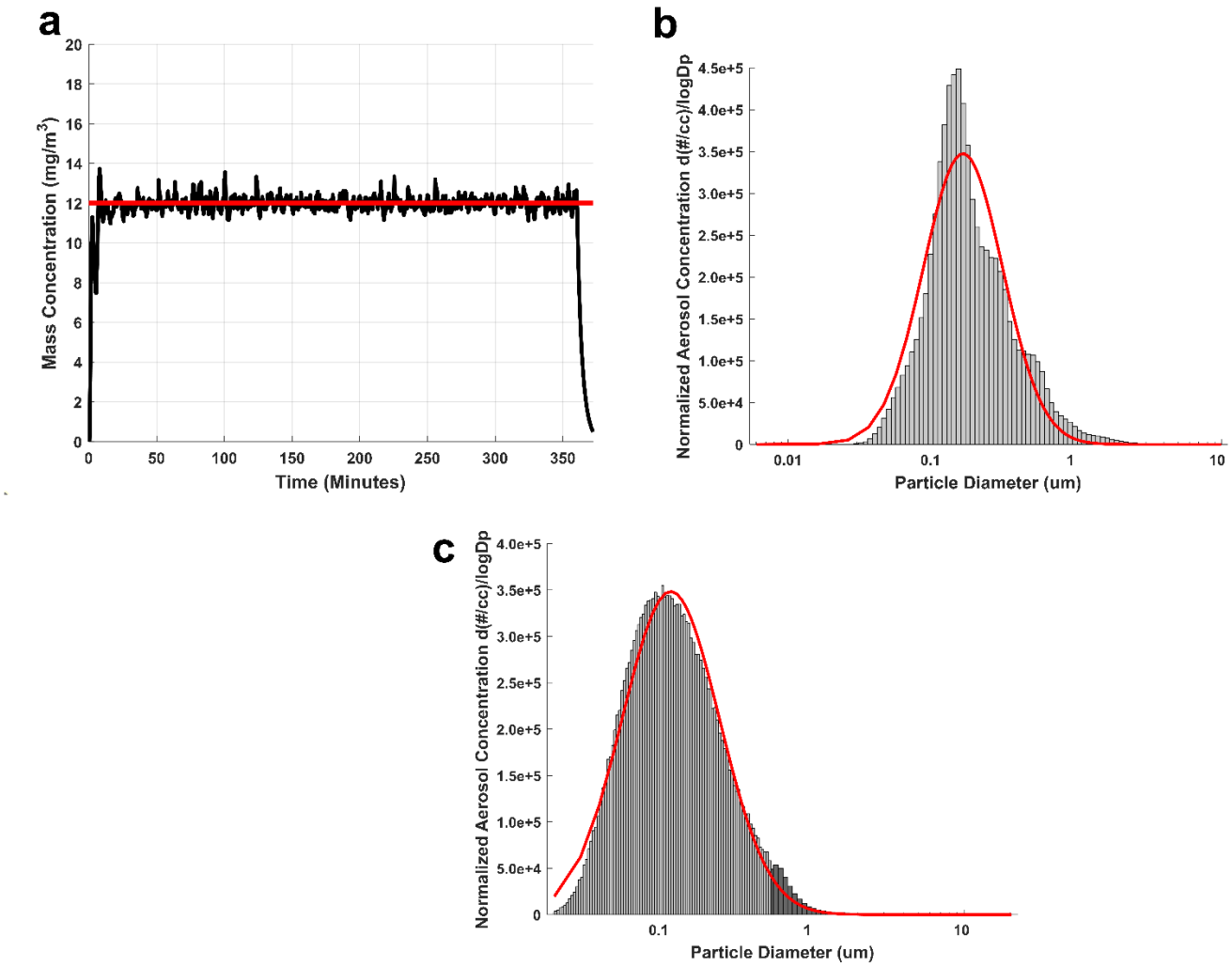
a
Mass Concentration (mg/m3)
Time (Minutes)
b
Normalized Aerosol Concentration d(#/cc)/logDp
Particle Diameter (um)
c
Normalized Aerosol Concentration d(#/cc)/logDp
Particle Diameter (um)

Fig. 2

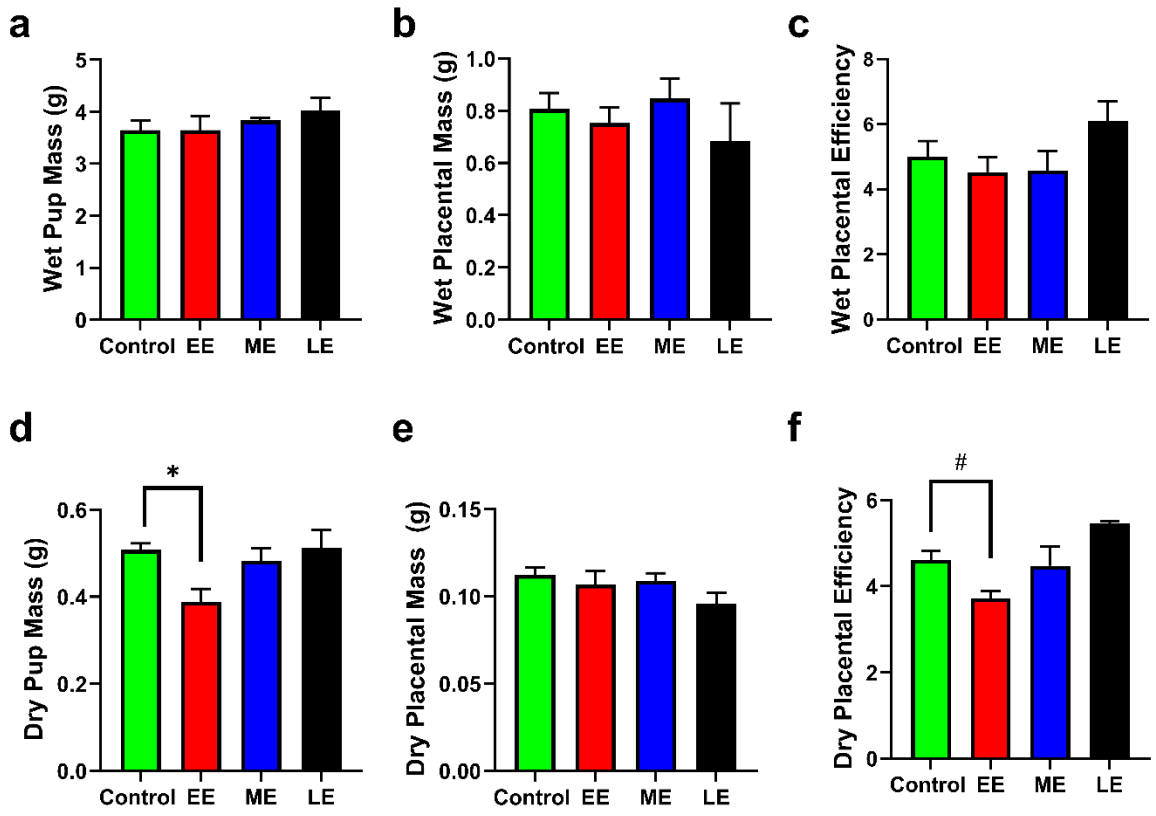
a
Wet Pup Mass (g)
0
1
2
3
4
5
Control EE ME LE
b
Wet Placental Mass (g)
0.0
0.2
0.4
0.6
0.8
1.0
Control EE ME LE
c
Wet Placental Efficiency
0
2
4
6
8
Control EE ME LE
d
*
Dry Pup Mass (g)
0.0
0.2
0.4
0.6
Control EE ME LE
e
Dry Placental Mass (g)
0.00
0.05
0.10
0.15
Control EE ME LE
f
#
Dry Placental Efficiency
0
2
4
6
Control EE ME LE

Fig. 3

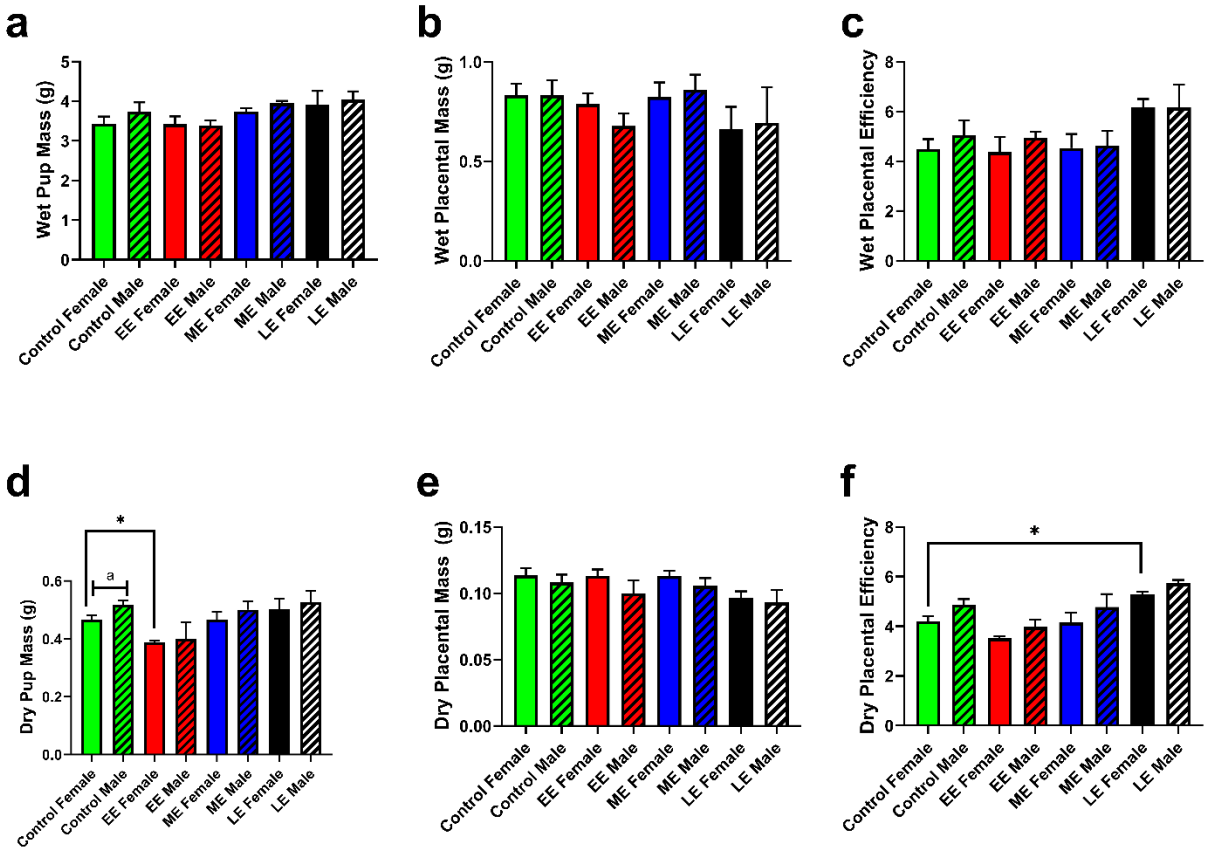
a
Wet Pup Mass (g)
0
1
2
3
4
5
b
Wet Placental Mass (g)
0.0
0.5
1.0
c
Wet Placental Efficiency
0
2
4
6
8
Control Female
Control Male
EE Female
EE Male
ME Female
ME Male
LE Female
LE Male
d
Dry Pup Mass (g)
0.0
0.2
0.4
0.6
*
a
e
Dry Placental Mass (g)
0.00
0.05
0.10
0.15
f
Dry Placental Efficiency
0
2
4
6
8
*

Fig. 4

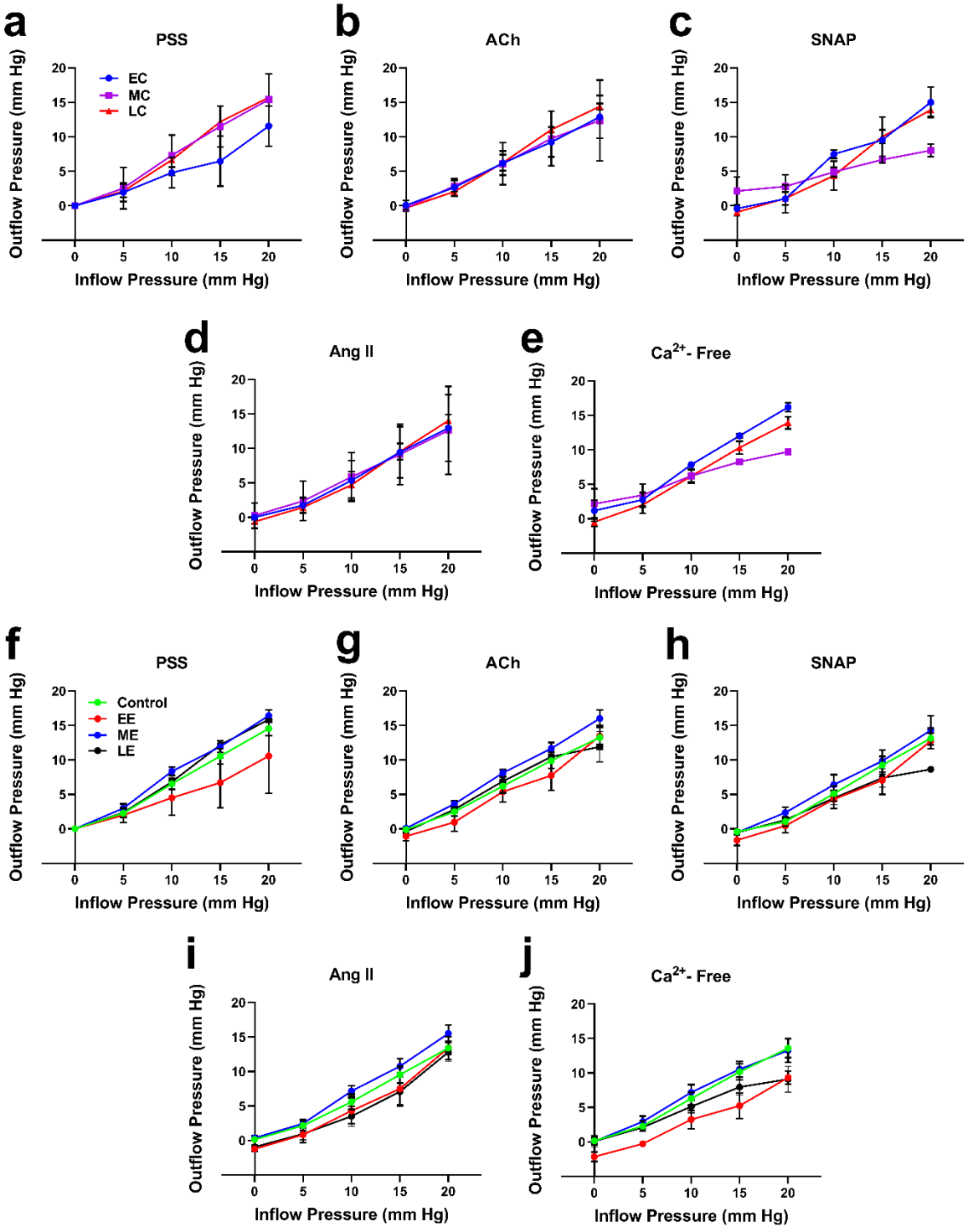
a
PSS
EC
MC
LC
b
ACh
c
SNAP
d
Ang II
e
Ca2+- Free
f
PSS
Control
EE
ME
LE
g
ACh
h
SNAP
i
Ang II
j
Ca2+- Free
Outflow Pressure (mm Hg)
Inflow Pressure (mm Hg)
0
5
10
15
20

Fig. 5

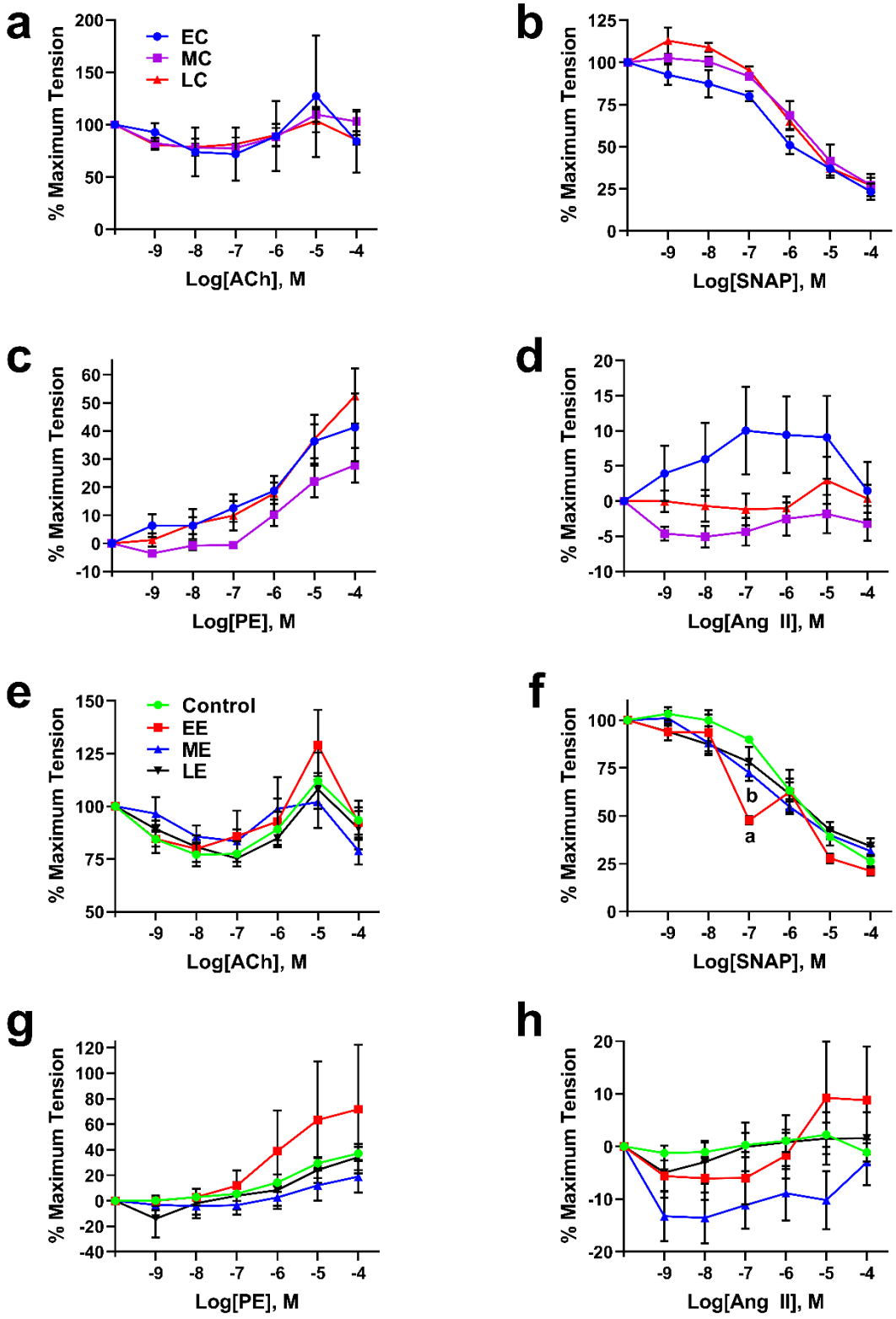
a
% Maximum Tension
EC
MC
LC
Log[ACh], M
b
% Maximum Tension
Log[SNAP], M
c
% Maximum Tension
Log[PE], M
d
% Maximum Tension
Log[Ang II], M
e
% Maximum Tension
Control
EE
ME
LE
Log[ACh], M
f
% Maximum Tension
b
a
Log[SNAP], M
g
% Maximum Tension
Log[PE], M
h
% Maximum Tension
Log[Ang II], M

Fig. 6

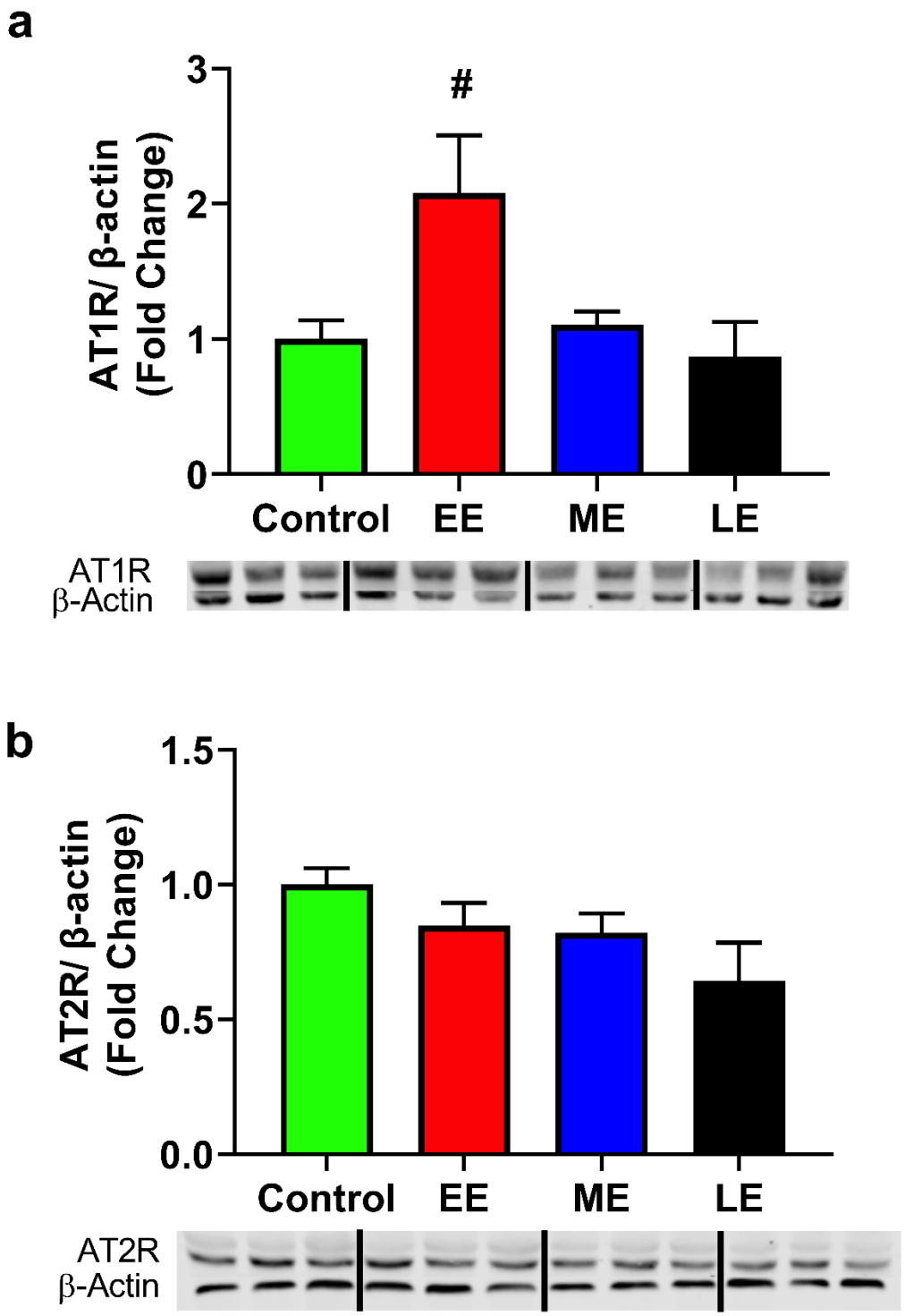
a
AT1R/ β-actin
(Fold Change)
3
2
1
0
#
Control
EE
ME
LE
AT1R
β-Actin
b
AT2R/ β-actin
(Fold Change)
1.5
1.0
0.5
0.0
Control
EE
ME
LE
AT2R
β-Actin

Fig. 7

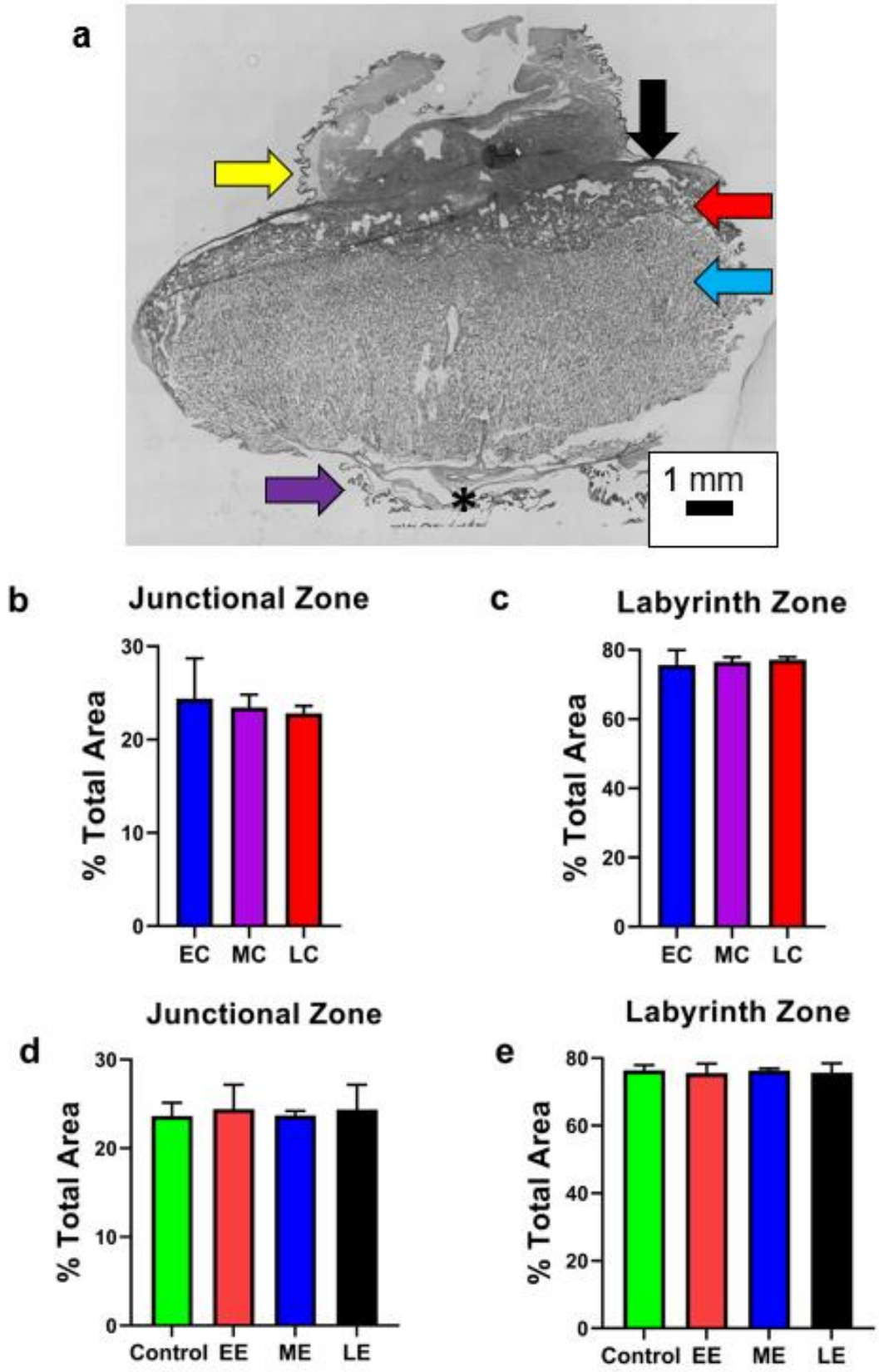
a
1 mm
b
Junctional Zone
% Total Area
30
20
10
0
EC MC LC
c
Labyrinth Zone
% Total Area
80
60
40
20
0
EC MC LC
d
Junctional Zone
% Total Area
30
20
10
0
Control EE ME LE
e
Labyrinth Zone
% Total Area
80
60
40
20
0
Control EE ME LE

VI. Chapter 6

3D Printer Emissions from Acrylonitrile Butadiene Styrene (ABS) Filament Result in Microvascular Consequences

Authors:

Garner, K.L.[1,2]

Bowdridge, E.C.[1,2]

Griffith, J.A.[1,2]

Farcas, M.T.[2,3,4]

McKinney, W.[3]

Qian, Y.[3]

Nurkiewicz, T.R. [1,2,3]

Affiliations:

[1]Department of Physiology and Pharmacology, West Virginia University School of Medicine, Morgantown, WV

[2]Center for Inhalation Toxicology (iTOX), West Virginia University School of Medicine, Morgantown, WV

[3]National Institute for Occupational Safety and Health, Morgantown, WV

[4]Pharmaceutical and Pharmacological Sciences, West Virginial University School of Medicine, Morgantown, WV

Abstract

3 dimensional printers (3D printers) are found extensively in commercial and household environments. During 3D printer use, volatile organic compounds (VOCs) and particulate matter, including ultrafine matter, are released into the air. While the benefits of the utilization of this technology are clear, little is known about the consequences of 3D printer emissions (3DPE) exposure. To identify the microvascular consequences associated with exposure, 5 different exposure groups were utilized to assess the effects of varying exposure lengths. Whole-body exposure was completed for 4 hours per day for either 1, 4, 8, 15, or 30 days. Mesenteric arteries were excised and microvascular responses were assessed including endothelial-dependent, -independent, and adrenergic responses. Artery wall thickness was shown to be increased on exposure groups 1-, 4- and 30-day. Wall tension was also shown to be significantly increased within the 15- and 30-day groups compared to the control. Endothelial-dependent response was shown to be altered within the 8-day group compared to the control and no differences were observed between any of the groups when assessing endothelial-independent vasodilation. When assessing adrenergic responses, the 1-, 4- and 30-day groups showed decrease response to phenylephrine compared to the control. This research showed that regardless of the length of the exposure, microvascular dysfunction was detected within each of the groups. Intriguingly, when assessing endothelial-dependent vasodilation, it appears that following 8 days of exposure the ability to respond to acetylcholine was improved, suggesting there may be a compensatory mechanism.

Introduction

The use of 3 dimensional (3D) printers has become commonplace throughout occupational and commercial environments as well as in domestic households. While the utilization of this technology has no doubt been beneficial for production, the consequences of exposure to these systems have yet to be fully elucidated. 3D printer emissions (3DPE) have been shown to be a complex mixture of particulate matter and volatile organic compounds (VOCs) [1, 2]. VOCs identified within these emissions include acetaldehyde, ethanol, acetone, isopropyl alcohol styrene and ethylbenzene [1]. Additionally, particulates were found well within the ultra-fine particle range during the use of the 3D printer [3]. This is of importance as VOCs may adsorb onto ultrafine particulates allowing them to further infiltrate the pulmonary system and reach deep within the terminal alveoli when inhaled [4]. Ultrafine particles may result in more toxic effects than other larger particulate matter due to the ability of ultrafine particles to embed not only throughout the pulmonary system, but because they have a greater deposition fraction within the terminal lung [5].

Inhalation of ultrafine particles has been linked to inflammatory effects as well as cardiovascular dysfunction [6-8]. Further, VOCs have been shown to cause irritation when inhaled as well as even may be linked to cancer [9]. Styrene has been labeled as Group 2A probably carcinogenic to humans by the International Agency for Research on Cancer (IARC) and ethylbenzene has been categorized as Group 2B possible carcinogenic to humans [10, 11]. Given the toxic concerns of VOCs as well as ultrafine particulate matter, it is of great concern to fully identify the risks of exposure to 3DPE.

Given the indoor use of this technology as well as the continued off-gas of VOCs from the object after printing [2], it is important to fully understand the ramifications of inhalation exposure to 3DPE. 3DPE has been linked to cardiovascular dysfunction, such as acute hypertension, as well as microvascular dysfunction [12]. Currently, the examination of these cardiovascular effects following continued use has not been investigated. In this study, five different exposure durations were examined over the course of either 1-, 4-, 8-, 15- or 30-day exposures to elucidate microvascular consequences associated with exposure.

Methods

Animal Characteristics

Male Sprague-Dawley rats were purchased from Hilltop Laboratories (Scottdale, PA) and housed as detailed in Farcas et al. 2020 [13]. All procedures were approved by the CDC-Morgantown Institutional Animal Care and Use Committee; accredited by the AAALAC International.

3D Printer ABS Filament Emissions Inhalation Exposure

A whole-body exposure chamber system was designed and utilized to conduct FFF 3D printer emissions exposures. Mass flow controller (MCRW-50-DS; Alicat Scientific, Tucson, Arizona) controlled flow rate during the exposures and was held at 30 L/min. A Differential pressure transducer (Model 264; Setra Systems, Inc. Boxborough, Massachusetts) assessed exposure chamber pressure during exposure. Temperature and relative humidity were monitored during the exposure. Three 3D printers were utilized to run using blue ABS filament currently commercially available. Rats were exposed to emissions for 4 h/day, with a single concentration of ~240 $\mu g/m^3$ ABS particle mass

concentration. There were 5 exposure groups exposed to either 1 day, 4 days, 8 days, 15 days or 30 days of 3D printer emissions. The exposure system is extensively detailed in Farcas et al. 2020 [13].

3D Printer ABS Emissions Characterization

Data RAM (DR-40000; Thermo Electron Co., Waltham, Massachusetts) was utilized to assess real-time aerosol mass concentration. Fast mobility particle sizer (FMPS, Model 3091; TSI Inc., Shoreview, Minnesota) was utilized as well as a field emission scanning electron microscope to assess physical characterization of particles (Hitachi S-4800, Tokyo, Japan). Volatile organic compounds (VOCs) were sampled by utilizing evacuated canisters (Entech Instruments Inc., Simi Valley, California) and analyzed as detailed in Farcas, et al. 2020 [13].

Euthanasia and Tissue Harvest

Rats were euthanized as detailed in Farcas, et al. 2020 [13]. The mesentery was dissected from the body and placed in a petri dish containing 4 ˚C physiological salt solutions (PSS, in mmol/L: 129.8 NaCl, 5.4 KCl, 0.5 NaH_2PO_4, 0.83 $MgSO_4$, 19.0 $NaHCO_3$, 1.8 $CaCl_2$, 5.5 glucose) and transferred immediately on ice. The mesentery was transferred to a dissection dish and A2 arterioles were cleaned and isolated.

Microvascular Reactivity

Mesenteric arteriole responses were evaluated following inhalation exposure for various time period lengths. Arterioles were isolated and transferred to isolated vessel chambers (Living Systems Instrumentation, Burlington, Vermont) containing PSS. Arterioles were cannulated and pressurized using glass pipette tips (Living Systems Instrumentation,

Burlington, Vermont) and were secured with 6-0 suture (AD Surgical, Sunnyvale, California). Arterioles were pressurized to 60 mm Hg and superfused (10 ml/min) with 37 ˚C PSS bubbled with 21% O_2/ 5% CO_2. Inner and outer diameter was measured with video calipers (Colorado Video, Boulder, Colorado). Vessels developed spontaneous tone before reactivity was assessed. The degree of constriction by a blood vessel relative to its maximally dilated states is spontaneous tone. Vascular tone ranges from 0% (complete relaxation, maximum dilation) to 100% (complete lumen closure, maximum constriction). Only vessels that developed tone ≥20% than initial tone were included in this study.

Mesenteric arterioles were treated with increasing cumulative doses of endothelium-dependent vasodilator acetylcholine (ACh, 10^{-9} - 10^{-4} M), endothelium-independent vasodilator S-nitroso-N-acetyl-DL-penicillamine (SNAP, 10^{-9} - 10^{-4} M) and α_1 adrenergic agonist phenylephrine (PE, 10^{-9} - 10^{-4} M). Steady state diameter was recorded following the addition of each dose. Following each dose response curve, the vessel was washed with fresh PSS until agonist was removed. Once all dose response curves were completed, PSS was removed and replaced with Ca^{2}- free PSS for 30 minutes for maximum passive diameter to be identified.

Pressure Myography Calculations

Spontaneous tone was determined using the following equations:

$$\boldsymbol{Spontaneous\ Tone}\ (\%) = \left[\frac{(\boldsymbol{Dm} - \boldsymbol{Di})}{(\boldsymbol{Di})}\right] \times \mathbf{100}\%$$

Dm represents the maximal diameter and Di is the initial steady-state diameter before experimental treatment. The vascular response to ACh and SNAP was calculated using the following equation:

$$\boldsymbol{Diameter}\ (\%\ \boldsymbol{Dilation}) = \left[\frac{(\boldsymbol{Dss} - \boldsymbol{Dcon})}{(\boldsymbol{Dm} - \boldsymbol{Dcon})}\right] \times \mathbf{100}\%$$

Dcon represents the diameter before treatment and Dss represents the steady-state diameter following the addition of agonist dose. The vascular response of PE was calculated using the following equation:

$$\boldsymbol{Diameter}\ (\%\ \boldsymbol{Constriction}) = -\left[\frac{(\boldsymbol{Dcon} - \boldsymbol{Dss})}{(\boldsymbol{Dcon})}\right] \times \mathbf{100}\%$$

Wall thickness (WT) of the vessels was calculated by measuring the inner (ID) and outer (OD) diameters and utilizing the following equation:

$$\boldsymbol{WT} = \frac{(\boldsymbol{OD} - \boldsymbol{ID})}{\mathbf{2}}$$

Wall-to-lumen ratio (WLR) of the vessels was calculated using the following equation:

$$\boldsymbol{WLR} = \frac{\boldsymbol{WT}}{\boldsymbol{ID}}$$

Statistics

Two-way repeated measures analysis of variance (ANOVA) was performed to identify point-by-point differences in dose response curves. A Dunnett's post hoc analysis was utilized when significance was found. Vessel % tone, wall thickness (WT) and wall tension were evaluated by one-way ANOVA and Dunnett's post hoc analysis when significance

was found. All data is reported as the mean ± standard error (SE). Significance was set as $p \leq 0.05$. All p-values are reported after multiple-comparison adjustments.

Results

Particle and VOC Characterization and Deposition

Gravimetric filters assess the average mass concentration to be 240 μg/m^3 and a standard deviation (SD) of 90 μg/m^3. Condensation particle counter determined the average count concentration per day to be 88,400 particles/cm^3 and a SD of 23,000 particles/cm^3. Particle size distribution plots and the scanning electron microscope image (SEM) are displayed in Farcas et al. 2020 [13]. In short, the geometric mean diameter started at 40 nm but increased after 20 minutes into the print job to 85 nm and steadied to 79-95 nm for the remaining 4h exposure with a geometric SD of 1.6 [13].

VOCs were analyzed via GC/MS and are detailed in Farcas et al. 2020 [13]. All levels were well within OSHA permissible exposure limits and NIOSH recommended exposure limits. VOCs detected in ABS emissions included acetaldehyde, benzene, and ethanol [13].

Mesenteric Microvascular Characteristics

Percent tone, vessel wall thickness and wall tension were calculated and measured to assess vascular adaptations that may have occurred following inhalation exposure. There were no statistical differences between any of the exposure groups and control when assessing percent tone (Fig. 1a) or WLR (Fig. 1c). When assessing wall thickness, control vessels (30 ± 2 μm) were significantly smaller compared to wall thickness from the 4-day exposure group (46 ± 5 μm). 1- day (44 ± 6 μm) and 30-day (42 ± 5 μm) exposures yielded

larger wall thicknesses trending towards significance (Fig. 1b). Wall tension was calculated and was significantly increased in the 15-day (1.73 ± 0.13 N/m) and 30-day (1.80 ± 0.04 N/m) group compared to the control (1.34 ± 0.08 N/m) (Fig.1d).

Mesenteric Microvascular Reactivity

When assessing point-by-point differences, endothelium-dependent vasodilation was significantly augmented within the 8-day group at ACh dose $1x10^{-6}$ M and $1x10^{-4}$ M (Fig. 2a). Point-by-point differences with endothelium-independent vasodilator SNAP yielded no significant differences between the groups and the control (Fig. 2b). Point-by-point differences when assessing α_1 adrenergic agonist PE were apparent between 1-day and control at $1x10^{-7}$ M, $1x10^{-5}$ M, and $1x10^{-4}$ M, showing a decreased response to PE. Response was also significantly decreased at $1x10^{-7}$ M for 4 day and at $1x10^{-5}$ M and $1x10^{-4}$ M for 15-day.

Discussion

Inhalation exposure to 3DPE has been linked to cardiovascular consequences and microvascular dysfunction [12]. Given the routine use of this technology, it is important to evaluate the consequences of long-term repeated exposure. In this study, we identified microvascular consequences associated with exposure for 1, 4, 8, 15 and 30 days. Regardless of the exposure paradigm, microvascular alterations to vascular anatomy and/or responses were identified in all exposure groups. Further, we were able to identify a potential compensatory response within the endothelial-dependent data following repeated exposure to 3DPE.

Wall thickness was shown to be significantly increased within the 4-day exposure group (Fig. 1b). An increase in wall thickness was trending withing the 1-day exposure as well as the 30-day exposure group, showing potential alterations within the shortest and longest exposure paradigm (Fig. 1b). While the inner and outer diameter was not significantly different between groups (data not shown), small alterations of these diameters could be a result of outward hypertrophic growths, as seen in pregnancy [14], or inward hypertrophic growth, which would cause an increased wall thickness following exposure. Inward hypertrophic growth is a response to hypertension [15]. Further, past data has shown an increase in blood pressure following inhalation exposure to 3DPE [12], additionally supporting evidence of cardiovascular ramifications. Wall tension was also shown to be increased in both 15- and 30-day exposure groups (Fig. 1d). High wall tension is required to withstand increased pressure and results in vasoconstriction in a stable, elastic vessel. If vascular dysfunction were to occur and wall tension were to be fixed, this could lead to collapse of the vessel [16]. While not significant, it was also interesting to see a steady increase in tone of the vessels to the 8-day exposure, followed by an inverse decrease to the 30-day exposure, perhaps suggesting a compensatory mechanism at play, as inhalation exposure to other ultrafine particulates has been shown to increase microvascular tone [8].

It was found that adrenergic response to PE was shown to be decreased significantly in 1-, 4- and 30-day exposures compared to the control (Fig. 2c). Additionally, endothelial-dependent vasodilation was significantly decreased within the 8-day exposure group (Fig. 2a). Interestingly, while not statistically significant, the ability to vasodilate appears to decrease from 1-day all the way to 8-day, from there, vasodilation increases from 15-day

to 30-day. This once again suggests the possibility of a compensatory mechanism after repeated exposure. One theory could be an increased antioxidant presence, which could lead to lowered reactive species and an increased nitric oxide bioavailability. While this is one theory, additional tests would have to be performed to assess if there is indeed a compensatory mechanism at play. Further, endothelial-independent vasodilation was not affected by 3DPE inhalation exposure (Fig. 2b). This suggests that endothelial dysfunction or nitric oxide bioavailability is driving these microvascular consequences.

All exposure groups were shown to result in some form of anatomical change or physiological response alterations following 3DPE exposure. One limitation of this study includes the transfer of tissues to our lab from NIOSH. While the tissue was transferred as soon as possible form NIOSH to our facility, kept on ice and in cold PSS, it is possible that differing transfer times may have affected the viability of the vascular network. This may have resulted in artifact when examining microvascular response and tone. Moving forward, these experiments should be done within the same lab to ensure proper preservation of the tissue and increased viability.

This study determined that 3DPE inhalation exposure, regardless of duration, resulted in microvascular consequences. These results further highlight the importance of increased ventilation and shield use when working with 3D printers in a commercial or household setting. With the increased presence of 3D printer technology, the cardiovascular consequences must be identified to fully understand the risks of use and exposure.

Figure Legends

Fig. 1 Microvascular characteristics following inhalation exposure to 3D printer emissions. (a) percent tone of mesenteric arterioles following ABS filament exposure. (b) microvascular wall thickness. (c) Wall-to-lumen ratio (WLR) of mesenteric arterioles assessed. (d) wall tension of mesenteric microvascular vessels. Data are mean ± SE. *, $P \leq 0.05$ vs control; #, $P \leq 0.07$ vs control

Fig. 2 Mesenteric arteriole dose response following inhalation exposure to 3D printer emissions for multiple time periods. (a) endothelium dependent response to ACh. (b) endothelium independent response to SNAP. (c) adrenergic response to PE. Data are mean ± SE. a, $P \leq 0.05$ control vs 1-day; b, $P \leq 0.05$ control vs 4-day; c, $P \leq 0.05$ control vs 8-day; d, $P \leq 0.05$ control vs 30-day

References

1. Byrley, P., et al., *Particle and volatile organic compound emissions from a 3D printer filament extruder.* Sci Total Environ, 2020. **736**: p. 139604.
2. Stefaniak, A.B., et al., *Characterization of chemical contaminants generated by a desktop fused deposition modeling 3-dimensional Printer.* J Occup Environ Hyg, 2017. **14**(7): p. 540-550.
3. Yi, J., et al., *Emission of particulate matter from a desktop three-dimensional (3D) printer.* J Toxicol Environ Health A, 2016. **79**(11): p. 453-65.
4. Zhang, X., et al., *Adsorption of VOCs onto engineered carbon materials: A review.* J Hazard Mater, 2017. **338**: p. 102-123.
5. Daigle, C.C., et al., *Ultrafine particle deposition in humans during rest and exercise.* Inhal Toxicol, 2003. **15**(6): p. 539-52.
6. Abukabda, A.B., et al., *Group II innate lymphoid cells and microvascular dysfunction from pulmonary titanium dioxide nanoparticle exposure.* Part Fibre Toxicol, 2018. **15**(1): p. 43.
7. Abukabda, A.B., et al., *Heterogeneous Vascular Bed Responses to Pulmonary Titanium Dioxide Nanoparticle Exposure.* Front Cardiovasc Med, 2017. **4**: p. 33.
8. Bowdridge, E.C., et al., *Maternal Engineered Nanomaterial Inhalation During Gestation Disrupts Vascular Kisspeptin Reactivity.* Toxicol Sci, 2019. **169**(2): p. 524-533.
9. Wolkoff, P., *Indoor air pollutants in office environments: assessment of comfort, health, and performance.* Int J Hyg Environ Health, 2013. **216**(4): p. 371-94.
10. *Evaluation of Carcinogenic Risks to Humans: some industrial chemicals. 15-22 February 2000, Lyon, France.* IARC Monogr Eval Carcinog Risks Hum, 2000. **77**: p. 1-529.
11. Humans, I.W.G.o.t.E.o.C.R.t., *IARC Monographs on the Evaluation of Carcinogenic Risks to Humans*, in *Styrene, Styrene-7,8-oxide, and Quinoline*. 2019: Lyon (FR).

12. Stefaniak, A.B., et al., *Inhalation exposure to three-dimensional printer emissions stimulates acute hypertension and microvascular dysfunction.* Toxicol Appl Pharmacol, 2017. **335**: p. 1-5.

13. Farcas, M.T., et al., *Pulmonary and systemic toxicity in rats following inhalation exposure of 3-D printer emissions from acrylonitrile butadiene styrene (ABS) filament.* Inhal Toxicol, 2020. **32**(11-12): p. 403-418.

14. Osol, G. and M. Mandala, *Maternal uterine vascular remodeling during pregnancy.* Physiology (Bethesda, Md.), 2009. **24**: p. 58-71.

15. Intengan, H.D. and E.L. Schiffrin, *Vascular remodeling in hypertension: roles of apoptosis, inflammation, and fibrosis.* Hypertension, 2001. **38**(3 Pt 2): p. 581-7.

16. Boron, W.F.e.a., *Elastic Properties of Blood Vessels*, in *Medical Physiology, 3rd Edition*. 2017.

Fig. 1

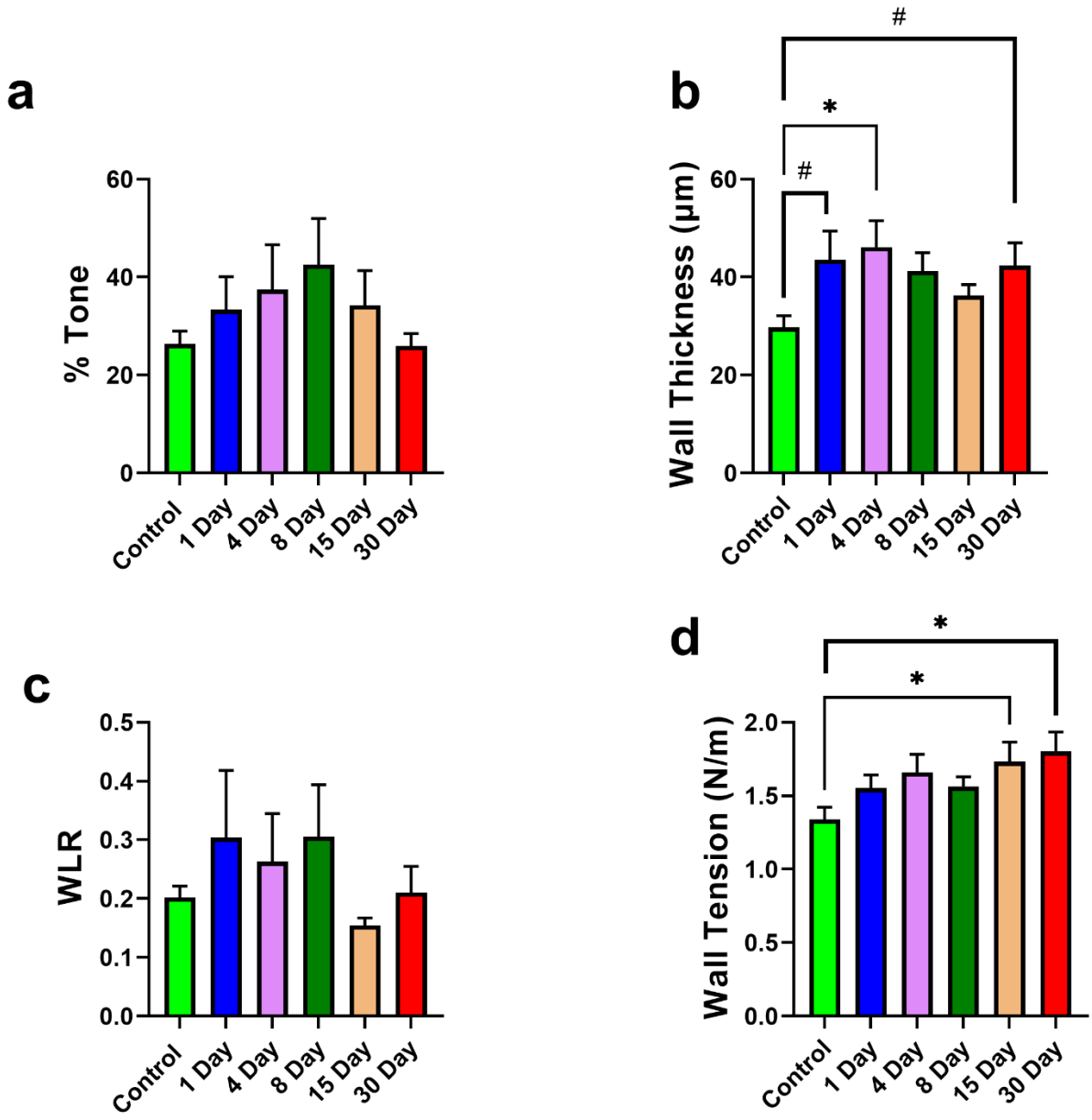
a
% Tone
60
40
20
0
Control
1 Day
4 Day
8 Day
15 Day
30 Day
b
Wall Thickness (µm)
#
*
#
c
WLR
0.5
0.4
0.3
0.2
0.1
0.0
d
Wall Tension (N/m)
2.0
1.5
1.0
0.5
0.0
*
*

Fig. 2

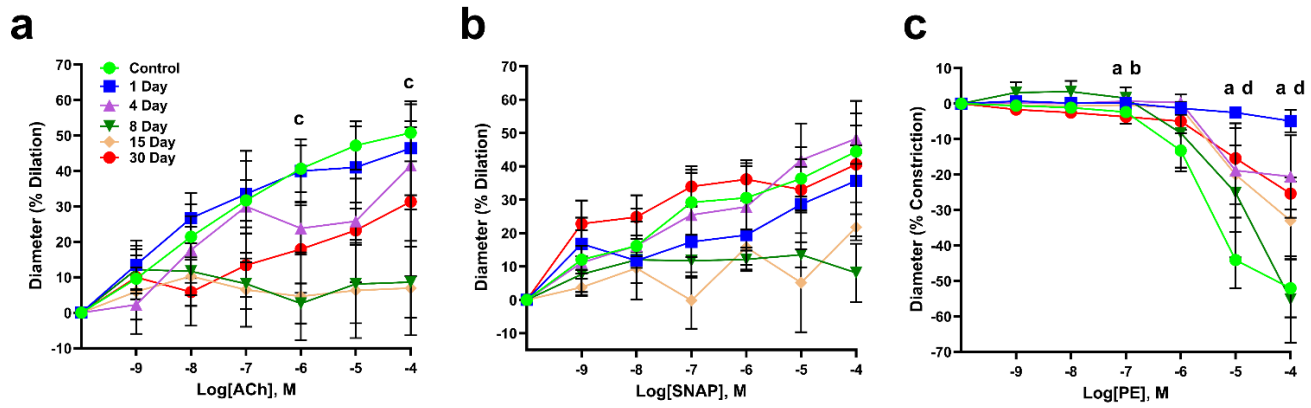
a
b
c
Control
1 Day
4 Day
8 Day
15 Day
30 Day
Diameter (% Dilation)
Log[ACh], M
Log[SNAP], M
Diameter (% Constriction)
Log[PE], M
c
c
a b
a d
a d

VI. General Discussion

The purpose of this dissertation was to further identify cardiovascular dysfunction associated with inhalation exposure to nano-TiO_2. Further, we wanted to identify the critical period of gestation at which maternal and fetal health is most susceptible to exposure. To do so, we assessed myogenic responsiveness within the maternal uterine microcirculation, fetal aortic responses, and angiotensin II (Ang II) influences within the maternal and placental microcirculation following specific gestational day (GD) maternal exposure. Through this, we were able to identify an Ang II specific mechanism by which early gestational exposure results in decreased pup weight. Further, we found that with this same exposure paradigm, the placenta does not seem to play a role in the fetal consequences reported here in.

In our first study, we found that myogenic responsiveness was not altered, regardless of adrenergic influence (Fig.3, page.87 and Fig.4, page 88). The myogenic response is an important component of vascular function of the microcirculation [1] and if not properly adapted during pregnancy, may result in reduced blood flow within the uterine circulation [2]. While evidence has shown that maternal inhalation exposure to nano-TiO_2 during gestation results in reduced pup mass (Fig. 3, page 127) [3-5], this data suggests that the myogenic response does not play a role in these reported consequences. If myogenic responsiveness had been increased following exposure, one may expect reduced blood flow within the uterus and therefore reduced nutrient delivery to the fetoplacental units, thereby resulting in reduced pup mass. Myogenic tone and actin polymerization within uterine arteries has been shown to be reduced following 17β-estradiol and progesterone

treatment [2]. Given that nano-TiO_2 maternal inhalation exposure during gestation resulted in reduction in circulating estradiol levels [3], this may inhibit the usual reduction in myogenic tone associated with pregnancy.

Additionally, within our first study, we found that maternal inhalation exposure to nano-TiO_2 during gestation can result in altered vascular response within the fetal circulation. These data showed reduced endothelium-dependent vasodilatory responses while displaying unaltered endothelium-independent vasodilation (Fig. 5, page 89). These findings suggest to us that the dysfunction must stem from the endothelial layer of the circulation, due to the ability of vascular smooth muscle to respond to nitric oxide (NO) directly. Given the inflammatory response that results from nano-TiO_2 inhalation [6], reduced NO activity may be a result of reduced bioavailability from enhanced reactive oxygen species (ROS) formation, such as superoxide anions [7]. The alterations observed within the F1 generation, such as aortic vascular responses, suggest that exposure within the F0 generation may result in effects transcending to the next generation. Transgenerational epigenetic inheritance occurs when the first unexposed generation exhibits effects from the F0 exposure [8]. Exposure to the F0 generation includes direct exposure of not only the F1 generation, but also any offspring within F2 generation, as eggs and sperm (F2) are already developed within the F1 generation in utero. We hypothesize that transgenerational consequences can occur through maternal nano-TiO_2 inhalation exposure. An example of transgenerational inheritance is F0 exposure to plastic additive bisphenol A, which has shown to result in F3 generational obesity, ovarian disease and heart disorders [9, 10]. While not transgenerational, our lab has shown multigeneration effects following maternal nano-TiO_2 inhalation exposure.

This study found that F1 dams, born from exposed F0 dams, had increased hydrogen peroxide (H_2O_2) production and therefore NF-κB activation [5]. Additionally, other nanoparticles, such as gold, have been shown to cause multigenerational effects, such as decreased reproduction rate [11].

These findings further suggest that developmental origins of health and disease (DOHaD) is a critical theory to consider when assessing fetal outcomes. If subsequent generations are affected following F0 exposure, epigenetic changes may be at play and these changes could have devastating effects. Moving forward, transgenerational effects of exposure need to be considered when assessing the full toxicological ramifications of gestational maternal inhalation exposure to nano-TiO_2.

To further examine the effects of maternal exposure to aerosolized nano-TiO_2, studies 2 and 4 were performed to assess the critical window of gestational exposure. This is important as pregnancy detection usually occurs after any potential insults have occurred in early gestation. Additionally, women typically do not stop working until their third trimester, allowing occupational exposure to proceed throughout pregnancy. In both studies, exposure time points were broken down into either early, mid or late gestation and all evaluation was performed on GD 20. In study 2, we found that, regardless of exposure group, endothelium-dependent vasodilation within uterine radial arteries were significantly reduced (Fig.5a-b, page 129). Further, it was found that Ang II sensitivity to vasoconstriction was significantly increased, but only within the early exposure (EE) group (Fig. 5g-h, page 129). Alterations in Ang II sensitivity or balance has been implicated in preeclampsia, gestational hypertension and fetal growth restriction [12, 13]. For a healthy pregnancy, Ang II sensitivity must decrease [14]. By doing so, this allows

for increased blood volume without increasing blood pressure, thereby enhancing blood flow to the uterus and fetus. While we did not have a model of preeclampsia, the data in study 2 showed that the exposure resulted in a hostile gestational environment, leading to decreased pup mass, therefore poor fetal outcomes.

We further determined that at least one mechanism through which increased vasoconstrictor sensitivity was occurring is through decreased presence of angiotensin II type 2 receptor (AT_2R) protein within the uterine circulation (Fig.6b, page 130). It has been shown that AT_2R is increased within the uterine circulation during pregnancy, while angiotensin II type 1 receptor (AT_1R) remained unchanged [15]. Given that AT_2R stimuli results in vasodilation, balancing the AT_1R responses, this would cause a decreased vasoconstrictive network regarding Ang II stimulation. AT_1R/AT_2R balance is crucial to suppress the Ang II pressor response while supporting the renin-angiotensin-aldosterone system (RAAS). RAAS stimulation results in release of aldosterone leading to reabsorption of sodium and water, thereby increase blood volume during pregnancy. Perturbations of this mechanism, such as during preeclampsia, is partly caused by increased AT_1R protein expression and decreased AT_2R expression [16].

We speculate that the cause for this receptor balance alteration may be due to a reduction of circulating estradiol levels following maternal inhalation exposure. This has been shown before with kisspeptin (Kiss), a peptide that plays physiological roles in trophoblast invasion and puberty [17, 18]. Similar to Ang II, Kiss is a vasoconstrictor that has been implicated in preeclampsia and intrauterine growth restriction [19]. Our lab has shown that inhalation exposure to nano-TiO_2 during gestation has resulted in decreased estradiol, leading to increased sensitivity to Kiss vasoconstriction within the uterine

arteries following exposure [3]. Similarly, estradiol has been linked to increased AT_2R protein levels within the uterine circulation and the kidney during pregnancy [15, 20]. Surprisingly, we were unable to show a reduction of estradiol at GD 20 in our EE group or any other exposure group (Fig.7, page 131). Given that the last day of exposure within the EE group occurred on GD 6, this insult may have affected estradiol levels and gone undetected due to the time of sampling. By GD 20, when these dams were euthanized, estradiol levels may have been improved, but the damage to the uterine microvasculature may have already been done. Future research must focus on assessing estradiol levels following exposure within the early and middle exposure groups before GD 20, as to capture these effects.

The EE group affected maternal uterine microvascular function, which may have potentially led to the decreased pup size observed in these dams at GD 20 (Fig. 3, page 127). Reduced blood flow due to this dysfunction within the uterus would have resulted in reduced pup size. This was reflected in our data and further suggests that exposure during early gestation results in the most critical adverse health effects. Our data also showed that placental efficiency was significantly reduced within the early exposure groups, meaning that the smaller pup required a much larger placenta to support any fetal growth or development (Fig. 3, page 127) [21]. Due to these results, we wanted to examine if placental anatomy and physiology may be altered as a result of maternal inhalation exposure, and if this may play a role in the poor fetal outcomes reported within the EE group.

Placental hemodynamics were assessed and was not altered within any of the exposure groups. We wanted to assess if Ang II may play a role in dysfunction placenta dysfunction,

as it did within the maternal uterine microcirculation, but this was not shown when assessing placental hemodynamics (Fig. 4, page 193) or umbilical artery function (Fig. 5, page 194). Additionally, Ang II receptor density was not significantly altered within any of the exposure groups (Fig. 6, page 194). Changes in placental zones or their function have been shown to reflect toxicological consequences following various exposures [22, 23]. Given this, we wanted to assess if placental zone surface area may have been affected following maternal inhalation exposure during gestation. Our study found that there were no changes to junctional or labyrinth zone area compared to the controls (Fig. 7, page 196). Given that there were no changes to placental anatomy or hemodynamics, we concluded that the placenta does not contribute to mechanism(s) responsible for smaller pup size within the EE group (Fig. 3, page 127). While zone area was not altered, it would be of interest to study placental anatomy, such as branching density within the placenta. If branching is reduced than overall placental resistance would increase within the unit, resulting in reduced blood flow [24]. This was one limitation of our study, that moving forward, should be explored.

These results were surprising, as past research has shown an increase in Ang II sensitivity, following maternal inhalation exposure, resulting in altered placental hemodynamics and reduced blood flow [25]. The difference observed between the two studies may be due to the exposure paradigm, which was 3 days in study 4 whereas it was 6 days in the previous experiment. Moving forward, prolonged exposures, beginning in early gestation, need to be performed to present a more accurate representation of occupational exposure during gestation. Perhaps an increased exposure period would

have resulted in placental dysfunction that was not able to be identified given the short 3-day exposure.

Due to gestation being an ongoing process, future experiments need to focus on exposures during the entirety of pregnancy. To fully appreciate the effects of maternal inhalation exposure to this ENM, a full scope experiment throughout gestation will be necessary. To gain even more insight into the reproductive consequences of these ENM aerosols, more experiments need to be completed to assess how exposure prior to mating may affect fertility. Given sex is a biological variable, this is in regard to not only female, but male fertility, and how this may impact pregnancy and future generations. While male outcomes were outside the scope of this dissertation, it is of equal importance in regard to multi- and transgenerational alterations following exposure. Evidence of multigeneration nano-TiO_2 exposure was shown in F1 males that exhibited cognitive deficits following in utero exposure [26]. Further, it would be interesting to explore potential differences between male and female placenta following exposure, given there has been evidence that pup sex ratio within the F1 generation tends to be favored towards females [5]. Given this finding, it could be possible that placental resistance is reduced within the female placental units compared to males.

In conclusion, this dissertation presents a mechanism involving Ang II, a critical hormone in pregnancy, in which maternal nano-TiO_2 inhalation exposure may result in poor fetal outcomes. Additionally, we found that early gestational exposure causes the most detriment to fetal health. This is significant due to the increased odds of occupational exposure prior to the third trimester, at which time most women will use maternity leave. Further, we found that these fetal outcomes, in part, stem from maternal uterine

microvascular dysfunction, including increased sensitivity to Ang II. Currently, the data here in suggests to us that these fetal outcomes are not related to placental dysfunction, as no differences were observed within our exposure groups. Moving forward, the future experiments presented above will need to be completed to fully appreciate the consequences of the growing field of advanced materials within our society.

References

1. Osol, G. and M. Cipolla, *Interaction of myogenic and adrenergic mechanisms in isolated, pressurized uterine radial arteries from late-pregnant and nonpregnant rats.* American Journal of Obstetrics & Gynecology, 1993. **168**(2): p. 697-705.
2. Xiao, D., et al., *Pregnancy downregulates actin polymerization and pressure-dependent myogenic tone in ovine uterine arteries.* Hypertension, 2010. **56**(5): p. 1009-15.
3. Bowdridge, E.C., et al., *Maternal Engineered Nanomaterial Inhalation During Gestation Disrupts Vascular Kisspeptin Reactivity.* Toxicol Sci, 2019. **169**(2): p. 524-533.
4. Garner, K.L., Bowdridge, E. C., Griffith, J. A., DeVallance, E., Seman, M. G., Engels, K. J., Groth, C. P., Goldsmith, W. T., Wix, K., Batchelor, T. P., & Nurkiewicz, T. R., *Maternal Nanomaterial Inhalation Exposure: Critical Gestational Period in the Uterine Microcirculation is Angiotensin II Dependent.* Cardiovascular Toxicology, 2022.
5. Bowdridge, E.C., et al., *Nano-titanium dioxide inhalation exposure during gestation drives redox dysregulation and vascular dysfunction across generations.* Part Fibre Toxicol, 2022. **19**(1): p. 18.
6. Abukabda, A.B., et al., *Group II innate lymphoid cells and microvascular dysfunction from pulmonary titanium dioxide nanoparticle exposure.* Part Fibre Toxicol, 2018. **15**(1): p. 43.
7. Galle, J., et al., *Endothelial dysfunction and inflammation: what is the link?* Kidney Int Suppl, 2003(84): p. S45-9.
8. Hanson, M.A. and M.K. Skinner, *Developmental origins of epigenetic transgenerational inheritance.* Environ Epigenet, 2016. **2**(1).
9. Manikkam, M., et al., *Plastics derived endocrine disruptors (BPA, DEHP and DBP) induce epigenetic transgenerational inheritance of obesity, reproductive disease and sperm epimutations.* PLoS One, 2013. **8**(1): p. e55387.

10. Lombo, M., et al., *Transgenerational inheritance of heart disorders caused by paternal bisphenol A exposure.* Environ Pollut, 2015. **206**: p. 667-78.

11. Kim, S.W., J.I. Kwak, and Y.J. An, *Multigenerational study of gold nanoparticles in Caenorhabditis elegans: transgenerational effect of maternal exposure.* Environ Sci Technol, 2013. **47**(10): p. 5393-9.

12. Yang, J., et al., *The role of the renin-angiotensin-aldosterone system in preeclampsia: genetic polymorphisms and microRNA.* J Mol Endocrinol, 2013. **50**(2): p. R53-66.

13. Delforce, S.J., et al., *Dysregulation of the placental renin-angiotensin system in human fetal growth restriction.* Reproduction, 2019. **158**(3): p. 237-245.

14. Irani, R.A. and Y. Xia, *Renin angiotensin signaling in normal pregnancy and preeclampsia.* Semin Nephrol, 2011. **31**(1): p. 47-58.

15. Mishra, J.S., K. Gopalakrishnan, and S. Kumar, *Pregnancy upregulates angiotensin type 2 receptor expression and increases blood flow in uterine arteries of rats.* Biol Reprod, 2018. **99**(5): p. 1091-1099.

16. Anguiano-Robledo, L., et al., *Renal angiotensin-II receptors expression changes in a model of preeclampsia.* Hypertens Pregnancy, 2007. **26**(2): p. 151-61.

17. Kotani, M., et al., *The metastasis suppressor gene KiSS-1 encodes kisspeptins, the natural ligands of the orphan G protein-coupled receptor GPR54.* J Biol Chem, 2001. **276**(37): p. 34631-6.

18. Bilban, M., et al., *Kisspeptin-10, a KiSS-1/metastin-derived decapeptide, is a physiological invasion inhibitor of primary human trophoblasts.* J Cell Sci, 2004. **117**(Pt 8): p. 1319-28.

19. Cetkovic, A., et al., *Plasma kisspeptin levels in pregnancies with diabetes and hypertensive disease as a potential marker of placental dysfunction and adverse perinatal outcome.* Endocr Res, 2012. **37**(2): p. 78-88.

20. Armando, I., et al., *Estrogen upregulates renal angiotensin II AT(2) receptors.* Am J Physiol Renal Physiol, 2002. **283**(5): p. F934-43.

21. Wilson, M.E. and S.P. Ford, *Comparative aspects of placental efficiency.* Reprod Suppl, 2001. **58**: p. 223-32.

22. Furukawa, S., N. Tsuji, and A. Sugiyama, *Morphology and physiology of rat placenta for toxicological evaluation.* J Toxicol Pathol, 2019. **32**(1): p. 1-17.

23. Kagawa, N., Y. Saito, and T. Nagao, *Early to middle gestational exposure to diethylstilbestrol impairs the development of labyrinth zone in mouse placenta.* Congenit Anom (Kyoto), 2014. **54**(2): p. 116-9.

24. Barapatre, N., et al., *Growth restricted placentas show severely reduced volume of villous components with perivascular myofibroblasts.* Placenta, 2021. **109**: p. 19-27.

25. Abukabda, A.B., et al., *Maternal titanium dioxide nanomaterial inhalation exposure compromises placental hemodynamics.* Toxicology and Applied Pharmacology, 2019. **367**: p. 51-61.

26. Engler-Chiurazzi, E.B., et al., *Impacts of prenatal nanomaterial exposure on male adult Sprague-Dawley rat behavior and cognition.* J Toxicol Environ Health A, 2016. **79**(11): p. 447-52.

VII. Curriculum Vitae

Krista L. Garner

Robert C. Byrd Health Sciences Center

1 Medical Center Drive • Morgantown, WV 26506

KLGarner22@gmail.com

Education

West Virginia University School of Medicine (2017-2022)

Division: Cellular and Integrative Physiology

Degree: PhD

Mount St. Mary's University (2009-2013)

Division: Biology

Degree: BS

Experience

West Virginia University School of Medicine (2017-2022)

Morgantown, WV

Graduate Research Assistant

Physiology and Pharmacology Advisor: Timothy R. Nurkiewicz, Ph.D

- Experience planning complex experimental designs and conducting inhalation toxicology experiments to assess cardiovascular and reproductive consequences
- Proficient with DMT wire myography and pressure myography systems
- Experience with handling and testing isolated pressurized perfused arterioles
- Murine handling and surgical experience
- Laboratory Training experience with undergraduate students, graduate students, postdoc fellows and research technicians

- Experience with immunohistochemistry staining, imaging, and quantification
- Scientific manuscript writing experience, including all aspects of submission, reviewer response and editing
- *Ad hoc* reviewer for several professional journals
- Independent problem solving and troubleshooting skills
- Excellent communication skills
- Experience presenting research at scientific meetings and departmental symposia

Lonza: Research and Technology (2015-2017)

Walkersville, MD

Cell Biology Research Associate

- Plan and execute experiments for new and improved processes for human primary cells
- Proficient in tissue isolations and cell culturing; primarily with human mammary epithelial cells (hMEC)
- Optimizing SOP protocols to increase success rates and improve the production of cellular products; including human mesenchymal stem cells (hMSC) and hMEC
- Selection and expansion of iPSCs and differentiation into neural cells
- Perform immunofluorescent staining for various cell types
- Experience with 3D tissue model development
- Training experience with production on new and improved primary cell isolation processes

Lonza: Cell Therapy (2013-2015)

Walkersville, MD

Core Technician II

- Perform client-specific cell manufacturing/culturing tasks in a cleanroom environment, including isolating, thawing, passaging, feeding and harvesting of multiple cell types
- Follow SOPs and batch records for processing of clinical grade cell therapy products
- Received individualized training for client projects
- Trained by Process Development on iPSC processing, including transfection, selection, and cell line expansion
- Designated as Lead Technician for client projects; responsible for process preparation, completion and accurate documentation
- Received GMP training and Aseptic Processing training for Iso-5 and Iso-7 environments

Abstracts Presented

1. **Garner KL**, Bowdridge EC, Griffith JA, DeVallance E, Schafner K, Engels KJ, Wix K, Goldsmith WT, Hussain S, Bachelor TP, Nurkiewicz TR. Nanomaterial Inhalation Exposure Alters Angiotensin II Sensitivity: Gestational Periods of Maternal and Placental Microvascular Outcomes. Society of Toxicology Annual Meeting (2022)

2. **Garner KL,** Bowdridge EC, Griffith JA, DeVallance E, Engels KJ, Wix K, Goldsmith WT, Hussain S, Batchelor TP, Nurkiewicz TR. Nanomaterial Inhalation During Gestational Windows Alters Angiotensin II Microvascular Sensitivity and Fetal Outcomes. Society of Toxicology Annual Meeting (2021).
3. **Garner KL**, Bowdridge EC, Griffith JA, Batchelor TP, Engels KJ, Goldsmith WT, Hussain S, Nurkiewicz TR. Critical Time-Point of Gestational Nanomaterial Inhalation Exposure: Alteration of Angiotensin II Response within the Maternal Uterine Microcirculation. Society of Toxicology Annual Meeting (2020)
4. **Garner KL,** Bowdridge EC, Griffith JA, DeVallance E, Engels KJ, Batchelor TP, Goldsmith WT, Nurkiewicz TR. Critical Window of Gestational Exposure: Uterine Microvascular and Fetal Consequences. Allegany-Erie Society of Toxicology Annual Meeting (2020).
5. **Garner KL,** Abukabda AB, Bowdridge EC, Batchelor TP, Hussain S, Goldsmith WT, Nurkiewicz TR. Uterine Adrenergic and Myogenic Microcirculatory Responses Influenced by Maternal Nano-TiO_2 Inhalation Exposure. West Virginia University, Van Liere Research Day (2019)
6. **Garner KL**, Bowdridge EC, JA Griffith, TP Batchelor, S Hussain, WT Goldsmith, TR Nurkiewicz. Impacts of Maternal Nano-TiO_2 Inhalation Exposure on Uterine Adrenergic and Myogenic Responses. Allegany-Erie Society of Toxicology Annual Meeting (2019)
7. **Garner KL**, Abukabda AB, Bowdridge EC, Batchelor TP, Hussain S, Goldsmith WT, Nurkiewicz TR. Influence of Maternal Engineered Nanomaterial Inhalation on

Uterine Adrenergic and Myogenic Microvascular Responses. Society of Toxicology Annual Meeting (2019)

8. **Garner KL**, Abukabda AB, Bowdridge EC, McBride CR, Batchelor TP, Goldsmith WT, Nurkiewicz TR. Fetal Vascular Consequences after Maternal Engineered Nanoparticle Inhalation. West Virginia University, Van Liere Research Day (2018)
9. **Garner KL**, Abukabda AB, Bowdridge EC, McBride CR, Batchelor TP, Goldsmith WT, Nurkiewicz TR. Consequences of Maternal Engineered Nanomaterial Inhalation of Fetal Vascular Reactivity. Allegheny-Erie Society of Toxicology Regional Chapter (2018)
10. Nie Y. **Garner K**, D'Souza T. A Three-Dimensional RAFT Co-Culture as Advanced Model for Breast Cancer Drug Discovery. American Association for Cancer Research (2017)

Publications

1. Griffith, J.A., **Garner, K.L**., Bowdridge, E.C., DeVallance, E., Schafner, K., Engels, K.J., Batchelor, T.P., Goldsmith, W.T., Wix, K., Hussain, S., Nurkiewicz, T.R. (2022). Nanomaterial Inhalation During Pregnancy Alters Systemic Vascular Function in a Cyclooxygenase-Dependent Manner. *Currently under review.*

2. Bowdridge, E.C., DeVallance, E., **Garner, K.L.,** Griffith, J.A., Stapleton, P.A., Hussain, S., Nurkiewicz, T.R. (2022). Cardiovascular System. P. Wexler (Ed.) *Encyclopedia of Toxicology 4th Edition. Accepted.*

3. Bowdridge, E.C., DeVallence, E., **Garner, K.L.,** Griffith, J.A., Schaffner, K., Seman, M.G., Engels, K.J., Wix, K., Batchelor, T.P., Goldsmith, W.T., Hussain, S., Nurkiewicz, T.R. (2022). Nano-Titanium Dioxide Inhalation Exposure During

Gestation Drives Redox Dysregulation and Vascular Dysfunction Across Generations. *Particle and Fiber Toxicology, 19(1),* 18. https://doi.org/10.1186/s12989-022-00457-y

4. **Garner, K.L.,** Bowdridge, E.C., DeVallance, E., Griffith, J.A., Kelley, E.E., Nurkiewicz, T.R. (2022) Using the Isolated Rat Placenta to Assess Fetoplacental Hemodynamics. *Frontiers in Toxicology: Developmental and Reproductive Toxicology, 4.* https://doi.org/10.3389/ftox.2022.814071
5. **Garner, K. L.**, Bowdridge, E. C., Griffith, J. A., DeVallance, E., Seman, M. G., Engels, K. J., Groth, C. P., Goldsmith, W. T., Wix, K., Batchelor, T. P., & Nurkiewicz, T. R. (2022). Maternal Nanomaterial Inhalation Exposure: Critical Gestational Period in the Uterine Microcirculation is Angiotensin II Dependent. *Cardiovascular toxicology*, *22*(2), 167–180. https://doi.org/10.1007/s12012-021-09712-8
6. Kunovac, A., Hathaway, Q. A., Pinti, M. V., Durr, A. J., Taylor, A. D., Goldsmith, W. T., **Garner, K. L.**, Nurkiewicz, T. R., & Hollander, J. M. (2021). Enhanced antioxidant capacity prevents epitranscriptomic and cardiac alterations in adult offspring gestationally-exposed to ENM. *Nanotoxicology*, *15*(6), 812–831. https://doi.org/10.1080/17435390.2021.1921299
7. He, Z., Huffman, J., Curtin, K., **Garner, K. L.**, Bowdridge, E. C., Li, X., Nurkiewicz, T. R., & Li, P. (2021). Composable Microfluidic Plates (cPlate): A Simple and Scalable Fluid Manipulation System for Multiplexed Enzyme-Linked Immunosorbent Assay (ELISA). *Analytical chemistry*, *93*(3), 1489–1497. https://doi.org/10.1021/acs.analchem.0c03651

8. Bowdridge, E. C., Abukabda, A. B., Engles, K. J., McBride, C. R., Batchelor, T. P., Goldsmith, W. T., **Garner, K. L.,** Friend, S., & Nurkiewicz, T. R. (2019). Maternal Engineered Nanomaterial Inhalation During Gestation Disrupts Vascular Kisspeptin Reactivity. *Toxicological sciences : an official journal of the Society of Toxicology*, *169*(2), 524–533. https://doi.org/10.1093/toxsci/kfz064
9. Abukabda, A. B., Bowdridge, E. C., McBride, C. R., Batchelor, T. P., Goldsmith, W. T., **Garner, K. L**., Friend, S., & Nurkiewicz, T. R. (2019). Maternal titanium dioxide nanomaterial inhalation exposure compromises placental hemodynamics. *Toxicology and applied pharmacology*, *367*, 51–61. https://doi.org/10.1016/j.taap.2019.01.024
10. Abukabda, A. B., McBride, C. R., Batchelor, T. P., Goldsmith, W. T., Bowdridge, E. C., **Garner, K. L**., Friend, S., & Nurkiewicz, T. R. (2018). Group II innate lymphoid cells and microvascular dysfunction from pulmonary titanium dioxide nanoparticle exposure. *Particle and fibre toxicology*, *15*(1), 43. https://doi.org/10.1186/s12989-018-0280-2

Career Development Activities

- 2020- Present: Biomedical Sciences Graduate Student Tutor
- 2020- Present: Acting Senior Graduate Student for Department of Physiology and Pharmacology
- 2020- Present: Student Representative for Graduate Advisory Committee
- 2020- Present: Aid in Cellular and Integrative Physiology Program Student Interviews

Memberships

- Toxicology Working Group — West Virginia University School of Medicine, Morgantown, WV (January 2018 – 2019)
- Center for Inhalation Toxicology (iTOX) – West Virginia University School of Medicine, Morgantown WV (2019 – Present)
- Society of Toxicology (August 2018— Present)
- Cardiovascular Toxicology Specialty Section
- Nanoscience and Advanced Materials Specialty Section
- Reproductive and Developmental Toxicology Specialty Section
- Inhalation and Respiratory Specialty Section
- Women in Toxicology
- Allegheny-Erie Regional Chapter of Society of Toxicology (August 2018-Present)

Participation in Scientific Meeting

- American Association for Cancer Research (2017)
- Allegheny-Erie Regional Chapter of Society of Toxicology Annual Meeting (2018)
- Society of Toxicology Annual Meeting (2019)
- Allegheny-Erie Regional Chapter of Society of Toxicology Annual Meeting (2019)
- Society of Toxicology Annual Meeting (2020)
- Allegheny-Erie Regional Chapter of Society of Toxicology Annual Meeting (2020)
- Society of Toxicology Annual Meeting (2021)
- Society of Toxicology Annual Meeting (2022)

Continued Education Symposia

1. **Garner KL** (2021) *Maternal Nanomaterial Inhalation Exposure: Critical Gestational Period in the Uterine Microcirculation.* Department of Physiology and Pharmacology Betschart Symposium
2. **Garner KL** (2021) *Determining the Sensitive Window of Gestational Exposure: The Impact on Uterine Microvascular Reactivity and Fetal Outcomes.* Stroke T32 Symposium
3. **Garner KL** (2021) *Nanomaterial Inhalation During Gestational Windows Alters Maternal Angiotensin II Microvascular Sensitivity and Fetal Outcomes.* Society of Toxicology Annual Meeting (Online)
4. **Garner KL** (2020) *Critical Window of Gestational Exposure: Uterine Microvascular and Fetal Consequence.* AESOT Rapid Fire Presentation
5. **Garner KL** (2020) *Determining the Critical Window of Gestational Exposure: Uterine Microvascular Reactivity and Fetal Consequences.* Physiology and Pharmacology Seminar Series
6. **Garner KL** (2019) *Critical Window of Gestational Exposure: Alteration of Uterine Microvascular Response and Fetal Outcomes.* Physiology and Pharmacology Seminar Series
7. **Garner KL** (2019) *Inhalation Exposure to 3D Printer Emissions (3DPE): Impacts on Microvascular Reactivity and Blood Pressure.* Department of Physiology and Pharmacology Betschart Symposium
8. **Garner KL** (2019) *Microvascular Responses to Diverse Xenobiotic Inhalation Exposures.* Physiology and Pharmacology Seminar Series

9. **Garner KL** (2018) *The Effects of Pulmonary Xenobiotic Particle Exposure on Systemic Microvascular Function.* Department of Physiology and Pharmacology Betschart Symposium

Awards and Honors

- 2009-2013: Presidential Scholarship
- 2009-2013: George Henry Miles Honor Society
- 2011-2013: Tri-Beta Biological Honor Society
- 2011-2013: Delta Sigma Epsilon Chemistry Honor Society
- 2019: Toxicology Working Group Student Travel Award
- 2019- 2021: Stroke T32 Training Scholar
- 2020: SOT Graduate Student Travel Award
- 2020: iTOX Outstanding Graduate Student Travel Award
- 2020: PPG Industries Graduate Student Oral Presentation Award at AESOT 2020
- 2021: Stroke Symposium Seminar Oral Presentation Award
- 2022: iTOX Graduate Student Travel Award